Establishment of a transgenic system for *in vivo* detection of apoptosis in the developing heart

Dissertation

zur

Erlangung des Doktorgrades (Dr. rer. nat.)

der

Mathematisch-Naturwissenschaftlichen Fakultät

der

Rheinischen Friedrich-Wilhelms-Universität Bonn

vorgelegt von

Kristel Martínez Lagunas

aus

Toluca, Mexiko

Bonn, 2017

Angefertigt mit Genehmigung der Mathematisch-Naturwissenschaftlichen
Fakultät der Rheinischen Friedrich-Wilhelms-Universität Bonn

Erstgutachter: Prof. Dr. Bernd K. Fleischmann
Zweitgutachter: Prof. Dr. Christa Müller

Tag der mündlichen Prüfung: 10.04.2018
Erscheinungsjahr: 2018

Die vorliegende Arbeit wurde von April 2012 bis November 2017 am Institut für Physiologie I der Rheinischen Friedrich-Wilhelms-Universität Bonn unter Anleitung von Prof. Dr. Bernd K. Fleischmann erstellt.

DEDICATION

I dedicate my Ph.D. journey to my parents because their unconditional love has made me the person who I am today and I would not have arrived here without your infinite support.

Les dedico mi viaje de doctorado a mis papis Toñita y Miguel porque su amor incondicional me ha convertido en la persona que soy hoy y sin su ínfinito apoyo no hubiera llegado hasta aquí.

To my grandparents for teaching me how beautiful Life is and that one has to live it on the edge despite the ups and downs.

A mis abuelitos Toñita y Rúben, Adelita y Jesús por enseñarme lo bonita que es la vida y que hay que vivirla al máximo a pesar de las altas y bajas.

To all who dare to make the Ph.D., for their endurance and determination to reach the finish line.

Y finalmente a todos los que se atreven a hacer el doctorado, por su aguante y perseverancia para llegar a la meta.

TABLE OF CONTENTS

1. INTRODUCTION

1.1. Programmed cell death during animal development

The German philosopher Arthur Schopenhauer mentioned that “life is a constant process of dying” (1). This phrase describes accurately the crucial role that programmed cell death (PCD) plays in the life of an organism. Actually, the life of an animal depends on the correct and constant elimination of cells via PCD during its development and a continuous cell turnover during its adulthood. PCD consists of different cell-suicide pathways that get activated at specific time frames of animal development. Since the nineteenth century, the relevance of this mechanism has been recognized and it was proven to occur naturally in many tissues of both vertebrates and invertebrates (2).

Jacobson and colleagues reviewed some of the main physiological functions of PCD. As shown in Fig. 1, it contributes to the sculpting of body parts in vertebrates, such as the formation of digits, inner ear and the four-chamber architecture of the heart. PCD is also involved in the deletion of tissues and organs, which are no longer needed in later developmental stages, or tissues that are not used in one sex. For example, the tadpole tail and intestine in amphibians are removed by PCD at older stages of development and the Müllerian duct that forms the uterus and oviducts in females is thought to be lost by PCD in males. PCD also adjusts cell numbers in organs where cells are overproduced. For example, in the vertebrate nervous system half of the neurons, which are generated in excess during embryonic development, are eliminated by PCD (3). It also eliminates more than 80% of oocytes prior to birth in human females (4, 5). In addition, it helps in the elimination of unwanted or dangerous cells such as self-reactive cells that could lead to autoimmunity in the human immune system or the removal of cells with unrepaired DNA damage, cell cycle perturbations or with fate and differentiation effects (3).

Developmental malformations and some human diseases are linked to an aberrant PCD (6). A decrease in cell death may be related to diseases such as cancer, autoimmune disorders or viral infections (7). For example, most of the cancer cells have developed resistance to undergo apoptosis, one of the 13 different types of programmed cell death (8), due to overexpression of anti-apoptotic proteins such as B-cell lymphoma 2 (BCL-2) or B-cell lymphoma X long (BCL-X_L) that prevents cell death (9, 10). New chemotherapeutic agents have been developed to promote cell death by activating specific genes of apoptosis. Similarly, in autoimmune disorders like systemic lupus and rheumatoid arthritis, a strategy to

reduce the lesion induced by auto-reactive T cells is to eliminate them from the circulation by adding death ligands from the tumor necrosis factor (TNF) receptor superfamily such as TNF-α or Fas ligand (FasL). These proteins activate the death-receptor pathway leading to cell death (11). On the other hand, an excess in the cell death program is often associated with diseases such as human immunodeficiency virus (HIV), neurodegenerative diseases like Alzheimer's disease, Parkinson, muscular atrophy, myocardial infarction and stroke. For instance, ischemia of both, neurons and cardiomyocytes induces programmed cell death (12).

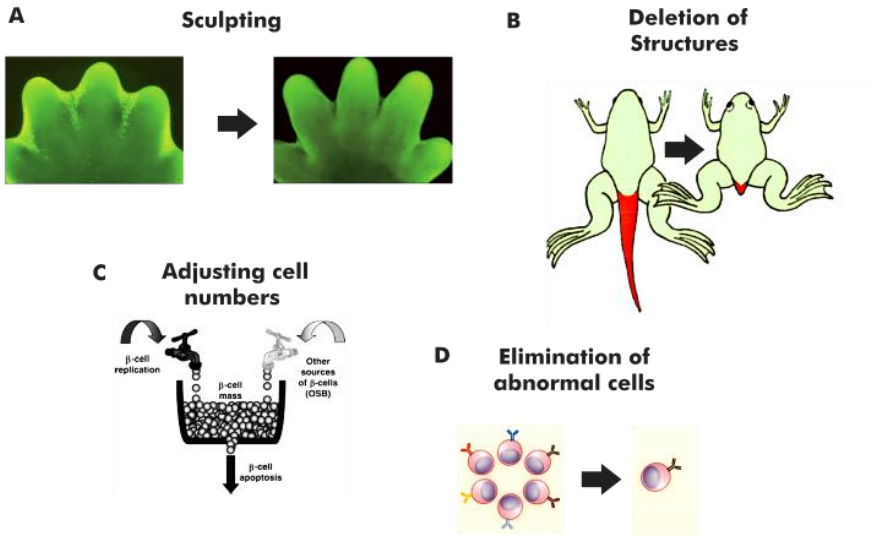

Fig. 1. Functions of programmed cell death during development.
Programmed cell death has different functions during animal development such as **(A)** sculpting of tissues, **(B)** deletion of structures mainly in insect or amphibian metamorphosis, **(C)** participation in cell turnover and **(D)** elimination of dangerous cells. (Taken and adapted from (3, 5, 13-16).

These diseases still represent a major health problem worldwide. According to the World Health Organization (WHO), cancer, neurodegenerative and cardiovascular diseases are still among the 10 top causes of death globally (17). Strikingly, ischemic heart disease is the world's biggest killer, causing almost 9 million deaths in 2015 (18).

It has been claimed that apoptosis is the major cause of cardiomyocyte's demise in myocardial infarction, ischemic injury and heart failure (19). These studies suggest that inhibiting apoptosis might be a potent strategy for treating heart diseases. However, this is still controversial, as it is not clear which type or types of programmed cell death are present in healthy and diseased hearts (20). This is mainly due to a lack of sensitive detection methods that can track and identify cells undergoing PCD in the myocardium. In order to establish effective therapies for heart diseases, it is necessary to deeper understand the distinct

physiological roles, the diverse mechanisms and signaling pathways of PCD in both, the embryonic and the adult heart. This will serve as a basis for further elucidation of its role in the diseased heart.

In the literature, it is still not specified if apoptosis, the most studied form of PCD, regulates the shaping and maturation of the mammalian heart (20, 21). Therefore, the focus of this work is to evaluate, if and to which extent this process is present during mouse development. For this, it is relevant to analyze the complex steps occurring during heart development in order to be able to evaluate in a second step, as to how apoptosis could be related to these developmental changes. The details of these processes will be described in the following paragraphs.

1.2. Heart Development and apoptosis

1.2.1. Formation of the heart

The word “heart” is defined in the dictionary as “the essential or most vital part of something” (22). This meaning resembles the vital function of the heart in the body. It plays a key role in the circulation of nutrients and removal of waste during the early stages of life and if the heart stops beating or pumping blood in the body, life will end (23).

The building of the heart involves a very detailed, sensitive and complex process. In order to form a proper and functional vertebrate heart, several morphological changes and different signaling pathways take place during development. These changes orchestrate the remodeling of the tubular heart into a mature four-chamber heart. Accurate heart organogenesis is the result of the interplay between proliferation, differentiation, cell growth and cell death (24). Alterations in these processes can lead to congenital heart diseases such as left ventricular non-compaction (LVNC), diastolic dysfunctions and arrhythmias and even might be lethal for the embryo (25). According to Samsa and colleagues, the drastic changes in the mammalian's heart’s shape, known as cardiac chamber maturation, can be divided into three interconnected processes: formation of the trabeculae (myocardial projections), the establishment of the conduction system and compaction of the myocardium (25).

The heart is the first organ to form and function in the embryo (26). It originates from mesodermal cells arising from the anterior part of the primitive streak in the embryo (Fig. 2). These cells migrate to the splanchnic (visceral) mesoderm in order to form the cardiac

crescent, which consists of two pools of cardiac progenitors. These cardiac precursors comprise the first and secondary heart fields (FHF, SHF) around embryonic day 7.5 (E7.5) in the mouse (27). As the embryo grows, the cardiac crescent fuses at the ventral midline to form the primitive heart tube at E8. The FHF will give rise to the left ventricle (LV), while the SHF will contribute to a large portion of the heart, including the outflow tract (OFT), right ventricle (RV), the sinus venosus (SV) and most of the atria (A). The early tubular mouse embryonic heart (between E7.5-8.5) is composed of an outer layer of myocardial cells framing it and an inner lining of endocardial cells derived from splanchnic mesoderm, separated by an extracellular matrix, which is better known as cardiac jelly (25, 28, 29). Even if in these early stages the heart lacks valves and a conduction system, it starts contracting and functioning as a peristaltic pump at about E8 (30). Around E8.25-E9, the heart tube starts to loop, the OFT and RV become distinguishable. Upstream the OFT, the future LV is formed at the outer curvature of the looped heart (Fig. 3A) (25). At E9, within the atrioventricular canal (AVC) and OFT, AV and OFT cushions develop by the accumulation of cardiac jelly. These cushions, populated by mesenchymal cells differentiated from endothelial and neural crest cells, will eventually form the cardiac valves (i.e. the mitral and tricuspid are derived from AV cushions and the aortic and pulmonary valves formed from OFT cushions) (31, 32).

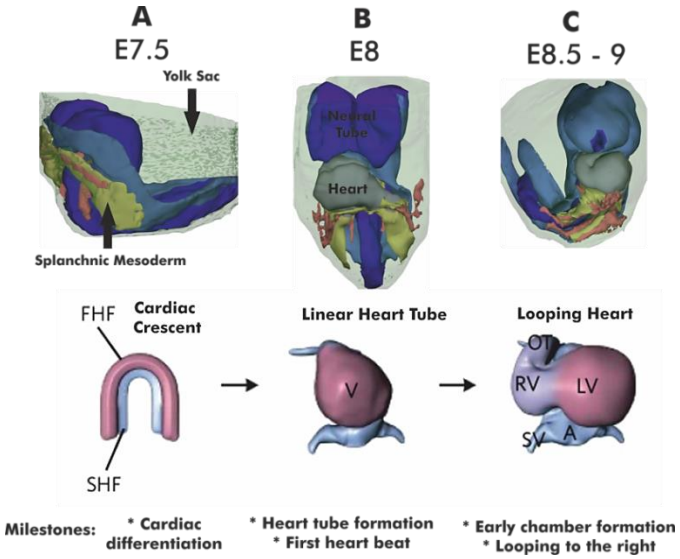

Fig. 2. Initial steps in heart formation.

3D diagrams of heart development with a whole embryo view (upper row) and ventral view of the primitive heart (lower row). **(A)** Cardiac crescent of the primitive heart at E.75. The cardiac crescent is derived from splanchnic mesoderm and it is comprised of two pools of cardiac precursors (the first and secondary heart fields (FHF, SHF). The first heart field (FHF) contributes to the left ventricle (LV), and the second heart field (SHF) contributes to the right ventricle (RV) and later to the outflow tract (OT), sinus venosus (SV), and left and right atria (LA and RA, respectively). **(B)** Primitive heart tube at E8. Fusion of the cardiac crescent at the ventral midline gives rise to the linear heart tube. **(C)** Looping heart at E8.5 – E9. Here the OF and the RV become visible. V = ventricle. (Schemes were taken and modified from (27, 29)).

After cardiac looping, around E9.5, trabeculae (myocardial cells covered by endocardial layer) emerge developing into the outer curvature of the primitive ventricle, extending villi-like on the luminal side of the wall. At this stage, the proliferation of endocardial and myocardial cells peaks in the developing chambers and in the OFT close to the LV (29) (Fig. 3B). The trabecular sheets or sponge-like structures are critical for the pumping function of the primitive heart. These myocardial protrusions increase cardiac output, allow nutrition and oxygen uptake in the embryonic myocardium and separate blood currents in the pre-septation heart before vascularization (33). Gradually, remodeling of trabeculae results in the formation of papillary muscles, pectinate muscles and is necessary for the formation of the conduction system (28, 33, 34). Despite its crucial role in heart chamber maturation, little is known about the molecular mechanisms that modulate formation and maturation of the trabeculae. Recently, it has been reported that perturbation in the process of trabeculation leads to cardiomyopathies such as LVNC (left ventricular non-compaction cardiomyopathy, hypertrabecualtion) as well as to cardiac failure, arrhythmias, and thromboembolism (34, 35). Therefore, due to its special attention will be given to the morphogenic events occurring during the process of heart trabeculation throughout this work.

After the emergence of initial trabecular ridges around E11-13.5, the trabecular sheets grow centripetally in the base of the ventricular wall and increase in length towards the lumen. Trabecular cardiomyocytes (CMs) are more differentiated than the ones in the compact wall (36). The proliferation pattern of CMs at this stage shows high rates on the mural wall and distal part of the OFT, and the septum becomes visible (29) (Fig. 3C).The last stage of trabecular growth ends with a phase of remodeling (between E14.5-E18.5). This process is also known as compaction or consolidation and starts when ventricular septation ends. At this stage, trabecular growth stops in luminal direction, it thickens radially and the trabeculae at the base regress to the point they cannot be distinguished from the myocardial wall (Fig. 3D). The spaces between trabeculae are filled with capillaries as the trabeculae compact.

Trabeculae in the LV are generally thicker and with larger intrabecular spaces that the ones in the RV. Furthermore, the trabeculae at the luminal LV merge to produce the anterior and posterior papillary muscles of the mitral valve (28). In addition, high proliferation rates are found at the base of the trabeculae and high differentiation rates of CMs occur at the luminal side (25, 28, 29). This compaction period is completed when a “mature” trabeculated network is evident at E14.5 in the mouse heart. The trabecular pattern varies between species and it is

considered to be like fingerprints, unique for each individual heart (28). After remodeling-compaction, the compact layer of the ventricles grows in size mainly by apposition, elongating the trabeculae and provoking an outward ventricular expansion. From E14.5 onwards, the myocardium thickening is accompanied by the invasion of the epicardium resulting in coronary vascularization of the myocardial wall. Further growth and compaction occur postnatally (28).

It is of relevance to mention other morphological changes that occur during heart chamber formation. For example, rotation and septation of the OFT occur around 9.5-10.5 connecting the right ventricle to the pulmonary trunk and the left ventricle to the aorta (28). In addition, the separation of the aorta and the pulmonary trunk is visible at E12.5-13.5 and it is accompanied by an increase in diameter and change in orientation of these great vessels (29). It is also around these stages (i.e. E11.5-E13.5) that the messenchymal cells of endocardial cushions (AV and OFT cushions) start to proliferate and that "myocardialization" at the margin of endocardial cushions occurs. Afterwards, the valve leaflets undergo apoptosis and several remodeling steps to finally become fully mature around E16.5 (37). Another important region of the heart is the intraventricular septum (iVS). It starts to be formed at E12.5 onward and at this stage, it shows high proliferation rate at its bottom and middle areas (29). Finally, Sedmera and colleagues emphasized the relevance of atrial trabeculation. Trabeculations in the atrium are visible around E12 coinciding with an increase of the atrioventricular pressure and therefore help to increase atrial contractility. The remodeling of atrial trabeculae results in the pectinate muscles (similar to the papillary muscles in the ventricle), which may improve atrial contractility as well (28).

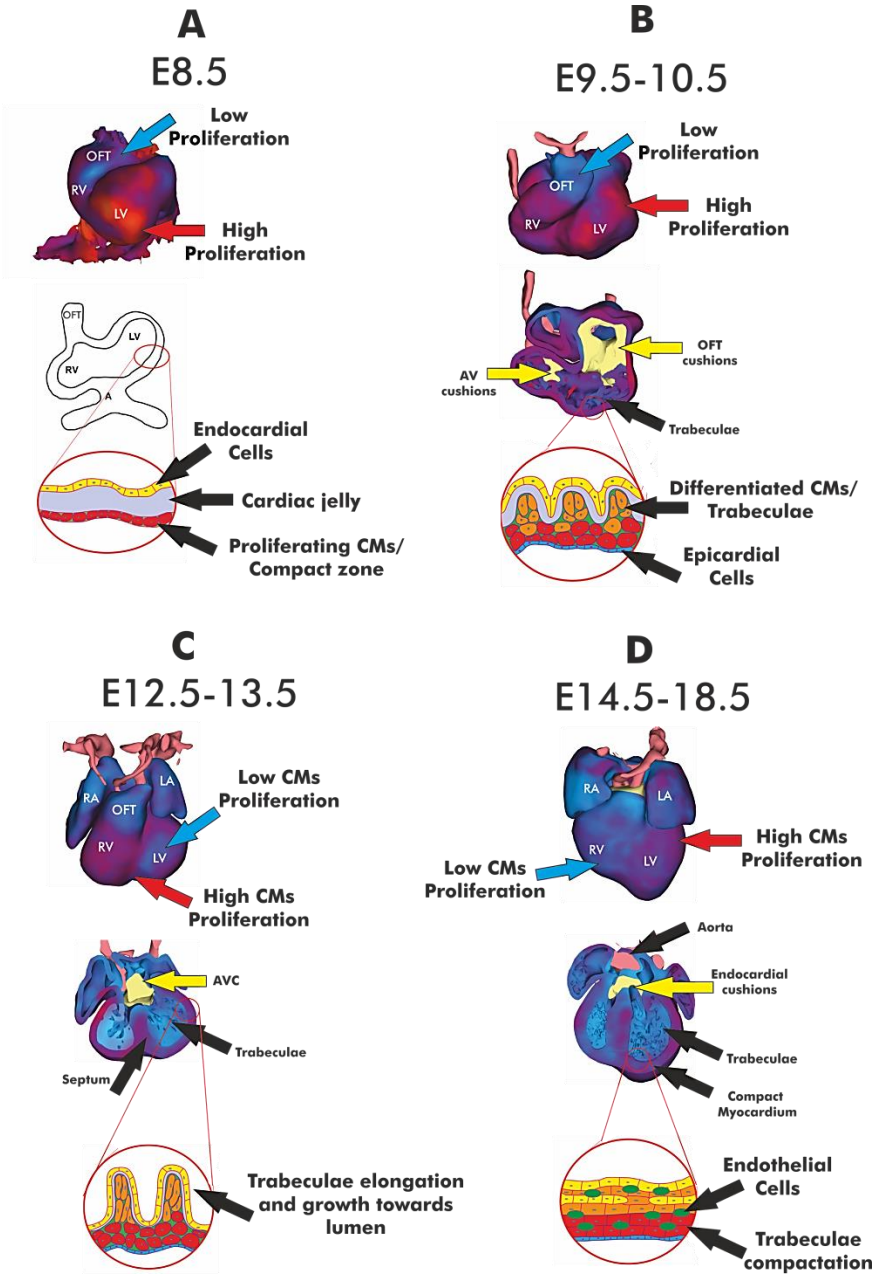

Fig. 3. Scheme of mouse heart chamber maturation.

(A) Structure and proliferation pattern of the mouse heart at E8.5. At this stage, the tubular heart starts to loop, the OFT, as well as primitive ventricles, can be distinguishable and CMs proliferation ($Brdu^+$ cells) is predominant at the ventricles. At this stage, the heart is composed only of myocardial cells, cardiac jelly, and endocardial cells. **(B)** Structure and CMs proliferation pattern of the mouse heart at E9.5-10.5. Trabeculae start to emerge from the ventricles wall extending towards the lumen and they contain differentiated cardiomyocytes as epicardial cells invade the heart wall. OFT and AV cushions are formed. At this stage, there is a high CMs proliferation incidence in the compact zone of the ventricles. **(C)** Structure and CMs proliferation pattern of the mouse heart at E12.5-13.5. Here, the ventricles and atria are already separated; the AVC and septum are clearly present. Notice that the trabeculae elongate more towards the lumen and proliferation rates are higher in the compact zone of the myocardium. **(D)** Structure and proliferation pattern of the mouse heart at E14.5-18.5. From E14.5 onwards, the 4 chamber-heart has formed. The trabeculae start to compact and stop growing. Endothelial cells fill the spaces between trabeculae sheets. The great vessels (aorta, pulmonary artery) are formed and the endocardial cushions will be converted into cardiac valves. (Proliferation 3D images were modified from (29) and cell types schemes were modified from (25, 31)).

1.2.2. Role of apoptosis during heart development

As described above, the developing heart undergoes several morphological transformations, during which cells proliferate, grow and differentiate in a matter of a few days. However, these mechanisms alone are not sufficient. It has been reported that cells in the heart as well as in other organs have to die trough apoptosis during development in order to sculpt correctly each part of the body (2, 3). Without genes of this controlled cell death process, several cardiac defects occur. For example, knockout mouse models for apoptosis genes (e.g. caspase 8, FADD (Fas-associated death domain protein)), and Casper (c-FLIP) develop abnormal hearts with aberrant ventricular chambers, with thin and disorganized trabeculae and hemorrhage, these mice die around E11 (38). This suggests an important role of apoptotic cell death, however, to understand its physiological function it is necessary to have a clear time course, localization and cell types of dying cells during different stages of heart development.

For more than 30 years, the chick heart has been the most studied model for cell death due to its easy accessibility and manipulation. In 1969, the first evidence of myocardial cell death in the embryonic chick ventricle was reported using electron-microscopy (39). These apoptotic cells suffered dramatic shape changes, their chromatin condensed, they had a comprised cytoplasm, and they started to lose their connections with adjacent cells rounding up to be finally expelled from the normal tissue mass into the intracellular spaces of the ventricle. A similar study, performed in 1972 by Tomas Pexieder, revealed degenerating cells in the bulbular cushions at early stages of development of the chick heart. These dying cells tended to be grouped, expelled to tissue boundaries (e.g. epicardio-myocardial, myocardio-endocardial or even into the lumen), and contained several liposomal vesicles suggesting autophagy activity. In addition, there were also neighboring mesenchymal cells in necrotic zones acting as macrophages to remove cells (40).

Other studies performed by Michiko Watanabe and colleagues in 1998 and by Katherine Schaefer and colleagues in 2004 (41, 42) in the chick embryo heart, confirmed a specific role of apoptosis in the shortening of the OFT during heart remodeling. In these studies, cell death was identified using more specific histological assays to detect apoptosis such as Terminal dUTP Nick End-labeling (TUNEL), Annexin V-biotin, cleaved caspase 3 and the supravital lysosomal dye, LysoTracker Red (LTR) (these techniques will be explained in section 1.4). Thus, they identified peaks of apoptosis during OFT septation and shortening. It was also

shown by co-stainings with markers for CMs (e.i. MF20 and anti-titin) that these specific cells die during OFT development.

The avian model has been helpful to confirm that apoptosis is active during the formation of the heart. However, until this date, there have been few comprehensive studies that show the distribution pattern of apoptotic cells in the developing mouse heart. One of these is the study from Sharma and coworkers in 2004 (43). They reported that apoptotic foci are distributed throughout different regions of the heart from E10.5 to 13.5. Using TUNEL assay they showed that high levels of apoptosis (more than 4%) occur at E12.5-13.5 at the endocardial cushions in the AVC and at the OFT. These apoptotic cells presented $TUNEL^{+}$ nuclei with a strong signal. Apoptosis in these areas coincides with the strong remodeling, fusion, and changes in cellular composition of the endocardial cushions to form the future atrioventricular valves. Less intense $TUNEL^{+}$ foci (less than 1%) were observed at the base of the ventricular wall and their number peaked at E11.5-12.5 being more abundant at the left ventricle and at the intraventricular septum. At the atria, the percentage of apoptotic cells was less than 0.5% and it was maintained during development. Sharma and colleagues suggested that apoptosis in different cardiac regions can be regulated by different cell death mechanisms and it can be associated with the removal of cell populations no longer required for later development, with the fusion of the atrioventricular cushions with the atrial septum induced by a probable removal of endocardial cells lying next to these structures, and with the separation and shortening of structures such as OFT.

The results presented by Sharma are similar to the ones shown by Barbosky and colleagues in 2006 using the LTR supravital dye, which marks the acidic compartments of the lysosomes. They confirmed that the number of apoptotic particles peak at E13-14.5 particularly at the OFT and significantly decrease after E15.5. They also showed co-localization of LTR^{+} particles with markers for cardiomyocytes suggesting a role of cardiomyocyte cell death in the remodeling of the OFT (21). Finally, another cardiac region in the embryonic mouse heart, where it has been shown that apoptosis is present, is the compact myocardium and in lesser extent also in the ventricular trabeculae. Consistent with this, Abdelwahid and colleagues determined the apoptosis index based on TUNEL staining at E10.5-15.5 of mouse heart development and reported its peak at E12.5 and a significant decrease at E15.5. In addition, they reported that apoptotic cell death might be associated with ventricular compaction and

differentiation of trabeculae and that it is mediated by the intrinsic (mitochondria) apoptosis pathway (44).

1.2.3. Role of apoptosis in congenital heart disease

As described above, the presence of cell death at different stages of the embryonic heart is indicative of a critical role in modulating proper heart formation, together with proliferation and differentiation. It has been demonstrated that excessive or diminished apoptosis is present in some congenital heart diseases (CHD) (45-49). According to the National Institute of Health (NIH), CHD are defects in heart's structure that very often change the normal blood flow through the heart. CHD manifest at birth and their incidence is 8 per 1000 newborns (50). It is still not known what the main cause of these defects is and its underlying molecular mechanisms remain unidentified. Environmental and genetic factors play an important role (51).

It is known that overexpression of the gene LYRM1, which is mainly expressed in adipose tissue and in the heart, does not affect cardiomyocyte differentiation, but it inhibits apoptosis and increases dramatically cardiomyocyte proliferation (52). This suggests that reduction of apoptosis during heart development can be associated with abnormal growth of the embryonic heart. For instance, one of the most common disorders of cardiac maturation is the left ventricular non-compaction (LVNC) or hypertrabeculation. It is characterized by excessive trabeculae growth and it is associated with mutations that cause mitochondrial dysfunction leading to abnormal apoptosis (25, 53). Furthermore, inhibition of apoptosis during chick heart development causes outflow tract defects similar to those observed in some human congenital heart defects (e.g. tetralogy of Fallot, double-outlet right ventricle, transposition of the great arteries, among others) (54, 55). Apoptosis can also play a role in pathologies of the cardiac conduction system postnatally (45, 47, 48, 56). Apoptotic cells have been found in the sinus node, atrioventricular node and His bundle of young human hearts with long QT syndrome, arrhythmias or conduction disturbances (48, 57, 58). Similarly, massive apoptosis in the right ventricle has been found in biopsy specimens of patients with Uhl's anomaly and arrhythmogenic right ventricular dysplasia (48, 59, 60).

If apoptosis is one of the mechanisms that can lead to CHD, then understanding its regulation and its manipulation can serve as alternative therapeutic approaches for these patients. Knockout mouse models provide a useful tool to find potential apoptosis checkpoints or

signals that trigger abnormal cell death in heart anomalies. Hearts of knockout mice of apoptosis genes such as caspase 8, FADD and c-FLIP developed noncompact myoarchitecture and impaired cardiomyogenesis (53, 61, 62). In addition, loss of Bax and Bak, pro-apoptotic mitochondrial genes, reversed doxorubicin-induced cardiotoxicity damage in neonatal mouse hearts (63). This suggests that specific inhibition of apoptosis modulators can improve cardiac damage caused by chemotherapy or radiation cancer treatments in young patients. Similarly, identification of active apoptosis mechanisms in congenital heart diseases may help to develop anti-apoptotic therapies based on stimulation of the IAP (inhibitors of apoptosis) family proteins, caspase inhibition, and inhibition of Bcl-2 for these diseases, among others (6).

1.3. Different types of PCD

1.3.1. Apoptosis

Apoptosis means "falling off" of leaves in Greek and it was coined for the first time by Kerr and colleagues in 1972 (64). It is a regulated cell suicide mechanism inherent to the majority, if not all, nucleated cells and it is the most extensively studied and well-characterized type of programmed cell death (6).

Cells that undergo apoptosis present a series of morphological changes that distinguishes this type of cell death from other programmed cell death processes. There are two stages of structural changes in apoptotic cells. In the first stage, the nucleus and cytoplasm condensate and the cell breaks up into membrane-bound fragments called apoptotic bodies, which contain compacted organelles with or without nuclear fragments (Fig. 4). In the second stage, these spherical or ovoid bodies are shed from tissue surfaces or are phagocytized by other cells (64, 65). If the phagocytosis fails, the apoptotic bodies disintegrate and release their content into the extracellular space by a process called secondary necrosis (66). Cells undergoing secondary necrosis are characterized by clear cytosol and rupture of the cytoplasmic membrane with extensive cell disintegration (67). On the contrary, apoptotic cells do not release their cellular components, and they are quickly phagocytized (6, 68).

Apoptotic bodies vary in size, they are often found in clusters at intercellular spaces, and they can move or disperse from their original site. Since 1972, the difficulty was noted to determine the precise duration of the formation and elimination of apoptotic bodies because the process appears to start in individual cells of same tissue at different times (64). The entire

apoptosis from the initial trigger to cell destruction can take hours or even days (69), however, specific biochemical apoptotic changes and removal of apoptotic cells can take less than ten minutes (70-72).

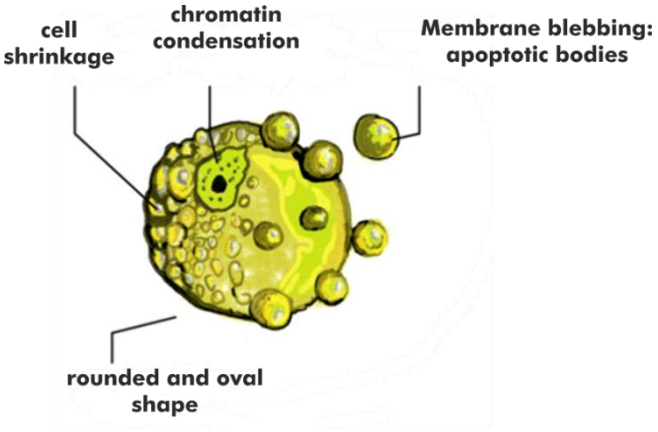

Fig. 4. Morphological features of apoptosis.
(A) Scheme of a typical apoptotic cell. (Modified from (65)).

1.3.2. Apoptosis Pathways

The molecular mechanism of apoptosis has been already elucidated. In 1986, Ellis and Horvitz demonstrated that the genes ced-3 and ced-4 are crucial to start apoptosis in the nematode *C. elegans* (73). Cloning studies in *Drosophila* and *C. elegans* have identified cell-death (CED) homologous genes in vertebrates and mammals, such as caspases and some mitochondrial genes like Bcl-2, which are conserved through evolution and play a role in the initiation or execution of apoptosis (74, 75).

Caspases, a group of cysteine proteases expressed constitutively as inactive precursors in almost all cells, are the key players in this cell death machinery and their activation decides the final fate of a cell (16, 68). There are two categories of caspases: initiator caspases (e.g., casp-8, -9 and -10) and effector caspases (e.g. casp-3,-6 and -7) (Fig. 5). These proteases contain an active-site (cysteine), a cleavage site (Asp-X sites) and a protein-protein interaction module domain (76). For the caspases to be activated they need to undergo dimerization after cleavage by specific upstream enzymes or by self-cleavage due to proximity (68, 77).

There are two main pathways by which apoptosis can be triggered: the intrinsic and extrinsic pathway (Fig. 5). The intrinsic pathway gets activated after a stress stimulus such a DNA damage which is sensed by damage sensors (e.g. p53), which send signals to turn on the pro-apoptotic Bcl-2 proteins (e.g. Bax, Bak), which then induce the release of mitochondrial

proteins such as cytochrome c (CytC) to the cytosol; CytC forms the apoptosome complex together with apoptotic protease-activating factor 1 (Apaf1) and caspase-9 (casp9). Casp-9 gets activated and it further stimulates executioner casp-3, 6 and/or -7. On the other hand, the extrinsic pathway is stimulated by steroid hormones or cytokines such as Fas ligand (FasL) or tumor necrosis factor alpha (TNFα), which binds to a death receptor (DR) (e.g. DR4, DR5, FasR, and/or TNFR1). Here, casp-8 is recruited by a death receptor and together with other molecules (i.e. Fas-associated death domain (FADD)), it forms the death-inducing signaling complex (DISC) at the plasma membrane. With this, casp-8 gets activated 8 (cCasp8) by self-cleaving due to close proximity and it starts the apoptotic cascade; it directly cleaves the executioner casp-3, 6 and/or -7 (cCasp-3,6,7) or it can further activate other proteins such as Bid that activates Bax and Bak to induce the release of CytC from the mitochondria (76).

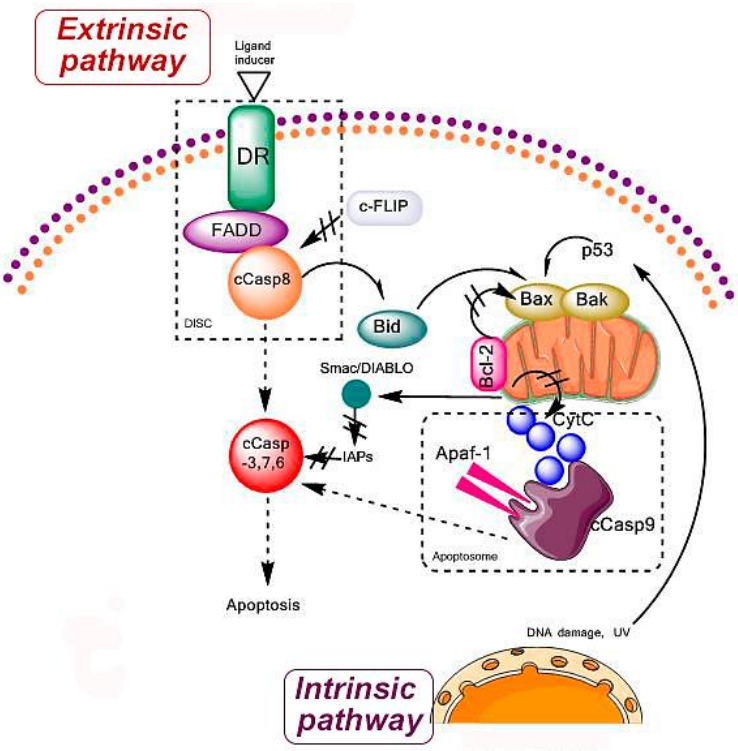

Fig. 5. Intrinsic and extrinsic apoptosis pathways.

The extrinsic pathway gets activated when a death receptor ligand (e.g. FasL, TNFα) binds its receptor (e.g. DR4-5, TNFR1 or FasR), which recruits other proteins to form the DISC complex. The DISC complex is necessary to activate casp-8 that furthers activates casp-3. The intrinsic pathway gets activated upon stress stimuli, such as DNA damage caused by radiation, toxins or hypoxia. It is sensed by damage sensor proteins such as the tumor protein p53, which activates the pro-apoptotic proteins Bax/Bak in the mitochondria, causing the release of cytochrome c (CytC) which forms the apoptosome complex together with Apaf-1 and casp-9. In this way casp-9 gets activated and it furthers cleaves casp-3 to continue with the apoptosis cascade. Caspase activation is antagonized by inhibitors of apoptosis proteins (IAPs), which themselves are inhibited and sequestered by Smac (second mitochondria-derived activator of caspases) or by DIABLO (direct IAP-binding protein with low pI). (Modified from (16, 68, 76) using the version 15.1 of the imaging sofware ChemDraw).

1.3.3. Necroptosis

This type of programmed cell death is also known as regulated necrosis, programmed necrosis, or necrotic cell death. It depends on the activation of receptor-interacting protein kinase-1 and/or 3 (RIPK1, RIPK3) and the phosphorylation of the pseudokinase mixed lineage kinase domain-like (MLKL). It is considered to be a back-up or innate mechanism of defense against pathogens like certain viruses that can inhibit caspase activation (68, 78). It plays a pathophysiological role in diverse disorders such as myocardial infarction, stroke, atherosclerosis, ischemia-reperfusion injury, pancreatitis, neurodegenerative pathologies, retinal detachment, and inflammatory bowel disease among others (78, 79). Therefore, it is of relevance to better understand the molecular pathways of necroptosis in order to find therapeutic options to fight these diseases by blocking or inducing this process. For example, triggering necroptosis might be an alternative therapy to eradicate apoptosis-resistant cancer cells (80). Several studies have shown that certain types of cancer (e.g. colorectal, leukemia and multiple myeloma cancer cells) are sensitive to necroptosis inducers such as TNF in combination with caspase inhibitors (81, 82). On the other side, inhibition of necroptosis might reduce the damage after myocardial infarction in mice. Luedde and colleagues (83) showed that the necroptosis complex RIPK1-RIPK3 is formed in the adult heart and that after myocardial infarction (MI) the mouse heart overexpresses RIPK3. Moreover, they observed that in hearts from RIPK3 knockout mice the effects of MI (e.g. inflammation, reduced ejection fraction, hypertrophy and adverse remodeling) were reduced after 30 days post-infarction, suggesting that inhibition of the RIPK3 protein can be a potential therapy for treatment of MI.

Hallmarks of necroptosis are “balloon-like” morphology, lysosomal, mitochondrial and plasma membranes rupture and there is cellular leakage, the release of intracellular content, and swelling of the cell and organelles. Necroptotic cells also show a translucent cytoplasm and condensed chromatin (small and irregular clusters) (66, 78) (Fig. 6).

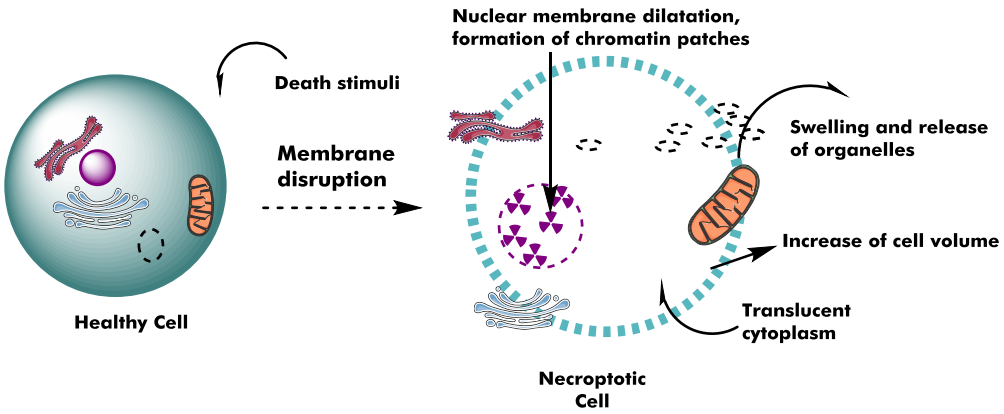

Fig. 6. Morphological features of necroptosis.

(A) Scheme of a typical necroptotic cell. (Modified from (66) using the version 15.1 of the imaging sofware ChemDraw).

1.3.4. Necroptosis Pathways

For several years, necrosis was considered as an accidental cell death caused by very strong stress or injury. However, it is now well reported that necrosis can be a regulated mechanism under certain circumstances (84, 85) (Fig. 7).

First, death stimuli such as DNA damage, viral or bacterial infection and cytokines, are sensed by specific death receptors at the membrane of the cell. When inducers such as TNFα or FasL bind their death receptors, FADD or TRADD are recruited to form a molecular complex, respectively. Casp-8 is also recruited in its inactive form; this is the reason why some scientist called this process "caspase-independent cell death". The assembly of these molecules leads to the activation of RIPK1, which subsequently phosphorylates RIPK3 (all together form the necroptosome complex). RIPK1 can be inhibited by Necrostatin 1 (Nec-1), a potent inhibitor that helped to identify RIPK1 activation as a critical step in the necroptosis pathway (86). Finally, RIPK3 phosphorylates MLKL resulting in its translocation to the plasma membrane leading to membrane rupture. In the case of viral or bacterial infection, the signal is sensed either by the DNA-dependent activator of interferon regulatory factor (DAI) or Toll/IL-1 receptor domain-containing adaptor inducing IFN-β (TRIF), respectively, which in turn activates RIPK3 and the further necroptosis cascade. Depending on cell type, lethal trigger and polyubiquitination state of RIP1, TNFα-TNFR1 ligation can also lead to the activation of the NF-kβ pathway resulting in cell survival (87, 88) by assembling different proteins such as TNFR-associated death domain (TRADD), RIPK1, cellular inhibitors of apoptosis 1 and 2 (cIAPS) (66, 89).

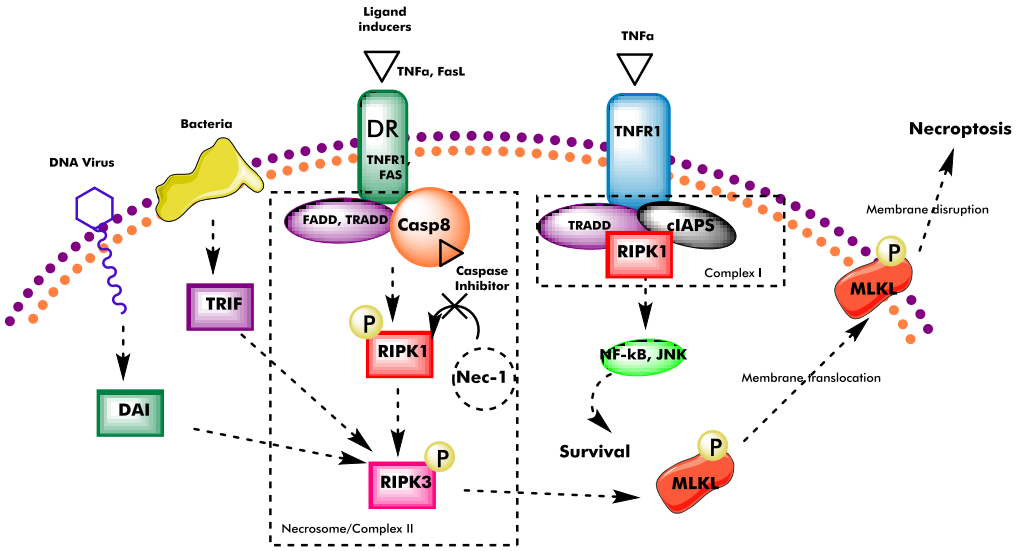

Fig. 7. Molecular pathways of necroptosis.

The main components of the necroptotic cascade are death receptors that, after triggering, form the necrosome complex that involve the activation of RIPK1 and RIPK3 or if the dead stimulus is a viral or pathogen infection it is sensed by damage sensor molecules (DAI, TRIF) which phosphorylate RIPK3. RIPK3 the leads to the phosphorylation of MLKL which translocates to the plasma membrane to cause cell membrane rupture. If the death stimulus is sensed by the TNFR1 receptor in presence of cellular inhibitors of apoptosis (cIAPS) the complex I is formed leading to the activation of the NF-kβ pathway resulting in cell survival. (Modified from (66, 78, 79, 89) and created with ChemDraw software version 15.1)

1.3.5. Autophagic Cell Death

The term autophagy is derived from ancient Greek and means "self-eating" and it was coined by the winner of the Nobel Prize in Physiology or Medicine 1972, Christian de Duve (90). In the 90s, Yoshinori Ohsumi—awarded with the Nobel Prize in Physiology or Medicine in 2016—has contributed substantial work in elucidating the molecular machinery and main functions of this process (91).

Autophagy is in charge of recycling cell organelles and proteins by lysosomal degradation and providing nutrients and energy to cells under starvation conditions in all living organisms (92). Furthermore, it is a quality control mechanism that maintains the cellular energetic balance under physiological conditions. However, as it is a multi-step regulated process, failure can occur at different levels. Defects in autophagy have been linked to different pathologies such as cardiomyopathies, myopathies, neurodegenerative disorders, cancer, immunological diseases, and metabolic dysfunctions (93).

Autophagy may also lead to cell death under certain conditions. For example, it was reported that autophagy mediates physiological cell death during the development of *D. melanogaster* (94) and knockdown of autophagy genes results in abnormal cardiac development in zebrafish

and mice (95). In addition, autophagy is responsible for cell death of certain cancer cells lacking apoptosis molecules (e.g. Bax, Bak or caspases) in response to cytotoxic agents (96). Bax/Bak-deficient cells treated with apoptotic stimuli contain massive cytoplasmic vacuolization (8, 97), a main feature of autophagy.

Up to date, it is still not clear which molecular mechanisms and as to how autophagy regulates cell death. However, autophagosome formation seems to be required for cells to die after starvation, hypoxia, high temperatures, or cytotoxic stimuli when apoptosis cascade is inhibited (97). Furthermore, upregulation of autophagy regulators such as Atg5 and Atg6 leads to cell death, whereas their downregulation results in cell survival (97). This type of cell death was named "autophagic cell death" by the NCCD. It is often morphologically characterized by the absence of chromatin condensation accompanied by massive autophagic vacuolization in the cytoplasm. However, in order to clearly classify cells undergoing autophagic cell death, the morphological analysis should be accompanied by the proof that autophagy can be suppressed by the inhibition or knocking down of at least two distinct autophagic related genes (e.g. Atgs, Beclin 1, or Vps34) (8).

1.4. Apoptosis detection methods

Programmed cell death research has substantially progressed over the past 15 years. According to the NCCD, there are at least 13 programmed cell death modalities (8). In order to detect each cell death type, it is critical to combine morphological characteristics with at least one biochemical assay. In addition, it has to be proven that the cell death modality does not occur when one or more key elements in its molecular pathway are inhibited. In this section, the most used and accepted methods to detect apoptosis *in vitro* and *in vivo* will be discussed.

As it was described in section 1.3, the molecular mechanisms of apoptosis are well studied. Therefore, several methods exist to identify this type of cell death. Still, its detection is challenging mainly because of the fast and asynchronous speed in which apoptotic cells die and disappear. Different cells within tissues are engulfed, shed or dispersed within minutes (72). Together with this, it is known that cells in the same tissue, organ or culture die at a different frequency or at specific sites, depending on the apoptotic stimuli and cell death machinery within each cell type (98). Therefore, the selected tool to detect apoptosis should be carefully chosen and optimized according to cell type.

Apoptosis has to be assessed at different time points and with at least two different principles. The oldest method of identification of apoptotic cells is transmission electron microscopy (TEM). Using TEM, one can observe the typical characteristics of the apoptotic cell: intact cellular membranes, dark and dense cytoplasm and nucleus, blebs at the cell surface, large vacuoles, nuclear fragmentation, and rounded cells expelled from the tissue or neighboring cells (99). Watanabe and colleagues mentioned that the advantages of TEM are that very often apoptotic cells can be identified even when engulfed in surrounding cells; the cell type sometimes can be as well distinguished via specific characteristics such as striated myofibrils in the case of cardiomyocytes or skeletal muscle cells (Fig. 8).

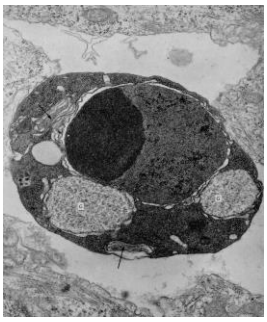

Fig. 8. Cardiomyocyte undergoing apoptosis in the embryonic chick ventricle.
This dying cell is located in the intercellular spaces of the developing myocardium. The cell has rounded up, expelled from the tissue, and the nuclear chromatin has condensed on one side of the nucleus. The cell was identified as cardiomyocyte by the presence of large glycogen pools and scattered myofilaments. This specimen was block stained with uranyl acetate and visualized via TEM. (Taken from (39)).

Another well-accepted indicator of apoptosis is DNA fragmentation. This feature occurs late in the apoptosis cascade, when the endonucleases are activated and cut the DNA at sites between the nucleosomes leaving fragments of similar sizes (e.i. approximately 200 bp). This can be evaluated by DNA laddering in an agarose gel or by TUNEL labeling. This technique detects the 3'-OH free ends of DNA fragments labeling them via the incorporation of labeled nucleotides to strand breaks through the action of terminal deoxynucleotidyl transferase (TdT). There are different labels, but the most commonly used are fluorescein labeled nucleotides, which can be detected by fluorescence microscopy or flow cytometry. This method is broadly used for histological tissue sections analysis (Fig. 9). However it has several disadvantages, first, it detects apoptosis in very late stages of the cascade, what means that cells which are initiating the apoptosis cascade can be missed leading to underestimation of the amount of apoptosis. On the other hand, DNA breaks are not only associated with apoptosis, but with DNA damage, in cells with high proliferative or metabolic activity or in

necrosis, leading to false positive results (100). For example, high variability (0.2 to 35 TUNEL$^+$ nuclei per 100 cardiomyocytes) in the reported apoptosis levels during end-stage heart failure in humans (101, 102) has been observed questioning the accuracy of TUNEL staining. In addition, this technique is very expensive and prone to false positive results due to sample processing (i.e. tissue sectioning). Therefore, the results obtained by this method have to be corroborated by at least one additional apoptosis assay (103).

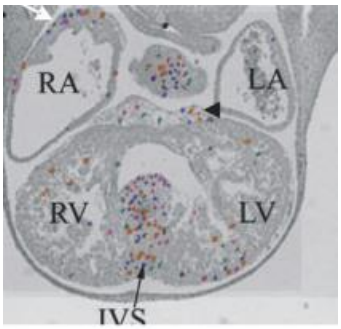

Fig. 9. Apoptotic cells detected in E13.5 mouse embryonic hearts using TUNEL assay and templating technique.
The template of apoptotic cells summated from ten transverse heart sections from two different E13.5 embryos. TUNEL$^+$ foci were found in the interventricular septum (IVS), atrioventricular cushions (arrowhead) and right atrium (white arrow). RA = right atrium, LA = left atrium, RV = right ventricle, LV = left ventricle. (Modified from (43)).

Another principle for apoptosis detection is based on identifying certain biochemical features of this cell death mechanism. These can be assessed by searching the activation or change of at least one molecule in the apoptosis cascade pathway (Fig. 5). For example, cells that undergo apoptosis by the extrinsic pathway can be detected by antibodies that bind to activated casp-8, 3, 7, 6 or 9, as well as Bid cleavage and mitochondrial outer membrane permeabilization (MOMP) (8). In addition, in order to observe caspase activation over time *in vitro*, there are some available assays based on fluorogenic protease substrates that contain a specific cleavage caspase sequence that associates with the cysteine of a fluoromethyl ketone (FMK) caspase moiety (6, 99). In this way, when apoptosis is present, this peptide is cut and the fluorescent protein released. This can be measured by fluorescence microscopy, flow cytometry or fluorescent readers giving the chance to have both, a qualitative and quantitative readout. This method works well in living cells, fixed cells, and tissues. However, it has also some disadvantages, such as limited permeability in dense tissues and it is also expensive for high throughput screenings. In addition, activation of caspases is not only associated with apoptosis, but with differentiation, cell proliferation and inflammation (104) leading to false positives. In order to confirm the presence of extrinsic apoptosis, it has to be proven that it can

be suppressed by pan-caspase inhibitors such as N-benzyloxycarbonyl-Val-Ala-Asp-FMK (zVAD-fmk) (8).

On the other hand, cells undergoing apoptosis by the intrinsic pathway is measured by changes in mitochondria. Early events in the intrinsic apoptotic pathway occur at the mitochondria: inner membrane depolarization, increase in Ca^{2+} concentration, MOMP, the release of cytochrome c (cytC) and other pro-apoptotic proteins such as Bid, Bax, and Bak. Pro-apoptotic proteins can be detected by antibody staining. To visualize MOMP there are different options, one is the transfection of cells with plasmids such as cytC-GFP, AIF-GFP, or mitochondrial localization sequences such as MLS-GFP. The cells can be monitored over time via fluorescence microscopy (105). In addition, there are some fluorescent dyes such as tetramethylrhodamine methylester (TMRM), which accumulates in the mitochondria in response to negative membrane potential (99). The advantages of mitochondrial assays are that they can be used *in vitro,* in live cells or in acute slices. The disadvantage is that changes in mitochondria also occur in necrosis and other PCD modalities (99, 105). Intrinsic apoptosis can be inhibited by zVAD or Bcl-2 overexpression.

Another approach to detect apoptotic cells is by assessing membrane alterations. Apoptotic cells externalize phosphatidylserine (PS) from the inside leaflet of its membrane to the outside part by the action of scramblase. PS externalization works as a signal for macrophages (99). Flipped PS can be detected by Annexin V, a protein that has high affinity to PS in the presence of Ca^{2+}. There are commercial fluorescent probes tagged to Annexin V to recognize apoptotic cells by flow cytometry and fluorescent microscopy. This method detects early apoptotic cells before the cell membrane is disrupted and the cell antigens destroyed. This allows the identification of cell type, thing that is not possible to assess when late apoptosis markers such as TUNEL or vital dyes are used. In spite of its advantages, Annexin V is also very expensive to use in a systemic way and in certain cases, it can also recognize necrotic cells (Fig. 10).

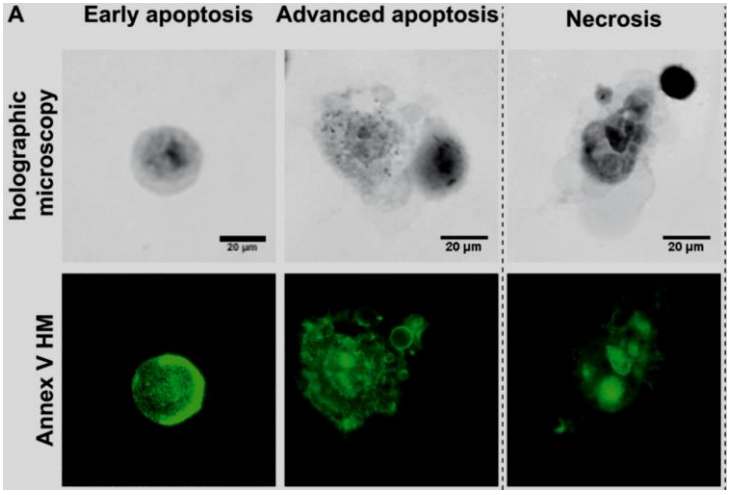

Fig. 10. Detection of alterations in the membrane of apoptotic and necrotic cells using Annexin V-FLUOS.

Annexin V can detect early apoptosis, advanced apoptosis, and necrosis. Note the morphological differences between the roundish apoptotic bodies formed in apoptosis in comparison to the swollen cell debris in necrosis. (Modified from (65))

Apoptotic cells in whole embryos have been broadly visualized by vital dyes, such as acridine orange (AO), Nile blue sulfate (NBS), neutral red (NR) or Lysotracker Red (LTR). These dyes concentrate in areas of high lysosomal and phagocytic activity. Due to their acidophilic nature, they stain acidic compartments (99). However, they cannot distinguish between lysosomes degrading apoptotic debris or another type of molecule due to autophagy. Therefore, as in the case of almost all described methods, it is critical to use a second technique to verify that apoptosis is triggered. Two of the main disadvantages of these dyes are the limited tissue penetration and photobleaching. This applies to all dyes with the exception of LTR, which has the advantage to penetrate easily into tissues due to its aldehyde-fixable capacity and in addition it does not fade (Fig. 11). The challenges with this technique are that it is limited to temperature, fixation and penetration conditions of the dye, together with the fact that it can also stain non-apoptotic cells containing large acidic compartments or undergoing autophagy.

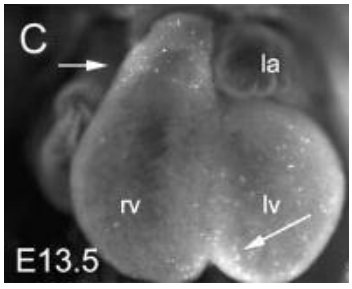

Fig. 11. Detection of apoptosis in mouse heart development using the supravital dye Lysotracker Red (LTR).

The bright LTR fluorescent particles mark apoptotic cells in specific areas of the embryonic mouse heart at E13.5. (Modified from (21)).

Finally, there are some genetically encoded probes for studying the complex progression of apoptosis *in vivo*. These live-imaging tools are mainly based on caspase activity detection (71, 106, 107) or on the visualization of PS translocation by Annexin V (108). The zebrafish (*Danio rerio*) model is suitable for live fluorescence imaging due to its optical transparency during early development (109). Van Ham and colleagues developed a transgenic zebrafish that expresses constitutively a secreted human AnnexinV-YFP protein (secA5-YFP), which is secreted into the extracellular space. In case the cell undergoes apoptosis, secA5-YFP binds to its PS residues on the outer leaflet of the membrane resulting in bright fluorescent signals (Fig. 12A-B). With this tool, it was possible to monitor patterns of apoptosis in living zebrafish during development and to visualize neural cell death *in vivo.* These genetic tools are very promising to detect cells at different stages of the apoptosis cascade in living organisms over time.

Here it is important to highlight the advantages of using genetic tools to monitor apoptosis in living contexts. Firstly, *in vivo* studies offer the possibility to analyze the importance of apoptosis in healthy and diseased organisms. Only in the living environment it is possible to evaluate the specific time point of appearance, progression and clearance of apoptotic cells, as well as their distribution within the tissues and their interaction with other cells, tissues or other cell death signaling pathways. From a pathophysiological perspective, Galluzzi and colleagues state that researchers should only consider the cell death modalities relevant to affect the embryonic or postnatal development or to be the cause of disease that have been shown to occur *in vivo* (8). Moreover, this complex environment should be aimed at in cell death studies to show, if there are other backup mechanisms after inhibition of a specific pathway and to show the functional role of specific genes of the pathway that might serve as the base to develop strategies to treat diseases. Finally, genetic live-imaging tools allow the monitoring of the complex and rapid changes of an individual apoptotic cell or group of cells in specific body tissues in real-time before engulfment.

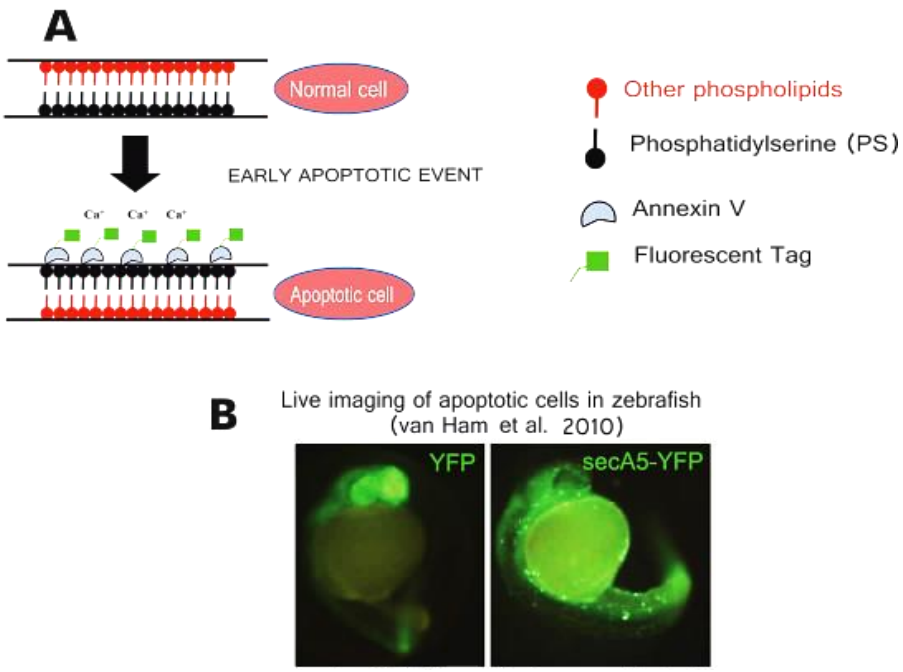

Fig. 12. Genetic tool to visualize PS translocation in apoptotic cells by Annexin V.

(A) Scheme for the detection of early apoptosis via binding of Annexin V to PS. When apoptosis occurs, PS is translocated to the outer leaflet of the cell membrane. Once there, Annexin V binds PS with high affinity and in a calcium-dependent manner. Annexin V conjugates are commonly used to detect early apoptosis *in vitro* and in tissue sections. **(B)** sA5-YFP labels apoptotic cells in live zebrafish embryos (Modified from (108)). Apoptotic cells can be identified as the brightest signals in the YFP channel. A5 = Annexin V, s = secretion signal, and YFP = yellow fluorescent protein.

1.5. Aims

Current methods that detect apoptotic cells are mainly based on evaluating only one time point of the apoptosis cascade. As this process is very dynamic and occurs at different times in cells of the same tissue the only way to estimate more accurately the rate of apoptosis is to monitor them over time. To date, there are some transgenic life-imaging tools available to detect apoptotic cells in living organisms such as the transgenic zebrafish expressing Annexin V from van Hamm et al. (108) or the SCAT3 mouse from Yamaguchi et al. (107). But unfortunately, there is no genetically encoded probe, which has been developed and used to track apoptosis in the mouse myocardium. A precise determination of cardiomyocyte apoptosis in the developing mouse heart may shed some light on the role of apoptosis in the context of physiological heart formation and in the pathogenesis of cardiovascular disease. Therefore, the main goal of the present work is to establish a straightforward live reporter-based method that allows the visualization and quantification of apoptotic cells in the embryonic mouse heart *in vivo.*

The proposed system for *in vivo* visualization of apoptosis is based on earlier work in zebrafish (108) with adaptations to the mammalian model. This system expresses a secreted human Annexin V (sA5) fused to yellow fluorescent protein (YFP) (Fig. 12). As cells undergo apoptosis, sA5-YFP binds with high affinity to its PS residues resulting in bright fluorescent signals. The ubiquitous expression will be ensured by the chicken β-actin promoter with CMV enhancer element (CAG). The functionality and specificity of the CAG-sA5-YFP reporter should first be evaluated in stably transfected, undifferentiated and differentiated mES cells as well as *in vivo* in a transgenic mouse model generated from the sA5-YFP mES cells. Apoptotic cells labeled by sA5-YFP should be confirmed by co-stainings with cCasp3 (early apoptosis marker) and TUNEL (late apoptosis marker).

After validating the system, I wanted to focus on the critical question, as to whether apoptosis occurs during mouse embryonic development in CAG-sA5-YFP mice. To achieve this goal a complete map of the distribution and rates of apoptotic cells and blebs during complete heart embryogenesis (E9.5 to P2) needs to be provided, the cell types undergoing apoptosis should be identified, the specific localization of the dying cells in the developing heart should be described. Additionally and importantly the changes occurring over time of apoptotic cells in living embryos and in the beating embryonic heart need to be documented.

2. MATERIALS AND METHODS

2.1. Materials

2.1.1. Reagents

Product Name	Company
Acetic acid	Sigma Aldrich, Steinheim, Germany
Acetic acid	Sigma Aldrich, Steinheim, Germany
Agarose	Carl Roth, Karlsruhe, Germany
Agar	Becton Dickinson, Heidelberg, Germany
Ampicillin	Gibco/Life Technologies, Darmstadt, Germany
Calcium Chloride ($CaCl_2$)	Sigma-Aldrich, Steinheim, Germany
Demecolcine	Sigma-Aldrich, Steinheim, Germany
DNaseI (3000 u/ml)	Promega, Madison, Wisconsin, Germany
DNA Gel Loading Dye (6X)	Thermo Fisher Scientific, Waltham, MA, USA
dNTP Mix (2.5 mM)	Qiagen, Hilden, Germany
Donkey Serum (DS)	Jackson ImmunoResearch, Suffolk, England
Dulbecco's Phosphate-buffered saline (DPBS)	Invitrogen/Life Technologies, Darmstadt, Germany
Enhancer Solution (5X)	Peqlab, Erlangen, Germany
Ethidium Bromide	Fluka/Sigma-Aldrich, Steinheim, Germany
Ethylenediaminetetraacetic Acid, EDTA	Sigma-Aldrich, Steinheim, Germany
Fetal Calf Serum (FCS)	PromoCell, Heidelberg, Germany
FLUKA Mounting Medium	Fluka/Sigma-Aldrich, Steinheim, Germany
Gelatin	Sigma Aldrich, Taufkirchen, Germany
Geneticin Sulfate (nmycin, G418)	Gibco/Life Technologies, Darmstadt, Germany
Hydrochloric Acid (HCl)	Sigma-Aldrich, Steinheim, Germany
4-Hydroxytamoxifen (4-OHT)	Sigma-Aldrich, Steinheim, Germany
Iscove's Modified Dulbecco's Medium (IMDM)	Gibco/Life Technologies, Darmstadt, Germany
Isopropanol	VWR, Darmstadt, Germany
Kanamycin	Gibco/Life Technologies, Darmstadt, Germany

Knockout Dulbecco's Modified Eagle Medium (KO-DMEM)	Gibco/Invitrogen, Karlsruhe, Germany
Leukemia Inhibiting Factor (LIF), ESGRO	Millipore, Schwalbach, Germany
L-Glutamine	Invitrogen/Life Technologies, Darmstadt, Germany
MasterAmp "x PCR Premix I (Buffer i)	Biozym Scientific, Oldendorf, Germany
Methanol	Merck, Darmstadt, Germany
β-Mercaptoethanol	Sigma-Aldrich, Steinheim, Germany
2-Methylbutan (Isopentanol)	Carl Roth, Karlsruhe, Germany
3-Morpholinopropanesulfonic Acid (MOPS)	Sigma-Aldrich, Taufkirchen, Germany
Non-Essential Aminoacids (MEM)	Gibco/Life Technologies, Darmstadt, Germany
O'GeneRuler 1 kb DNA Ladder, ready-to-use	ThermoFisher Scientific, Waltham, MA, USA
Paraformaldehyde (PFA)	PanReac AppliChem, Barcelona, Spain
Penicillin/Streptomycin	Gibco/Life Technologies, Darmstadt, Germany
Phosphate-Buffered Saline (PBS)	Sigma-Aldrich, Steinheim, Germany
Potassium Chloride (KCl)	Sigma-Aldrich, Steinheim, Germany
Rat Serum	PAN Biotech, Aidenbach, Germany
RNA-Loading Buffer	New England Biolabs, Frankfurt am Main, Germany
Sodium Acetate	Sigma-Aldrich, Steinheim, Germany
Sodium Citrate	Sigma-Aldrich, Steinheim, Germany
Sodium Chloride (NaCl)	Sigma-Aldrich, Steinheim, Germany
Sucrose	Sigma-Aldrich, Steinheim, Germany
TaqMan Master Mix	Applied Biosystems/Life Technologies, Darmstadt, Germany
Taq Polymerase	Invitrogen/Life Technologies, Darmstadt, Germany
Tissue-Tek® O.C.T.™ Compound	Sakura Finetek Europe B.V., Zoeterwoude, Netherlands
Tris-(Hydroxymethyl)-Aminomethan-Hydrochlorid (Tris-HCl)	Sigma-Aldrich, Steinheim, Germany

Trypsin/EDTA 0.05% /w/v) 100X	Gibco/Life Technologies, Darmstadt, Germany
Tryptone	Becton Dickinson, Heidelberg, Germany
TritonX-100	Sigma Aldrich, Steinheim, Germany
TRIzol® Reagent	Invitrogen/Life Technologies, Darmstadt, Germany
Yeast Extract	Becton Dickinson, Heidelberg, Germany
Z-Val-Ala-As (OMe)-FMK (zVAD-fmk)	Abcam, Cambridge, UK

2.1.2. Enzymes

The following enzymes were purchased from the company Fermentas, Leon-Rot, Germany: BamHI, Calf Intestine Alkaline Phosphatase (CIAP), HincII, Klenow Fragment of the DNA-Polymerase I, NotI, SacII and T4 Ligase.

2.1.3. TaqMan Probes

The following TaqMan probes were purchased from the company Applied Biosystems/Life Technologies located in Darmstadt, Germany:

Name	**Reporter**
eGFP	FAM-MGB
TFRC	VIC-MGB
18S rRNA	VIC-MGB

2.1.4. Primers

All primers were designed and ordered to the company Invitrogen/Life Technologies, Darmstadt, Germany:

Name	**Sequence (5'-3')**
Sec Signal_Fw	**5'** - AGGTTTTGCTGGCACTGTTC - **3'**
YFP PolyA_Rev	**5'** - TGCCGATTTCGGCCTATTGG - **3'**
YFP_1Fw	**5'** - CCGCGTTACATAACTTACGG - **3'**
CAG_1Fw	**5'** - CCGCGTTACATAACTTACGG - **3'**
CAG_2Fw	**5'** - TTCGGCTTCTGGCGTGTGAC - **3'**
A5_1Fw	**5'** - ACCCTCTCGGCTTTATGATG - **3'**
A5_2Fw	**5'** - AGCTCTTCTGCTGCTCTGTG - **3'**

2.1.5. Kits

Name	Company
Annexin V-FITC Apoptosis Detection Kit	Calbiochem/Millipore, CA, USA
EndoFree® Plasmid Maxi Kit	Qiagen, Hilden, Germany
Gentra Puregene Mouse Tail Kit	Qiagen, Hilden, Germany
In Situ Cell Death, fluorescein detection Kit	Roche, Mannheim, Germany
QIAprep Spin Miniprep Kit	Qiagen, Hilden, Germany
QIAquick Gel Extraction Kit	Qiagen, Hilden, Germany
QIAquick® PCR Purification Kit	Qiagen, Hilden, Germany
SuperScript VILO cDNA Synthesis Kit	Invitrogen/Life Technologies, Darmstadt, Germany

2.1.6. Solutions, Media, and Buffers

Name	Composition
1x Tris-Acetate-EDTA (TAE Buffer):	20 mM Sodium Acetate 40 mM Tris (pH 7.6) 1 mM EDTA
LB-Medium (1x):	1% Tryptone 0.5% Yeast Extract (w/v) 1% Tryptone 1% NaCl (w/v) in deionized water
LB-Agar-Plates:	Prepared as LB-Medium plus: 1.5% Agar (w/v) pour into Petri dishes
SOB Medium:	2% Tryptone (w/v) 10 mM NaCl 0.5% Yeast Extract (w/v) 2.5 mM KCl pH 7.0, autoclave 10 mM $MgCl_2$ and $MgSO_4$
MOPS-Buffer:	10 mM EDTA 200 mM MOPS 50 mM NaAc

Ampicillin:	Stock Solution: 100 mg/ml Ampicillin in pure water Working Solution: 100 µg/ml
Kanamycin:	Stock Solution: 50 mg/ml Ampicillin in pure water Working Solution: 50 µg/ml
Sucrose Solution:	20% Sucrose (w/v) in DPBS 2.5 mM $CaCl_2$
DPBS Washing Solution:	2.5 mM $CaCl_2$ in DPBS
PFA Fixing Solution:	2.5 mM $CaCl_2$ in PFA
Permeabilization Solution:	0.2% (v/v) TritonX-100 in DPBS
Blocking Solution:	5% (v/v) Donkey Serum (DS) in DPBS
mESCs culture medium (15% KO-DMEM):	15% FCS (v/v) 100 U/ml Penicilinin 100 µg/ml Streptomycin 0.1 mM MEM 2 mM L-Glutamin 0.1 mM β-Mercaptoethanol in KO-DMEM
LIF-Culture Medium:	15% KO-DMEM LIF: 1000 - 2000 U/ml
Differentiation Medium (20% IMDM):	20% FCS (v/v) 100 U/ml Penicilinin 100 µg/ml Streptomycin 0.1 mM MEM 2 mM L-Glutamin 0.1 mM β-Mercaptoethanol in IMDM
Freezing Medium:	1:1; 20% DMSO-80% FCS (v/v):15% KO-DMEM
Fixing Solution:	3:1; Methanol: Acetic Acid
1% Gelatin Solution:	100 mg Gelatin 100 ml PBS
Hoechst Solution (1 µg/ml):	1 mg/ml Hoechst 33342 in PBS

	999 ml PBS
0.01 M Sodium citrate buffer (pH 6.0):	2.94 g Sodium Citrate
	1000 ml Pure Water
	pH 6.0 with 1 N HCl
0.01 M Sodium citrate buffer (pH 6.0):	2.94 g Sodium citrate
	1000 ml pure water
	pH 6.0 with 1 N HCl
IMDM and Opti-MEM imaging mediums:	50% rat serum
	1 % Penicillin/Streptomycin
	1% HEPES
	2.5mM $CaCl_2$
4-OHT tamoxifen:	Stock solution: 12.9 mM in methanol
	Working solution: 40 µM
zVAD-fmk:	Stock solution: 20 mM in DMSO
	Working solution: 50µM

2.1.7. Plasmids

Name	**Company**
pBH-UAS-secA5-YFP	Provided by Randall T. Peterson, Harvard Medical School, Massachusetts, USA
CAG-Neo3-eGFP	CLONTECH Laboratories, Inc., USA
CAG-sA5-YFP	Cloned by Kristel Martinez Lagunas (Section 3.1)

2.1.8. Equipment and Materials

Name	**Company**
Analytical balance XS205	Mettler Toledo, Columbus, OH, USA
Balance 440-45	KERN, Balingen, Germany
Cell culture dishes (10 cm)	Greiner Bio-One, Frickenhausen, Germany
Centrifuge 5415D	Eppendorf, Wesseling-Berzdorf, Germany
Centrifuge Multicentrifuge 4KR	Heraeus, Hanau, Germany
Colibri Illumination System	Carl Zeiss, Jena, Germany
Cryo 1°C Freezing Container	Nalgen/Sigma-Aldrich, Steinheim, Germany

Cryostat apparatus (Kryotom CM 3050S)	Leica, Solms, Germany
Cryovials	Nunc A/S, Roskilde, Denmark
Falcon 15 ml tubes	Falcon, Gräfeling-Lochnam, Germany
Falcon 50 mL tubes	Falcon, Gräfeling-Lochnam, Germany
Gel electroporation chambers	BioRAD, Munich, Germany
Gel documentation system	Gel documentation system
GenePulser cuvettes (0.2 cm)	GenePulser cuvettes (0.2 cm)
GenePulser electroporation system	BioRAD, Munich, Germany
Incubator HERAcell 240	Heraeus, Hanau, Germany
KOS Microwave HistoStation	Milestone, Sorisole, Italy
Laser Scanning Microscope Eclipse Ti	Nikon instruments, Düsseldorf, Germany
Macroscope AXIO Zoom V16	Carl Zeiss, Jena, Germany
Microscope Axiovert40CFL	Carl Zeiss, Jena, Germany
Microscope Axiovert200	Carl Zeiss, Jena, Germany
Microscope Observer Z1 with Apotome	Carl Zeiss, Jena, Germany
NanoDrop 100 Spectrophotometer	Peqlab, Erlangen, Germany
Pipettor	Eppendorf, Wesseling-Berzdorf, Germany
Rotorgene-qPCR machine	Corbett/Qiagen, Hilden, Germany
Serological pipettes	Greiner Bio-One, Frickenhausen, Germany
Shaker Excella E24	New Brunswick Scientific, Nürtingen, Germany
Slides for tissue sections	Menzel-Gläser/VWR, Darmstadt, Germany
Sterile bank HERAsafe	Heraeus, Hanau, Germany
Stereomikroskop AxioZoom V16	Carl Zeiss, Oberkochen, Germany
T-flasks - 25 cm^2	BD Biosciences, Heidelberg, Germany
Tissue culture dish vacuum gas plasma	Falcon, Gräfeling-Lochnam, Germany
Tissue pen ImmEdge	PEN Vector Laboratories, Burlingame
Thermocycler TProfessional TRIO	Biometra, Göttingen, Germany
Thoma counting chamber	Marienfeld, Lauda-Königshofen, Germany
24-well glass bottom plate	In Vitro Scientific, Wien, Austria
6- and 24-well cell culture plates	BD Biosciences, Heidelberg, Germany
2-well glass bottom chamber	Ibidi, Martinsried, Germany

2.1.9. Cell lines and biological material

Name	Company
Mach1™-T1R E.Coli cells	Invitrogen/Life Technologies, Darmstadt, Germany (ATCC #9637, S. A. Waksman)
G4 mESCs (SV129;BL/6 background)	Provided by Nagy Lab, Toronto, Canada (110)
Embryonic Fibroblast (PMEF-NL) (Feeder cells)	Millipore, Schwalbach, Germany
cDNA EBs derived from R1- CAG-ChR2-EYFP	Provided by Tobias Bruegmann, Institute of Physiology I, University of Bonn, Germany

2.1.10. Mouse Lines

Name	Company
CAG-sA5-YFP CD1-Tg(CAG-sA5-YFP)KML	Generated by Dr. Michael Hesse and Patricia Freitag from the Institute of Physiology I, University of Bonn via diploid aggregation of CAG-sA5-YFP Clone 27 (described in 2.5.1)

2.1.11. Primary Antibodies

Primary Antibody (Isotype, Dilution, Temperature, Incubation Time)	Company
Anti-Vimentin (Chicken IgGY, 1:800, RT, 2h)	Chemicon, Millipore, Schwalbach, Germany
Anti-α-Actinin (Mouse IgG1, 1:400, RT, 2h)	Sigma-Aldrich, Steinheim, Germany
Anti-MF20-eFluor® 660 (Mouse IgG2b, 1:200, RT, 2h)	eBioscience, Frankfurt am Main, Germany
Anti-α-SMCs (Mouse IgG2b, 1:400, RT, 2h)	Sigma-Aldrich, Steinheim, Germany
Anti-cleaved caspases 3, 7 and 8 (cCasp3-,7-,8) (Rabbit IgG, 1:50 in tissue and 1:200 in mESCs, 4°C, overnight) *Needs Antigen Retrieval treatment	Cell Signaling Technology, Danvers, Massachusetts, USA
Anti-eGFP (Goat IgG, 1:50, 4°C, overnight) *Needs Antigen Retrieval treatment	Santa Cruz Biotechnology, Heidelberg, Germany
Anti-PECAM (Rat IgG2a, 1:800, RT, 2h)	Becton Dickinson, Heidelberg, Germany

Anti-CD45 (Rat IgG, 1:800, RT, 2h)	Chemicon, Millipore, Schwalbach, Germany
Anti-human Annexin V (Mouse IgG1, 1:50, 4°C, overnight) *Needs Antigen Retrieval treatment	Abcam, Cambridge, United Kingdom

2.1.12. Secondary antibodies

All secondary antibodies were ordered from Jackson ImmunoResearch, Suffolk, England:

Secondary antibody-Fluorochrome (Isotype, Dilution)

Anti-chicken-Cy5 (Donkey IgGY, 1:400)

Anti-goat IgG-Cy3 (Donkey IgG, 1:400)

Anti-mouse-Cy5 (Donkey IgG1, 1:400)

Anti-rabbit-Cy5 (Donkey IgG, 1:400)

Anti-rat-Cy5 (Donkey IgG, 1:400)

2.2. Molecular Biology Methods

2.2.1. Restriction enzyme reaction

This basic cloning technique was used in several steps (linearization of DNA, cleavage of double DNA strands at specific nucleotide sites of target vectors and to identify correct product orientation of recombinant DNA) of the cloning strategy to create the CAG-sA5-YFP construct. The method uses restriction enzymes also called endonucleases, which are able to cut the phosphodiester bonds between nucleotides. There are two types of restriction enzymes: blunt end cutters, which cleave double-stranded DNA at the same spot leaving blunt ends, and sticky end cutters, which cleave at different spots resulting in 3'- or 5'-overhangs or sticky ends (111). The general procedure to carry out the restrictions consisted of the reaction mix protocol (Table 1) followed by the Klenow Fragment of the DNA-Polymerase I reaction (Table 2) in order to fill-in nucleotides at 5’-overhangs strands to get blunt ends when needed. Afterward, the cut DNA plasmid was purified by using the QIAquick® PCR Purification Kit (112). If needed, another enzyme cut was run after DNA purification. To finish, before ligation it was necessary to remove 5’- or 3’-phosphate groups of the cut vectors by using the Calf Intestine Alkaline Phosphatase (CIAP) reaction (Table 3) in order to avoid re-ligation.

Table 1. Restriction enzyme reaction protocol

Component	Volume (per 30 µl)
Buffer (10x)	3 µl
DNA (5 – 10 µg)	x µl
Enzyme (10 U/µl)	2.5 µl
Pure water	Add up to 30 µl
Reaction temperature (°C) and time (h)	37 °C, 1 h *Enzyme specific
Inactivation temperature and time	65 or 80 °C, 20 min *Enzyme specific

Table 2. Nucleotide Fill-in: Klenow Fragment reaction protocol

Component	Volume (per 40 µl)
Klenow Buffer (10x)	4 µL
DNA solution	30 µl
dNTPs (2 mM)	2 µl
Klenow Fragment (10 U/µl)	2
Pure water	Add up to 40 µl
Reaction temperature (°C) and time (h)	37 °C, 0.5 h *Enzyme specific
Inactivation temperature and time	75 °C, 10 min *Enzyme specific

Table 3. CIAP: DNA dephosphorilation protocol

Component	Volume (per 40 µl)
DNA solution	30 µl
CIAP (1 U/µL)	1 µL
Reaction temperature (°C) and time (h)	37 °C, 1 h
Inactivation temperature and time	85 °C, 15 min

2.2.2. Analysis of DNA fragments by gel electrophoresis

To evaluate if the desired DNA fragment sizes were obtained after a restriction reaction, a gel electrophoresis was run. This is a basic method to separate nucleic acids or proteins based on their size and charge, in which the macromolecules move through an agarose gel under the influence of an electrical field (13). Briefly, the DNA samples (approximately 20 µl each) were mixed with 4 µl 6x loading buffer and they were loaded on a polymerized 1% agarose-ethidium bromide (EtBr) gel (1 g agarose in 100 ml of 1x TAE-Buffer and 6 µl EtBr). The gel was submerged into a 1x TAE buffer containing chamber and run for 45 min at 90-110 Volts (5-8 V per cm of gel). As each DNA nucleotide has a negative charge, the DNA moved towards the positive field. The smallest and linear fragments run fastest. Afterward, the gel was analyzed under UV light to expose DNA bands tagged with EtBr. In order to identify band sizes, 5 µl of a ready to use 1 kb DNA ladder was loaded onto the gel.

2.2.3. DNA gel extraction

This procedure was used to purify the desired DNA fragment bands from an agarose gel. For this purpose, the QIAquick Gel Extraction Kit (112) was used. Using this kit different impurities (i.e. nucleotides, enzymes, salts, agarose or EtBr) were removed from the DNA to get efficient ligation or a reliable sequencing. Briefly, after the restriction reaction, 15 µl of DNA solution were loaded on a 1% agarose gel and the gel was run as previously described; the desired DNA bands were cut out using a scalpel and they were weighed using an analytical balance in grams scale. Generally, 200 mg of gel bands were dissolved in 600 µl of QG buffer. Afterward the bind-wash-elute procedure from the kit was followed. Finally, the DNA was eluted with 30 µL pure water.

2.2.4. Plasmid Ligation

A ligation reaction is the formation of a covalent bond between 2 DNA fragments, normally the gene of interest and the plasmid vector. This reaction is carried out by the T4 DNA ligase, which has the ability to bind both sticky and blunt ended fragments by catalyzing the formation of phosphodiester bonds between phosphate and sugar groups of DNA strand (113). The ligation reaction consisted of insert, vector, T4 ligase and enzyme buffer containing adenosine triphosphate (ATP) that served as a cofactor (Table 4); the reaction was carried out at 16°C overnight. Two control ligation reactions were run in parallel: DNA of the vector alone with ligase and both DNA, vector, and fragment, but without ligase. The ratio relation between insert and vector was calculated with the following formula assuring not to exceed 300 ng of total DNA using a 3:1 ratio:

$$DNA\ fragment\ mass\ (ng) = 3 * \left(\frac{Number\ of\ base\ pairs\ of\ fragment * vector\ mass\ (ng)}{Number\ of\ baise\ pairs\ of\ vector}\right)$$

Table 4. Ligation reaction

Component	Volume (per 20 µl)
DNA Vector	x µl
DNA Fragment	x µl
T4 Ligase (1 U/µl)	1 µl
Ligase Buffer (10x)	2 µl
Pure water	Add up to 20 µl
Reaction temperature (°C) and time (h)	16 °C, overnight
Inactivation temperature and time	65 °C, 10 min

At the next day, 5 µL of the ligation solution were analyzed via gel electrophoresis to verify that the DNA band of the new product was larger than that of the vector alone and of the ligation reaction without ligase. Furthermore, approximately one-third of ligation solution was used to transform chemical competent bacteria (see method 2.2.5), which later were seeded in Kanamycin LB-Agar plates. As in blond-end ligations is likely that the recombinant colonies have inserts incorporated in the wrong orientation, the resistant clones had to be further analyzed (see method 2.2.6).

2.2.5. Transformation of plasmid DNA in chemical competent Bacteria

In order to replicate the cloned plasmid DNA, it was introduced into the chemically competent Mach1™-T1R E.Coli cells by applying a heat shock. Briefly, 50 µl of Mach1 bacteria were thawed on ice, then, up to 100 ng of the DNA ligation solution was added and incubated for 30 min on ice; in this step, the plasmid was taken up by the bacteria. Afterward, the transformed bacteria were exposed to a heat shock at 42°C for 45 s; this served to close the bacteria cell's wall. Next, 250 µL of SOB medium were added followed by an incubation at 37°C for 1 h with shaking (400 rpm). After that, they were plated on kanamycin (1:1000)-containing LB agar plates overnight at 37°C and in this way for selection. For amplification of plasmid-DNA, single colonies were picked and were grown in 5 ml kanamycin (1:1000)-LB medium at 37°C on a shaker at 220 rpm for 8-16 h.

2.2.6. Isolation of plasmid DNA from bacteria cultures (Miniprep)

The QIAprep Spin Miniprep Kit was used to isolate plasmid DNA from bacteria cultures at small scale. The kit is based on a silica matrix spin-column to which DNA strongly binds in the presence of high concentration of chaotropic salts and which can later be eluted using low-salt buffer. Briefly, 2 ml of bacteria culture were centrifuged for 5 min at 9000 x g at RT

followed by binding-washing-eluting steps as stated by the Kits instructions (114). In the final step, the isolated DNA pellet was resuspended in 30 µl of pure water. Afterward, the recombinant DNA was ready to be analyzed by restriction enzyme digestion and gel electrophoresis to verify the inserts correct size and orientation.

2.2.7. Isolation of endotoxin-free plasmid DNA from bacteria cultures (Midiprep)

Using the EndoFree® Plasmid Purification Kit DNA from bacteria clones containing the correct plasmid was amplified and purified to an endotoxin-free grade. This improves transfection efficiency as well as avoids unspecific immune responses after application in mouse models due to the effect of endotoxins, which are cell membrane components of Gram-negative bacteria (115). The EndoFree purification protocol is based on a modified alkaline lysis procedure, followed by a strong binding of plasmid DNA to a Qiagen anion-exchange resin, as well as by washing and eluting steps. The purification was carried out following the Kit's instructions (116). Shortly, 100 ml of kanamycin-LB medium were inoculated with 100 µl of previously selected starter bacteria culture, these were incubated at 37°C, at 500 rpm overnight and they were centrifuged at 6000 x g for 15 min at 4°C. Afterwards, the lysate buffers were added, followed by a washing step to remove endotoxins. Next, the DNA was bound to the resin, further washed and eluted. Finally, the purified DNA was resuspended in 50 µl of the endotoxin-free buffer. Endotoxin-free plasmid DNA was sequenced and later transfected into mouse embryonic stem cells (mESCs) (see methods 2.2.8, 2.2.9).

2.2.8. Plasmid DNA sequencing

The desired plasmid DNA was sequenced by Eurofins MWG Operon (Ebersberg). For sequencing 20 µl samples consisting of a mixture of plasmid DNA (100 ng/µl), primers (15 pmol) and pure water were sent to this company.

2.2.9. Transfection of plasmid DNA in mESCs

In order to analyze the gene expression of the cloned plasmid, the desired foreign DNA was introduced into mESCs by electroporation. This method is based on the use of high-voltage electric fields that open temporarily the pores of cell membranes allowing non-polar molecules such as foreign DNA to enter the cell (117).

In order to generate a stable transfection, 20 µg of linearized plasmid DNA plus 5 x 10^6 wild type G4 mESCs were used. Briefly, DNA was linearized using a one-site-cutter restriction

enzyme. Afterward, G4 mESCs were cultured for two days and were trypsinized at 75% confluence (see method 2.3.1). 5 x 10^6 cells were resuspended in 5 ml of 15% KO-DMEM medium and seeded in 10 cm dishes pre-coated with 1% gelatin solution to remove feeder cells (inactivated fibroblasts) for 10 min at RT. Later, the medium containing the mESCs was collected from the dish, transferred to a 15 ml reaction tube and centrifuged at 5000 rpm for 5 min. The pellet was resuspended in 800 µl ice cold-PBS containing 20 µg of linearized plasmid DNA and transferred into a 2 mm electroporation cuvette. The cell suspension was then subjected to an electric pulse of 250 V (Volts), 500 µF (micro Farad) using the GenePulser electroporation system from Biorad followed by incubation on ice for 15 min. Finally, 2.5 x 10^6 cells were seeded on 10 cm dishes pre-coated with feeder cells containing 10 ml of 15% KO-DMEM and 1000 U/ml of LIF to maintain the cells in a non-differentiation state. Cells were incubated at 37°C for 24 h followed by media change. After 48 h of incubation, the cells were selected with 175 µg/ml Geneticin Sulfate G418 for 8 days. Surviving clones expressing the neomycin resistant gene were picked by using a microscope and were further expanded.

2.2.10. RNA isolation from mammalian cells

To be able to analyze the relative expression of the gene of interest in transfected mammalian cells, RNA of these cells was isolated using the TRIzol® Reagent protocol under RNase-free conditions. This method is based on layers separation. Following the manufacturer instructions, 1 ml of Trizol reagent was added to approximately 5 x 10^5 adherent cells, which were homogenized by pipetting up and down 5 times. After addition of chloroform, three separate layers formed. The first upper layer was a clear aqueous phase containing the RNA, followed by an interphase and a red organic layer containing DNA and proteins. Next, RNA was precipitated from the carefully extracted aqueous layer by addition of isopropanol and it was centrifuged at 12,000 × g for 10 minutes at 4°C. The RNA pellet was washed with ethanol and vortexed for 5 min followed by centrifugation at 7,500 × g for 5 min at 4°C. The washed RNA pellet was then resuspended in 50 µl RNase-free water. RNA samples were analyzed by agarose gel electrophoresis (1% agarose gel) using 1x MOPS-buffer to verify its quality. Approximately 200 ng of RNA were mixed with RNA-Loading buffer; samples were loaded and the gel was run at 80 V for 15 min. The RNA integrity was evaluated as intact when the 28S and 18S RNA subunits bands were clearly visible, without smearing.

2.2.11. Reverse transcription of RNA to cDNA

In order to be able to measure relative gene expression by real-time quantitative reverse transcription PCR (RT-qPCR) (method 2.2.12), it was first necessary to perform a reverse transcription from isolated RNA to complementary DNA using a reverse transcriptase (RT). For that, the SuperScript VILO cDNA Synthesis Kit was used. A reaction mix for each sample was prepared as shown in Table 5. The obtained cDNA was then used as the template for the qPCR reaction.

Table 5. Reverse transcription reaction

Component	Volume (per 20 µl)
Reaction mix (5x) (buffer, dNTPs, SuperScript III RT)	4 µl
Enzyme mix (10x)	2 µl
RNA (200 ng)	x µl
RNase-free water	Add up to 20 µl
Reaction temperature (°C) and time (h)	25°C for 10 min and 60 min at 60°C
Inactivation temperature and time	85 °C, 5 min

2.2.12. Relative expression analysis via RT-qPCR

By using RT-qPCR it was possible to assess the amount of mRNA expressed by transgenic cells and to analyze how many copies of the transgenic DNA were integrated into their genome. This method measures the increase in fluorescence during the amplification reaction. The starting template can be either cDNA or genomic DNA (gDNA) which is labeled by a TaqMan probe, which binds specifically to the desired DNA sequence. The probe contains a reporter molecule at its 5' end, a quencher at the 3' end and gene-specific set of primers. Trough FRET (Fluorescence Resonance Energy Transfer) the reporter molecule transfers its fluorescence energy to the quencher whenever the probe is intact and they are in a close proximity, but when they bind the cDNA strand, they are separated due to the 5'-exonuclease activity of the Taq-polymerase and the reporter fluorescence is no longer quenched. This fluorescence intensity is directly proportional to the number of PCR product molecules (amplicons) generated (118).

In order to detect the relative expression of the YFP transgene, a TaqMan probe against eGFP containing the carboxyfluorescein (FAM) reporter was used which was measured in the green channel. YFP and eGFP protein sequences only differ in the amino acid Thr-203, a Tyrosine

mutation that results in approximately 20 nm shift to longer wavelengths for both the excitation and emission spectra (119). Therefore, it was assumed that YFP sequence could be detected by an eGFP probe. In order to verify this fact, cDNA of an eYFP expressing cell line was used as a positive control. The results were normalized to the housekeeping gene 18S rRNA fused to VIC reporter (yellow channel). When copy number analysis was performed, the samples were normalized to an endogenous reference gene, known to be present in two copies in a diploid genome such as the transferrin receptor gene (TFRC). The qPCR reactions were prepared in triplicates as follows (Table 6):

Table 6. qPCR reaction setup

Component	Volume (per 20 µl)
TaqMan Master Mix (2x)	10 µl
TaqMan probe (20x) Diluted 1:3	4 µl
cDNA (~100 ng) or gDNA (50 ng/ µl)	4 µl
Pure water	2 µl

The samples were pipetted in a 72 sample disc and were run in the Rotorgene-qPCR machine using the following two-step qPCR protocol Table 7:

Table 7. qPCR protocol

Step	Temperature	Time	
Initial denaturation	95 °C	10 min	
Denaturation	95 °C	10 s	**40 cycles**
Primer hybridization and elongation	60 °C	45 s	
	4 °C	hold	

The relative transgene mRNA expression was calculated with the ΔCt-method (120) as follows:

$$\text{Relative expression} = 2^{-(\text{Ct of gene of interest (eGFP)-Ct of reference gene (18s sample)})}$$

In order to be able to compare different qPCR runs it was important to always assume the same threshold for Cts and to have the same control in each run. The Ct value threshold was set to 0.022 in relation to the 18S reference samples in the exponential phase of the qPCR.

2.2.13. Genotyping by PCR

The polymerase chain reaction (PCR) was used to detect the transgene of interest in the genome of transgenic sA5-YFP mice. This method has been described in 1986 by Mullis and coworkers (121). Using this method it was possible to amplify specific DNA fragments and later to verify them in an agarose gel electrophoresis if the desired fragment size was present. The starting template can be gDNA, cDNA or plasmid DNA. Specific oligonucleotide primers (Sec Signal_Fw and YFP PolyA_Rev; see sequences at section 2.1.4) were designed to bind complementary CAG-sA5-YFP DNA sequences. Primers act as starter strands for the amplification. In order to determine the genotype of the generated sA5-YFP mice, 5 mm tail tissue samples were taken. From these, gDNA was isolated following the instructions of Gentra Puregene Mouse Tail Kit (122). The PCR mix was prepared for each sample as indicated in Table 8 and the PCR was run in a Thermocycler using the protocol from Table 9:

Table 8. PCR reaction

Component	Volume (per 20 µl)
gDNA (300ng)	x µl
Buffer i (2X)	10 µl
Enhancer (5X)	4 µl
dNTPs (10 µM)	1 µl
Sec Signal_Fw (10 µM)	3 µl
YFP PolyA_Rev (10 µM)	3 µl
Taq Polymerase	0.25 µl

Table 9. PCR protocol

Step	Temperature	Time	
Initial denaturation	95 °C	4 min	
Denaturation	94 °C	45 s	**29 cycles**
Annealing	65 °C	45 s	
Extension	72 °C	1 min	
Final Extension	72 °C	10 min	
	4 °C	hold	

2.2.14. Apoptosis induction in sA5-YFP mESCs by 4-Hydroxytamoxifen (4-OHT) and DMSO.

It is known that tamoxifen induces apoptosis in breast cancer cells through the activation of both intrinsic and extrinsic apoptosis pathways (123). Its derivative 4-hydroxytamoxifen (4-OHT) has 50 to 100 fold higher affinity than tamoxifen to estrogen receptors and therefore greater potency to induce apoptosis (124). In this work 4-OHT compound was used to induce apoptosis in mESCs. It has been reported that a concentration of 40 μM tamoxifen caused the highest caspase activity in human hepatocellular carcinoma cells after 4 hours of addition (125). Therefore, this concentration of 4-OHT was tested in mESCs and it was concluded that it induced cell death after a 3 h incubation based on blebs formation, rounding up of the cells and caspase-3 activation. Thus, this concentration was used in all the *in vitro* experiments to induce apoptosis.

Another reagent used to induce apoptosis in this work was dimethyl sulfoxide (DMSO). It has been shown that a concentration of 1% or more DMSO induces apoptosis in a wide variety of cells, mainly through the intrinsic pathway (mitochondria) via activation of cCasp9 and cCasp3, both in vitro and in vivo (126). Therefore, 1% DMSO was used to assure induction of apoptosis in mESCs.

2.3 Cell Culture Methods

2.3.1. Thawing, Culture and Freezing mESCs

Transgenic and wild-type G4 mESCs stored in nitrogen tanks were briefly thawed at 37 °C in a water bath. In order to avoid cell damage caused by DMSO, which is contained in the freezing medium, the cell suspension was resuspended in 5 ml culture medium (15% KO-DMEM) followed by centrifugation at 1500 x g for 5 min. The pellet was resuspended in 1 ml of LIF-culture media (15% KO-DEMEM-1000 U/ml LIF). Approximately 5 x 10^5 cells were seeded in 25 cm^2 T-flasks containing either 1.3 x 10^6 feeder cells or coated with 0.1% gelatin solution. It was important to double the amount of LIF (2000 U/ml) when the cells were seeded on gelatin coated flasks to avoid differentiation. At the following day, the medium was changed.

In order to expand and culture the cells, they were passaged when reaching approximately 70% confluency (every 2^{nd} or 3^{rd} day). For that, cells were washed with PBS and trypsinized with 1 ml of 0.5% Trypsin/EDTA, a proteolytic agent which cleaves proteins chains at the

amino acids Arginine or Lysine. The trypsin reaction was stopped with 5 ml culture medium. Afterwards, the cell solution was centrifuged at 1500 x g for 5 min and the pellet was resuspended in 1 ml LIF culture medium. Cells were counted using a Thoma-cell chamber and approximately 150,000 cells were further seeded in 25 cm^2 flasks with either feeder cells or gelatin-coated containing 5 ml of LIF culture medium and incubated at 37°C, 5% CO_2 and 96% humidity. The rest of the cells (0.5 – 1 x 10^6 cells) were resuspended in 1 ml freezing medium (1:1; 20% DMSO (v/v) in Fetal Calf Serum (FCS):15% KO-DMEM) and stored in cryovials. The vials were first stored in cryo-chambers containing isopropanol at -80°C, this allows to get a slow freezing (- 1°C/h), this avoiding crystal formation due to the DMSO. After 2 days, vials were stored in a liquid nitrogen tank.

2.3.2. Differentiation of mESCs: Embryoid Bodies formation

ESCs maintain their undifferentiated state when they are grown in co-culture with feeder cells or in presence of LIF or both, however, when they are cultured in suspension in absence of these components, ESCs differentiate spontaneously by forming three-dimensional multicellular aggregates called Embryoid Bodies (EBs) (127). EBs are able to differentiate into derivatives of all three germ layers (128) giving rise to more specialized cells such as cardiomyocytes. The differentiation of transgenic and wild-type mESCs was carried out by mass culture also known as a liquid suspension culture (Fig. 13). This method facilitates the differentiation of mESCs into cardiomycytes (129). Briefly, approximately mESCs grown in feeder cells were trypsinized as described in method 2.2.1. Afterwards, these cells were re-suspended in 10 ml differentiation medium (20% IMDM without LIF) and seeded in 10 cm adherent cell culture dishes to allow feeder cells to attach for 20 min. Afterwards, the feeder cells remained attached and the mESCs suspension was transferred to a 15 ml reaction tube to determine the number of viable cells. To generate EBs, 2 x 10^6 mESCs were transferred into 10 ml of differentiation medium in 10 cm^2 bacterial-grade (non-adherent) culture dishes and incubated at 37°C, 5% CO_2 on a horizontal shaker at 70 rpm. This day was defined as day 0 of differentiation. After 2 days of differentiation, the EB number was determined by transferring the EBs solution into a 15ml tube to allow the EBs to sink down for 5 min. Then, the medium was aspirated leaving 1 ml medium. The number of EBs was counted from 2 drops of 5 µl of EBs solution. 750 EBs were seeded in five 10 cm^2 bacterial-grade culture dishes containing 10 ml differentiation medium which were incubated at 37°C, 5% CO_2 on a horizontal shaker at 70 rpm for 5 more days. After this time, the first medium change was

performed. At day 7 of differentiation, the EBs started beating and at day 11 of differentiation, they were fixed and further analyzed.

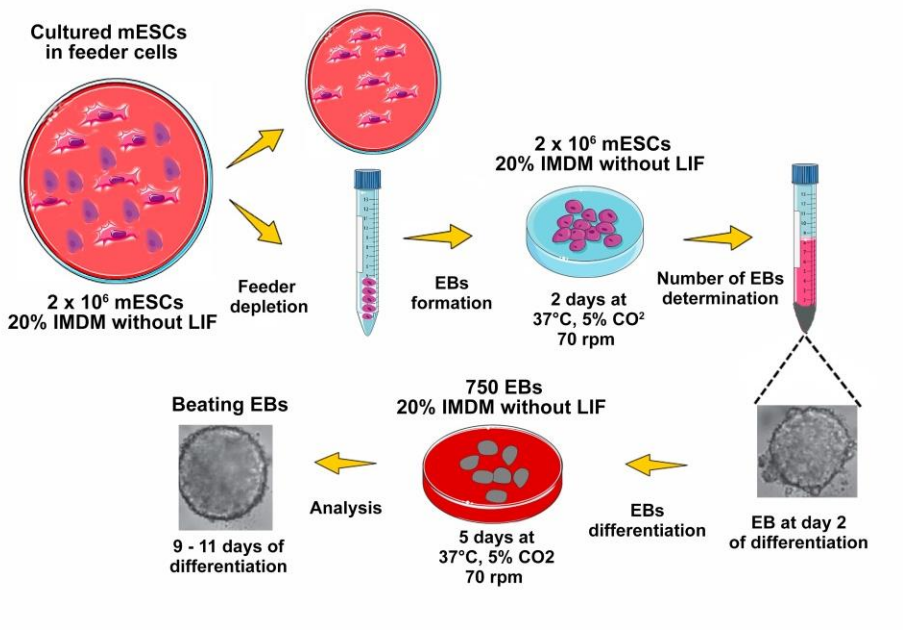

Fig. 13. Scheme of ESCs differentiation to embryoid bodies by mass culture.

Mouse embryonic stem cells (mESCS) were differentiated to embryoid bodies (EBs) using the mass culture or liquid suspension protocol. (This scheme was created using and modifying images and clipart from (128, 130)).

2.3.3. Karyotyping of transgenic mESCs clones

In order to determine the number of chromosomes in the CAG-sA5-YFP mESCs clones, a metaphase chromosome spread preparation was performed. For that, mESCs at 70% confluency in a 25 cm^2 flask were incubated for 3 h with 5 ml culture medium and Demecolcine (0.1 µg/ml) in order to arrest the cells in metaphase. After this time, the cells were trypsinized as in method 2.2.1. Cells were centrifuged and the pellet was resuspended in 5 ml of 75 mM Calcium-Chloride (KCl) solution followed by 15 min incubation at RT. Subsequently, cells were centrifuged for 5 min at 210 x g and the pellet was fixed with 1 ml ice-cold fixing solution (3:1; methanol: acetic acid) for 30 min at RT. Then, it was gently resuspended and 0.5 ml of the fixed cell suspension were taken with a Pasteur-pipette and approximately 100 µl drops were dropped from a height of 50 cm onto slides previously washed with ice-cold ethanol. Then, the slides were shortly dried and later they were submerged in 1 µg V/ V of Hoechst solution in order to stain the chromosomes. Finally, the slides were washed twice with PBS and mounted with mounting medium (FLUKA). At the following day, fluorescent pictures of chromosomes were taken using the fluorescent microscope Axiovert 200M and the DAPI filter set at 40x magnification. At least 30 spreads

were counted for each clone and if more than 70% of the spreads contained 40 chromosomes the clone was considered for generation of a transgenic mouse line.

2.3.4. Caspase Inhibition by zVAD-fmk

In order to inhibit the activity of caspases in the mESCs, the pan-caspase inhibitor zVAD-fmk was used. Briefly, 3 x 10^4 transgenic mESCs per well were seeded in 24 well glass bottom plates. When cells were at approximately 70% confluency, 50 µM of zVAD-fmk were added 2 hours before cell death induction. Cell death was then induced with 1% DMSO. After 24h, cells were fixed and stained against cCasp3.

2.3.5. Long-term observation of apoptotic mESCs

Transgenic and non-transgenic mESCs were grown on gelatin-coated 24-well plates under culture conditions described in method 2.2.1. After 2 days in culture and approximately at 60% confluency, cells were treated with 40 µM 4-OHT for 24 h and non-transgenic cells were treated with 1 µM Annexin V-FITC for 30 min at 37°C before tamoxifen addition. Next, images were taken with the fluorescence microscope Observer Z1, the Colibri Illumination System (blue and white LED), the 20x air-objective, the transmission light and GFP filters at 37°C and 5% CO_2. Using the ZEN 2 Blue Edition Software, a long-term program was set up to take serial pictures every 5 min for 24 h.

2.3.6. Fluorescence measurements in mESCs using Image J software

Transgenic sA5-YFP mESCs either induced or non-induced with 4-OHT for 24 h, were first fixed with 4% Paraformaldehyde (PFA) containing 2.5 mM $CaCl_2$ (PFA solution) for 20 min at RT, stained for cCasp3 (see method 2.3.1) and imaged using a fluorescence microscope (Observer Z1, ZEN 2 Blue Edition Software). Pictures of at least 4-6 areas of 3 different wells of transgenic induced, transgenic non-induced and wild-type induced cells were taken. Mean fluorescence intensity of each area in the green channel was quantified using the tool "Integrated density measurements" from the image analysis software "Image J", version 1.37A. Sample's total fluorescence was calculated by deducting sample's fluorescence from background's fluorescence. 2 different experiments were run and statistical analysis (Student's t-test) was performed.

2.4 Immunohistochemistry Methods

2.4.1. Immunostainings in mESCs

Transgenic and non-transgenic mESCs were shortly washed with a washing solution and fixed at RT with fixing solution for 30 min. The addition of calcium to all solutions and mediums was important to ensure the binding of Annexin V to PS when apoptosis induction experiments were carried out. After fixation, the fixing solution was removed and cells were washed two times with DPBS. For the immunostainings, cells were permeabilized at RT with permeabilization solution for 10 min. In order to avoid unspecific staining, cells were blocked at RT with blocking solution for 20 min. After a quick washing step with DPBS, primary antibodies (see dilutions in section 2.1.11) were diluted in blocking solution and added to the cells. Afterwards, cells were incubated at 4°C overnight or 2 h at RT, depending on the antibody (specified in section 2.1.11). After three washing steps with DPBS, cells were incubated at RT for 1h with specific secondary antibodies (see dilutions in section 2.1.12), which were diluted in Hoechst solution. The cells were shortly washed with washing solution, mounted with 1 drop of mounting medium and coverslips, stored at RT to let them dry overnight and stored at 4°C in darkness until their analysis.

2.4.2 Immunostainings in EBs and embryonic tissue sections

Transgenic and non-transgenic EBs, embryos and embryonic hearts were fixed overnight in fixing solution. Then they were washed twice with washing solution followed by incubation at 4°C in sucrose solution overnight. Tissue was frozen in Tissue-TEK O.C.T compound using isopentanol and dried ice. Afterward, 10 µm tissue sections were cut with a Cryostat device. For some antibodies (specified in section 2.1.11) it was necessary to perform antigen retrieval (AR) (high-temperature heating treatment) to be able to disrupt cross-links between formalin and protein enabling epitope detection. It is known that formalin fixation causes protein's structure modifications hiding antigen sites (131). Therefore, sections were pre-treated with 0.01 M sodium citrate buffer (pH 6.0) for 15 min at 93°C using a Microwave HistoStation. After heating, sections were allowed to cool at RT for 15 min. After AR the native YFP signal was lost, therefore it was necessary to stain the tissue against YFP together with the other primary antibodies. After AR, tissue sections were permeabilized, blocked, stained, mounted and stored in the same way as described in section 2.4.1.

For the detection of late apoptotic cells, the *In Situ* Cell Death, fluorescein Detection Kit from Roche was used. This method is based on the detection of DNA strand breaks by labeling of

free 3’-OH termini using the terminal deoxynucleotidyl transferase (TdT), which catalyzes polymerization of labeled nucleotides to free 3’-OH ends (TUNEL reaction). Briefly, TUNEL positive (sections treated with 3000 u/ml DNaseI for 5 min at RT) and negative controls (sections incubated with Kit´s Labeling solution) were prepared. Later, sample sections were washed twice with DPBS and they were treated with the Kits' TUNEL reaction mix followed by incubation for 1h at 37°C in a humidified space. Finally, slides were quickly washed with DPBS and mounted. The detection of apoptotic cells was analyzed under a fluorescence microscope using FITC and Cy3 filter sets.

2.5. Animal experiments

2.5.1. Generation of the CAG-sA5-YFP mouse line

The transgenic CAG-sA5-YFP mouse line, which official name is CD1-Tg(CAG-sA5-YFP)KML according to the International Committee on Standardized Genetic Nomenclature for Mice, was generated from the CAG-sA5-YFP mESCs line by complementation assays with diploid embryos from wild-type CD1 mice (132) (the aggregation was kindly performed by Dr. Michael Hesse and Patricia Freitag from the Institute of Physiology I, University of Bonn).

Briefly, 3 days before aggregation, clones 27 and 28 from the CAG-sA5-YFP mESCs were thawed and cultured 25 cm^2 flasks with feeder cells as described in method 2.2.1. At the following day, the medium was changed. When the cells were at ~70% confluency they were trypsinized the same way as performing a passage. After stopping the trypsin reaction with medium, approximately 10 ml of the cell suspension were left for 10 min in a 0.1% gelatin coated 6 cm^2 cell culture dish to remove feeder cells. Afterwards, different dilutions (1:12.5, 1:25, 1: 50, 1:100 and 1:200) of the mESCs were prepared in culture medium containing 2000 U/ml LIF. These were then seeded on 0.1% gelatin coated 6 cm^2 culture dishes containing 6 ml LIF-culture medium. Cells were incubated at 37°C and 5% for 24 h on the day before aggregation. For aggregation with diploid embryos, the protocol described by Takanaka and coworkers was followed in which clumps of approximately 6 -10 ESCs were aggregated with previously prepared zona pellucida-free embryos flushed from oviducts 2.5 days post coitum (dpc) from pregnant mice. One day after aggregation, embryos in blastocyst stage (3.5 dpc) were transferred to pseudopregnant CD1 recipient females. After approximately one month, the first germline transmission chimera embryos were analyzed under fluorescence

macroscope to make the first evaluation of YFP expression. Afterward, chimera offspring was genotype and analyzed by PCR (method 2.1.13.).

2.5.2. Isolation of mouse embryos and embryonic hearts

Embryos at different embryonic stage (E9.5 - P2) were taken out from pregnant mice at the respective day. The day of embryonic development was determined by counting the day of the vaginal plug as day 0.5. The pregnant mice were killed by cervical dislocation and the embryos were dissected and then placed in ice-cold PBS containing $CaCl_2$. The placenta and in some cases also the yolk sac were removed. As fast as possible, embryos were scanned under a fluorescent macroscope to distinguish transgenic and wild-type embryos. Immediately after, embryos were fixed in fixing solution for 2-4 h; they were quickly washed and incubated in sucrose solution for 24 h.

For the isolation of embryonic hearts (E11.5-P2), embryos' head was removed, the thorax was opened and the heart was taken out with small forceps. All connective tissue was removed and hearts were then fixed in the same way as the isolated embryos.

2.6. Preparation, *ex-vivo* culture and live imaging of A5-YFP embryos and hearts at E8.75-9.5

Pregnant mice were killed by cervical dislocation at day 8.75 - 9.5 postcoitum. The uterus was dissected and immersed in 37°C warm IMDM or Opti-MEM culture medium and embryos removed from the uterus and yolk sac under a stereomicroscope. Embryos were scanned under a fluorescent microscope to select for sA5-YFP expression and heart beating. Approximately 500 µl of 2% low-melting agarose were poured into an imaging chamber with glass bottom. Holes were dug into the agarose before embryo dissection. Selected embryos were placed in the agarose holes and the imaging chamber was filled with IMDM imaging medium. These culture conditions were used to document massive apoptosis in E8.75 embryos as a proof of concept of the system. Later, I change the following culture conditions: embryos were immersed directly in liquid 2% low-melting agarose and hold into the desired position until the agarose polymerized. The chamber was filled with Opti-MEM imaging medium. For the live imaging, the chamber was positioned into an inverted confocal microscope live imaging system and incubated at 37°C and 5% CO_2. Whole body or the heart of transgenic sA5-FYP embryos was imaged for 15 to 20 h. Pictures were taken every 5 - 10 min using a 10x air objective. YFP was excited by a 515 ± 30 nm laser (8-15% power) and a

595 ± 50 nm laser (8-15% power) was used to excite autofluorescence. The transmission light source was simultaneously used. Z-stack slices depth was defined between 4-6 µm, depending on the experiment (Fig. 14).

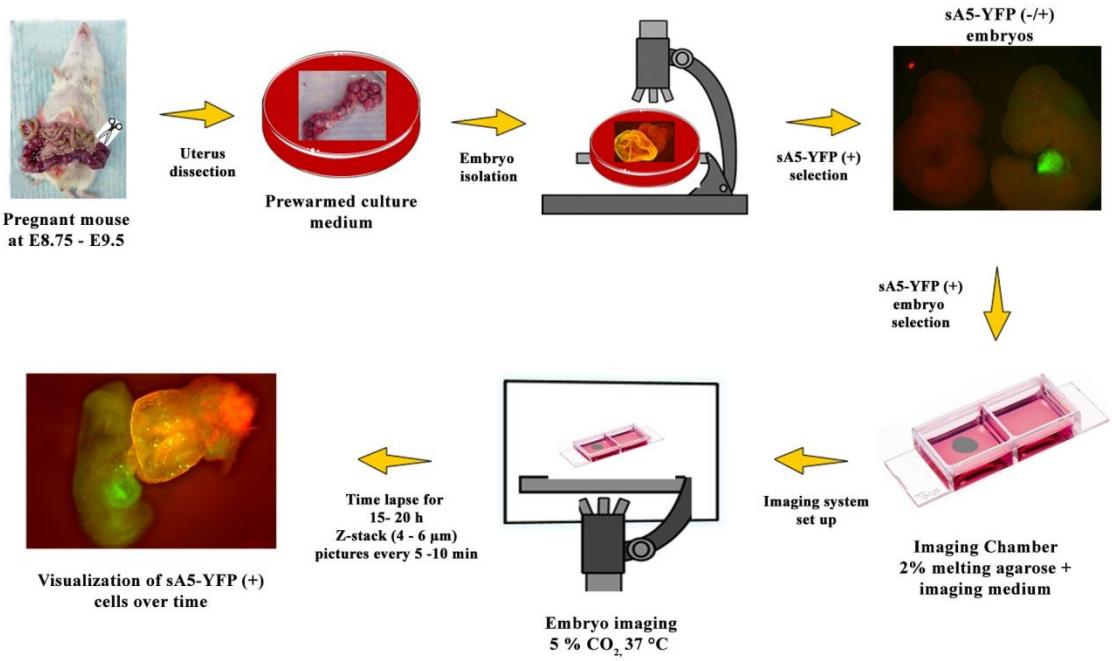

Fig. 14. Scheme of the live-imaging setup for monitoring apoptosis in sA5-YFP embryos.

sA5-YFP embryos were isolated and imaged using the depicted imaging set up. (This scheme was created using and modifying images and clipart from (130, 133-136)). Fluorescent images of E8.5-9.5 sA5-YFP embryos were generated in this work.

3. RESULTS

3.1. Generation of a CAG-sA5-YFP expression cassette

As mentioned in section 1.5, the main goal of this PhD thesis is to generate a straightforward genetic tool for the identification of apoptotic cells in the developing mouse heart *in vivo*. For that, the first step was to create via molecular cloning the desired plasmid cassette that contains the ubiquitous promoter, CAG, and our gene of interest, sA5-YFP (see Fig. 15). The CAG (chicken β-actin promoter with CMV enhancer) promoter has been proven to drive expression of transgenes in all types of mammalian cells, with predominant expression in muscle cells during all stages of development (137-140).

The CAG-sA5-YFP construct (6995bp) was generated using the pBH-UAS-secA5-YFP vector (provided by Randall T. Peterson, Harvard Medical School, Massachusetts, USA) and the CAG-Neo3-eGFP (CLONTECH Laboratories, Inc.) vector. The first vector was cut with the restriction enzyme SacII, its ends were modified with Klenow-Fragment leaving a blunt end and it was further cut with BamHI. The vector was then analyzed by gel electrophoresis. Three DNA fragments (3692, 3569 and 1892 bp) were obtained. The 1892 bp fragment was removed from the gel and it was ligated to the 5109 bp fragment obtained by cutting the CAG-Neo3-eGFP vector with the restriction enzymes NotI and BamH1. The ligation resulted in a 6995 bp product named CAG-sA5-YFP (Fig. 15A). Afterward, this plasmid was transformed into chemical competent MACH-1 E.coli cells and clones were selected on LB-Agar plates with Ampicillin. On the following day, 6 resistant clones were isolated and amplified in LB suspension culture. The correct orientation of the CAG-sA5-YFP construct was verified by cutting the plasmid with the restriction enzyme HincII. Four clones out of six showed the expected band sizes, 5267 bp and 1732 bp (Fig. 15B). DNA of clone number 2 was sequenced using the following primers: CAG_1Fw, CAG_2Fw, A5_1Fw, A5_2Fw, and YFP_1Fw (see 2.1.4.). The expected nucleotide sequence was confirmed by sequencing (Method 2.2.8.). Finally, DNA of clone number 2 was purified in an endotoxin-free preparation and linearized with the enzyme Alw44I for it to be introduced in mammalian cells as explained in the following section.

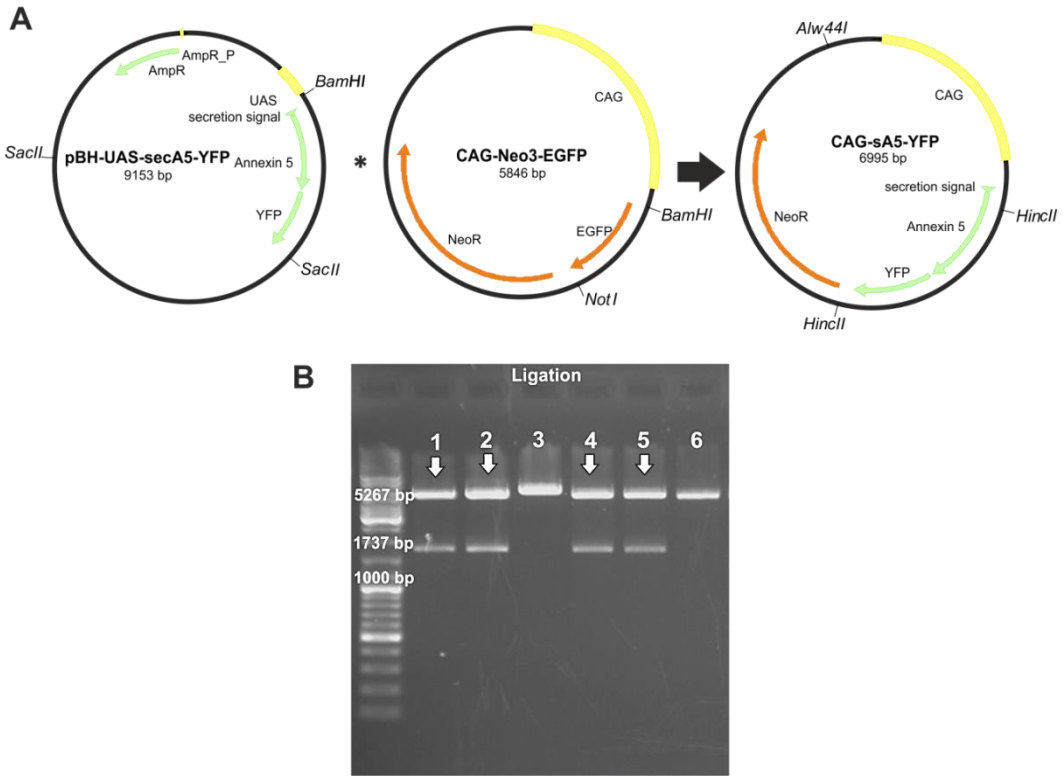

Fig. 15. Generation of the CAG-sA5-YFP expression cassette.

(A). Scheme of the cloning strategy for the generation of the CAG-sA5-YFP plasmid. **(B)** Gel electrophoresis of DNA samples of bacteria transformed clones cut with the restriction enzyme HincII. The expected fragment sizes with correct orientation are 5267bp and 1737bp. Positive clones are marked with white arrows.

3.2. Apoptosis detection in sA5-YFP transgenic mESCs as a proof of principle.

Once the CAG-sA5-YFP construct was successfully cloned and sequenced, it was tested *in vitro* with the purpose to evaluate its functionality as an apoptosis marker. For that, transgenic mESCs stably expressing sA5-YFP were generated by electroporation (Method 2.2.9). After 8 days of neomycin selection, approximately 46 clones were picked under fluorescence light to detect YFP expression. From these, 3 clones (27, 37 and 38) displayed a stable YFP expression (Fig. 16A-B). As explained in section 3.1, the CAG promoter drives the expression of sA5-YFP ubiquitously. Thus, this expression was defined as "background-ubiquitous expression", which was darker than that of apoptotic cells (bright sA5-YFP signal). In addition, the YFP expression level was analyzed by qPCR. Relative YFP expression level of clone #27 was comparable to that of a control mESC line stably expressing EYFP under the control of the CAG promoter (RNA sample kindly donated by my colleague Tobias Bruegmann (141). As part of clone characterization and to be able to use it later to generate transgenic mice, the newly generated mESCs lines were karyotyped (Method 2.3.3.). All three clones contained 40 chromosomes in more than 70% of the counted spreads corresponding to

a normal karyotype (Fig. 16C). Therefore, they were considered to have a high chance to contribute to the germline.

Next, the system was tested upon apoptosis stimuli using 4-Hydroxytamoxifen (4-OHT) at 40 µM, as a proof of concept. This concentration was chosen based on the report of Riss and Moravec (125) (Method 2.2.14). Within 24 hours after apoptosis induction, bright YFP-fluorescence signals could be observed due to accumulation of sA5-YFP at flipped PS residues in the membrane of apoptotic cells (Fig. 12). In order to corroborate that apoptosis was induced 24h after 4-OHT addition cells were fixed and stained against cCasp3, an early marker of apoptosis. YFP^+ and $cCasp3^+$ fluorescence signals increased after apoptosis induction. Labeled cells became roundish and detached from the bottom of the culture wells showing the typical apoptosis morphology (Fig. 16D). In addition, fluorescence measurements were performed via image software analysis (Image J, Version 1.37 A). A significant increase in YFP-fluorescence intensity over time of two independent experiments was observed, confirming the accumulation of YFP at the membrane of apoptotic cells (Fig. 16E).

In addition, as apoptosis is a very dynamic process (142), it was of interest to track apoptotic cells over time using this transgenic system. To do so, long term observation experiments were run (Method 2.3.5). Briefly, transgenic sA5-YFP and non-transgenic G4-mESC cells were grown on 1% gelatin coated plates and when they reached 60-80% confluency, apoptosis was induced with 4-OHT at 40 µM. As a control and to validate the efficacy of the sA5-YFP system against a commercial Annexin V probe, wild type mESCs were incubated with 1 µM Annexin V-FITC for 30 min at 37°C before apoptosis induction. Afterwards, time-lapse images were taken every 5 min for 24 hours using the Axiovision Observer Z1 fluorescence microscope. During the first 6 hours it was possible to detect apoptotic cells emerged from mESCs colonies. After approximately 50 min the first sA5-YFP labeled cells were detected and it was possible to observe a dot-like formation of blebs 175 and 275 minutes after induction (Fig. 17, upper row). These cells were comparable in morphology to the ones marked by a commercial Annexin V-FITC probe (Fig. 17, lower row). Examples of rounded cells and blebs are marked with white arrows. From these results, it could be concluded that the sA5-YFP transgenic system is able to detect apoptotic cells in a way comparable to commercially available Annexin V probes.

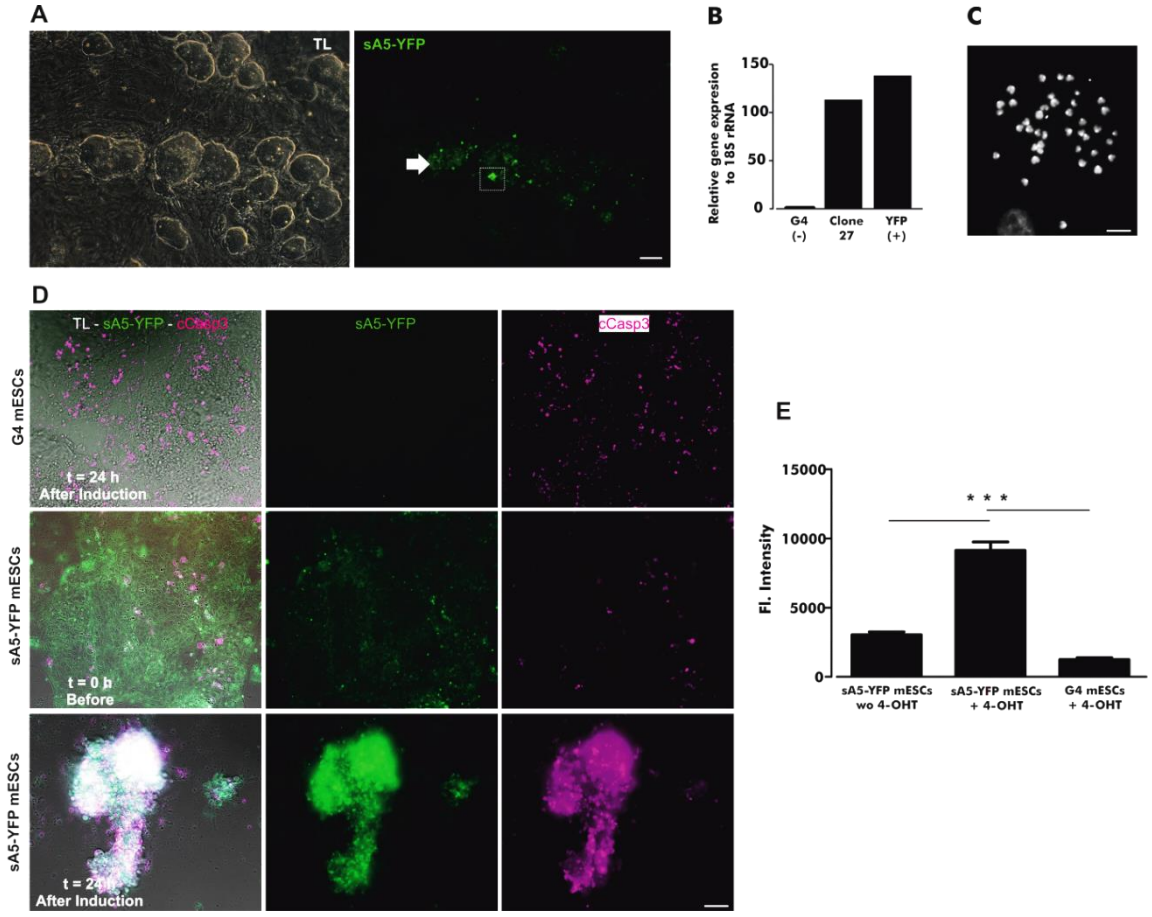

Fig. 16. Apoptosis detection in A5-YFP transgenic mESCs.

(A) Transgenic mESCs stably expressing sA5-YFP. Note the "background-ubiquitous" YFP expression (white arrow) and the few bright YFP^+ cells (white square). **(B)** Relative expression levels of sA5-YFP in a stable expressing mESCs clone compared to wild type G4 mESCs and mESCs expressing YFP. **(C)** Normal karyogram of the transgenic mESCs clone 27. **(D)** Fluorescent images revealing the accumulation of sA5-YFP in the membrane of apoptotic cells and co-localization of YFP^+ (green) and $cCasp3^+$ (purple) signals after apoptosis induction. **(E)** Quantitation of sA5-YFP fluorescence signals from (D) over time. Fluorescence intensity of YFP significantly increased 24 h after apoptosis induction by 4-OHT addition. G4 (-) = G4 mESC line, YFP (+) = mESC line expressing EYFP, 4-OHT = 4-hydroxytamoxifen, TL = transmission light, eGFP = enhanced green fluorescent protein, Afl = autofluorescence, cCasp3 = cleaved caspase 3. Data are shown as mean ± s.e.m., n =2, *** = $P < 0.001$ (Student's t-test). Bars are 50 µm (A, D) and 5 µm (C).

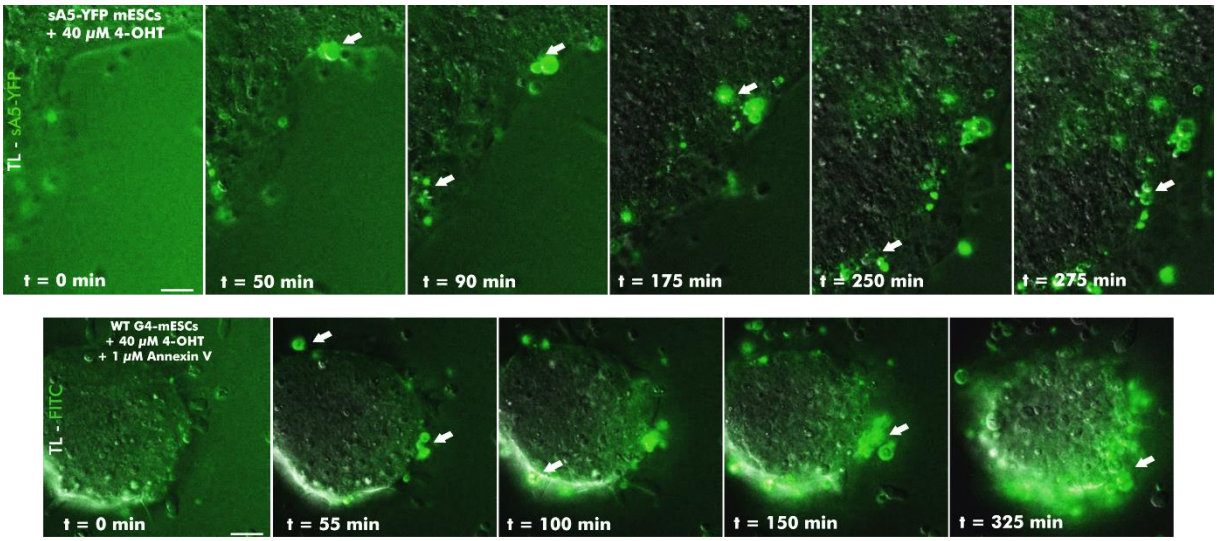

Fig. 17. Long term observation of apoptotic cells in sA5-YFP and control mESCs.

Time course of apoptotic cells in transgenic sA5-YFP (upper row) and non-transgenic mESCs (lower row) upon apoptosis induction. Transgenic sA5-YFP mESCs were treated with 4-OHT at 40 µM for 24 hours. Wild type mESCs were pre-incubated for 30 min with 1 µM of commercially available Annexin V-FITC before 4-OHT addition. Time-lapse images were recorded every 5 min. Examples of apoptotic cells labeled by sA5-YFP or Annexin V-FITC are shown by white arrows. Bar is 20 µm.

3.3. sA5-YFP marks apoptotic cells in differentiated cells

Transgenic mESCs stably expressing sA5-YFP were differentiated to embryoid bodies (EBs) (Fig. 13). EBs are 3-dimensional cell aggregates consisting of all three germ layers (i.e. endoderm, ectoderm, and mesoderm). They recapitulate early stages of mammalian development. EBs, cultured in suspension for 8 - 15 days, form structures homologous to the visceral yolk sac (mesoderm and endoderm) of post-implantation embryos (143). It is well known that apoptosis takes place during development (107, 144) and that massive cell death is present during EBs formation at the periphery and in the center of the body due to cavitation (145). Therefore, EBs are a good model to test and validate the sA5-YFP system in a more physiological environment in which apoptosis occurs.

For this purpose, EBs at day 11 of differentiation were fixed, sectioned and co-stained with cCasp3 (early apoptosis marker) and TUNEL (late apoptosis marker) (Fig. 18B-E). Bright YFP^+ signals were present at the periphery and in the center of the EBs in the same regions where $cCasp3^+$ and $TUNEL^+$ events were found. Quantitation revealed approximately 1.7 ± 0.48% $cCasp3^+$, 1.5 ± 0.26% $sA5\text{-}YFP^+$ and 3 ± 0.5% $TUNEL^+$ signals of total nuclei in the analyzed EBs. As mentioned before, the YFP positive signals followed the same pattern as the two apoptosis markers; however, it was observed that 30 ± 2.5% of the $cCasp3^+$ signals co-

localized with sA5-YFP$^+$, whereas only 13 ± 3.8 % of the TUNEL$^+$ signals co-localize with sA5-YFP$^+$ (Fig. 18F-G).

These results could indicate low specificity of the sA5-YFP system, as more than 50% of the signals do not co-localize with cCasp3 and TUNEL markers. However, based on the typical morphological and biochemical changes of the apoptosis cascade, it is known that the apoptotic cells show a very clear membrane ring-like morphology at the early stages of apoptosis and then start to form blebs. These blebs contain cellular components to avoid their release to the extracellular space which would cause inflammation (8). Thus, as caspase activation occurs in the cytoplasm, some membrane sA5-YFP$^+$ blebs will contain caspase residues. In addition, it is known that caspase 3 activation is initiated in the cytosol and later translocates to the nucleus. Moreover, caspase 3 activation is transient and reaches in less than 10 min its maximal activation (71). On the other side, TUNEL marks nuclei of cells in a late apoptotic state, meaning that the early apoptotic cells should not contain fragmented nuclei. Therefore, this is the first indication that the sA5-YFP transgenic system might detect cells at different stages of apoptosis (early-intermediate-late).

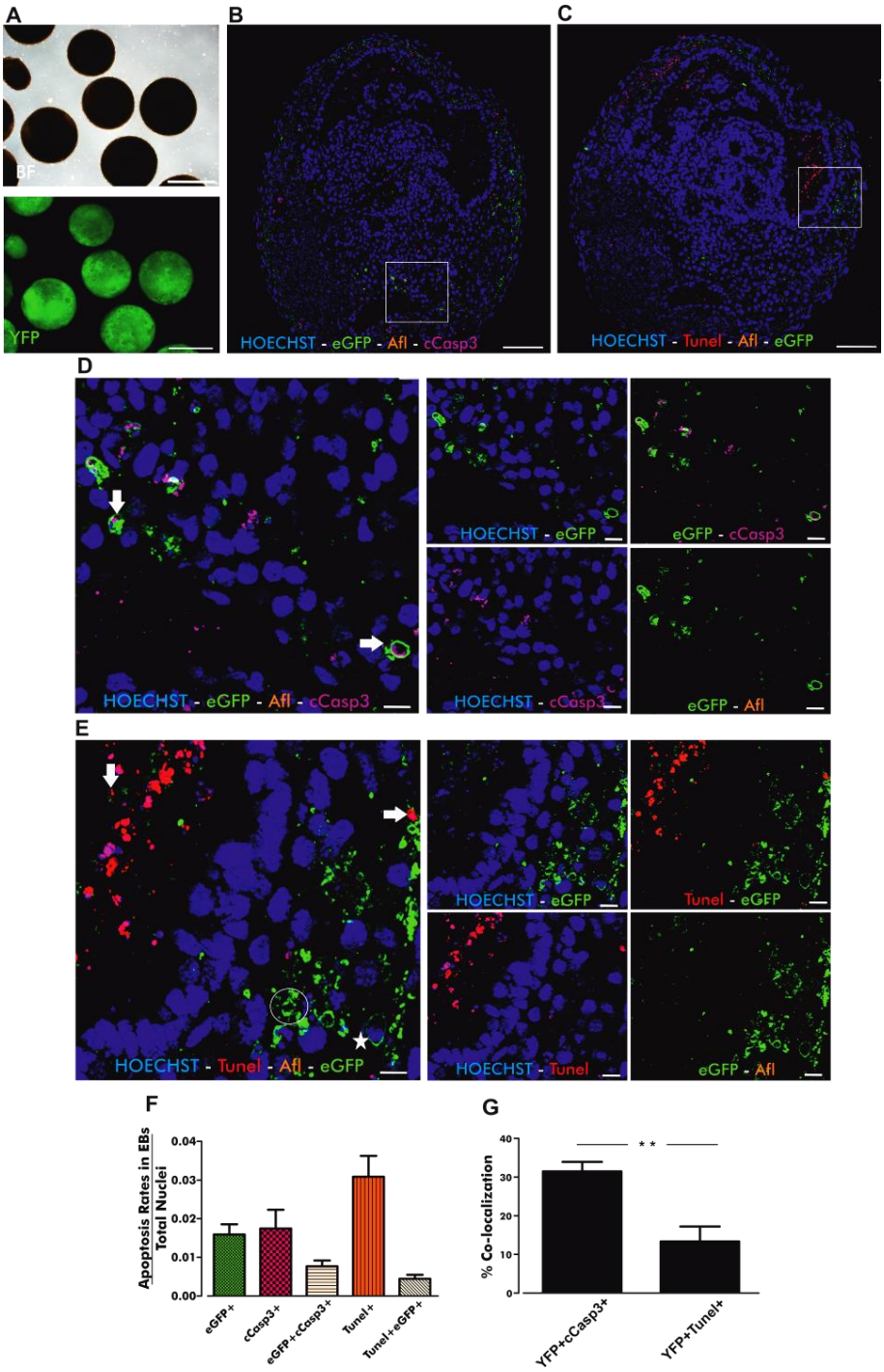

Fig. 18. Detection of apoptotic cells in differentiated mESCs.

(A) Transgenic EBs at d11 of differentiation derived from mESCs stably expressing sA5-YFP. **(B, C)** Frozen section of a transgenic sA5-YFP EB co-stained against cCasp3 and TUNEL stained, respectively**. (D, E)** Magnification of the area marked by a white box in (B and C) showing apoptotic bodies with co-localization of YFP^+ signals and $cCasp3^+$ or $TUNEL^+$ (white arrows). Note membrane ring-like sA5-YFP signals (white star) and membrane blebs (white circle). **(F)** Quantitation of early ($eGFP^+$ and $cCasp3^+$) and late apoptosis ($TUNEL^+$) rates in transgenic EBs at d11 of differentiation. (G) Percentage of co-localization of GFP^+ with total $cCasp3^+$ or total $TUNEL^+$ signals. Data are shown as mean ± s.e.m. **P < 0.01 (Student's t-test), n=4. BF = bright field, Afl = autofluorescence, HOECHST = nuclear staining, cCasp3 = cleaved caspase 3, TUNEL = Terminal deoxynucleotidyl transferase dUTP nick end labeling and sA5-YFP = secreted Annexin V-yellow fluorescent protein. *Sections were stained with eGFP antibody after antigen retrieval treatment to detect the YFP signal. Bars are 200 µm (A), 100 µm (B, C) and 10 µm (D, E).

3.4. Detection of apoptotic cells by sA5-YFP is independent of caspase activation

Apoptosis is not the only programmed cell death process, as cells can still die even in the presence of caspase inhibitors (79, 146). Necroptosis has been described as programmed necrosis, in which the caspase activation cascade is inhibited and a specific molecular pathway is activated. Therefore, it was of interest to test if the sA5-YFP transgenic system depends exclusively on caspase activation to detect dying cells. For this purpose, I cultured transgenic sA5-YFP mESCs in the presence or absence of zVAD-fmk, a widely used pan-caspase inhibitor (147, 148). After 2 h of caspase inhibition with 50 µM of zVAD-fmk, I added 1% DMSO to induce cell death for 24 h (Method 2.3.4). After this time, I fixed and stained the cells for cCasp3 (Method 2.4.1). I observed that cleaved Caspase 3 was significantly reduced in cells treated with zVAD-fmk (Fig. 19). Furthermore, I could also notice that sA5-YFP marks dead cells even if cCasp3 is not active. These bright sA5-YFP^{+} cells had a condensed nucleus and sA5-YFP accumulation in the membrane, which occur in both apoptotic and necroptotic cells. This indicates that the sA5-YFP transgenic system is independent of caspase activation and it might be capable of detecting other types of programmed cell death such as necroptosis.

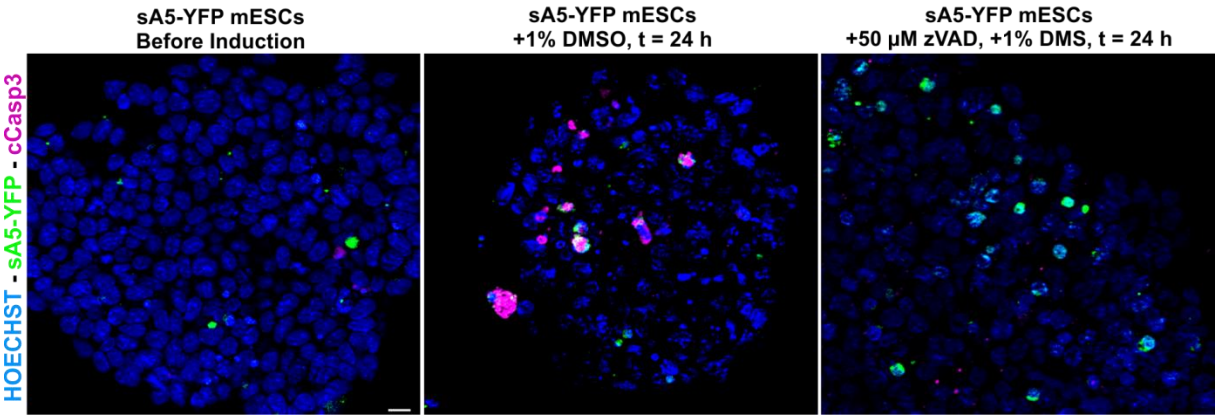

Fig. 19. Inhibition of caspase activity in sA5-YFP mESCs.

Transgenic sA5-YFP mESCs were incubated with the pan caspase inhibitor (zVAD-fmk) at 50 µM 2 h before cell death induction. Cell death was induced with 1 % DMSO. After 24 h, cells were fixed and stained against cCasp3. Casp-3 activity was clearly inhibited and bright YFP^{+} signals could still be observed after inhibition. This indicates that sA5-YFP cell death reporter is caspase independent and it may detect other types of programmed cell death such as necroptosis. Bar is 20 µm, n=3.

3.5. sA5-YFP marks apoptotic cells during mouse embryonic development

In order to understand the dynamics of apoptosis and to be able to visualize and observe apoptotic cells in living animals, the sA5-YFP transgenic system was tested *in vivo*. For that, a transgenic mouse line was generated from the CAG-sA5-YFP mESC line by complementation assays with diploid embryos as described in section 2.5.1 (the aggregation was kindly performed by Dr. Michael Hesse and Patricia Freitag from the Institute of Physiology I, University of Bonn).

As a proof of concept and because apoptosis is known to occur during embryonic development (107), 8.5 days old chimeric embryos of the first transgenic litter were dissected and scanned under fluorescence macroscopy for bright YFP signals, such as those described in the zebrafish sA5-YFP transgenic model (Fig. 12B). Small and roundish bright YFP particles within the heart and the yolk sac could be identified in the isolated embryos (Fig. 20).

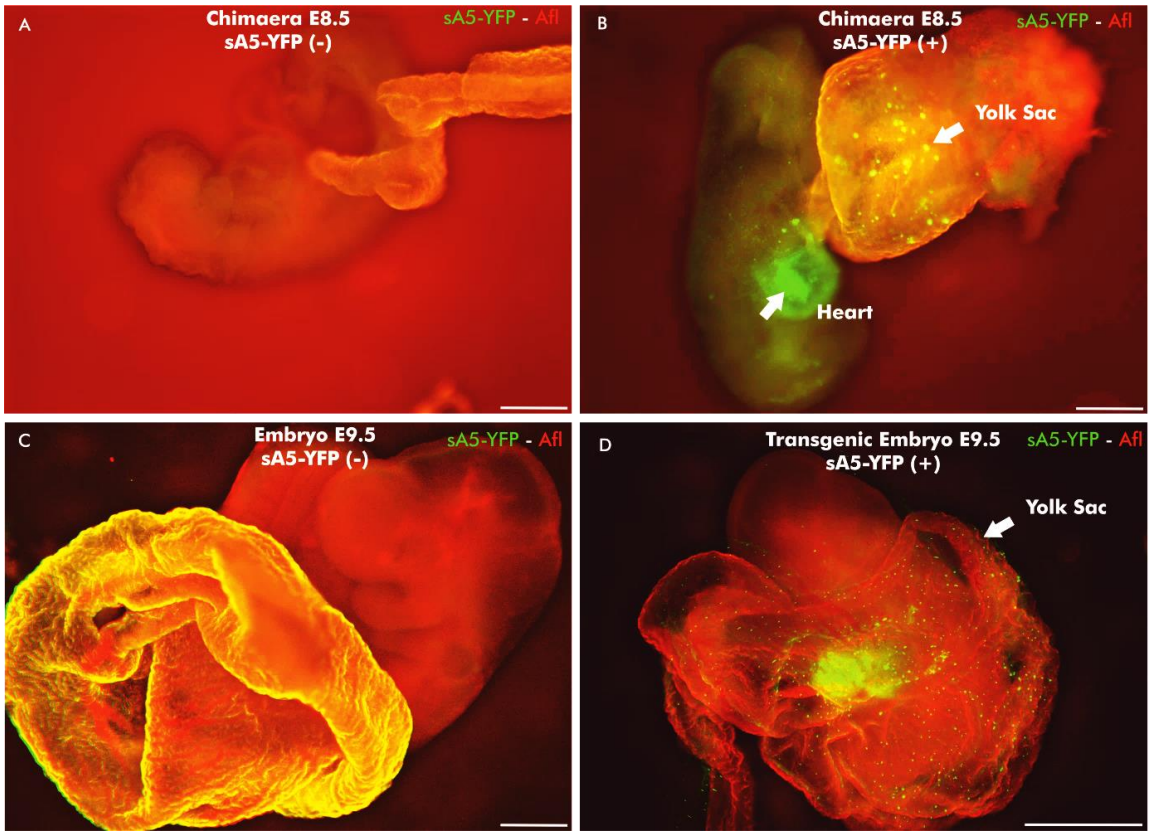

Fig. 20. Macroscopic pictures of sA5-YFP chimeric and transgenic embryos.

(A, B) Chimeric embryos at day 8.5 and **(C, D)** transgenic embryos at E9.5 expressing sA5-YFP are shown. Bright green fluorescent signals (white arrows) show typical apoptotic features: accumulation of sA5-YFP in the outer layer of the membrane and roundish morphology. sA5-YFP = secreted Annexin V-yellow fluorescent protein, Afl = autofluorescence. Bars are 200 µm (A, B and C) and 500 µm (D).

To evaluate if those small particles were apoptotic cells, transgenic embryos at E9.5-10.5 and hearts from transgenic embryos at E10.5 were dissected and analyzed by fluorescence macroscopy and immunostainings. Macroscopic pictures revealed very bright YFP^+ signals in embryos within the yolk sac, otic placode, hind brain and heart (Fig. 21A-E), as reported earlier (107, 144). Additionally, co-stainings with cCasp3 and TUNEL staining were performed in frozen sections of transgenic E9.5 embryos (Fig. 22A-D). Co-localization of YFP^+ signals with $cCasp3^+$ was observed within the otic placode, in the neural tube, and in the heart. In addition, it was observed that these positive cells also exhibited nuclear condensation (a hallmark of apoptosis), as shown by Hoechst counterstaining. However, it was also noted that few of the $sA5\text{-}YFP^+$ signals co-localized with TUNEL positive cells suggesting that this reporter system mostly detects cells in early/intermediate stages of apoptosis.

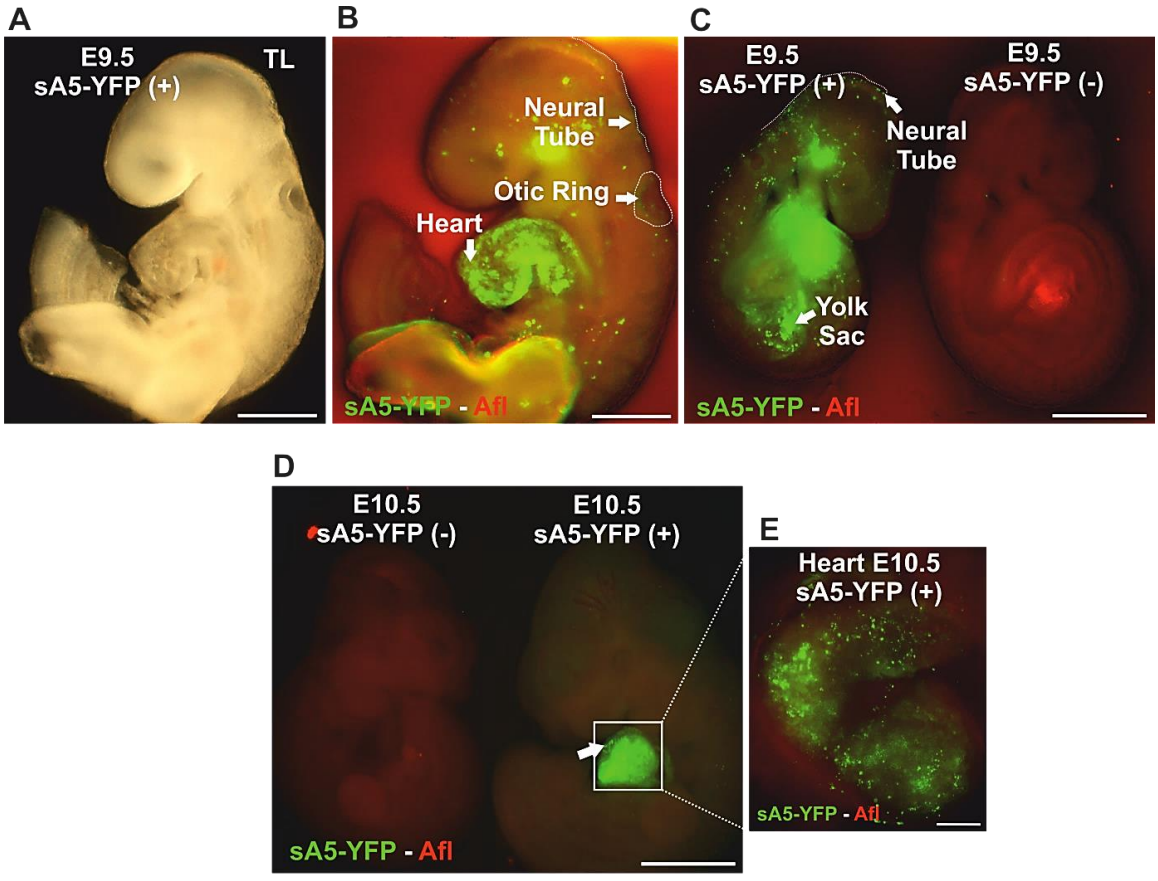

Fig. 21. Apoptosis detection in sA5-YFP mouse embryos.

(A, E) Macroscopic pictures of transgenic embryos at E9.5, 10.5 and a transgenic heart at E10.5 expressing sA5-YFP. Bright green fluorescent signals (white arrows) label apoptotic cells during embryonic development within the otic ring, the neural tube and the heart. These signals can be distinguished from the background expression by the roundish morphology and higher YFP intensity. TL = transmission light, sA5-YFP = secreted Annexin V-yellow fluorescent protein and Afl = autofluorescence. Bars are 200 µm (A, B), 500 µm (C, D), and 200 µm (E).

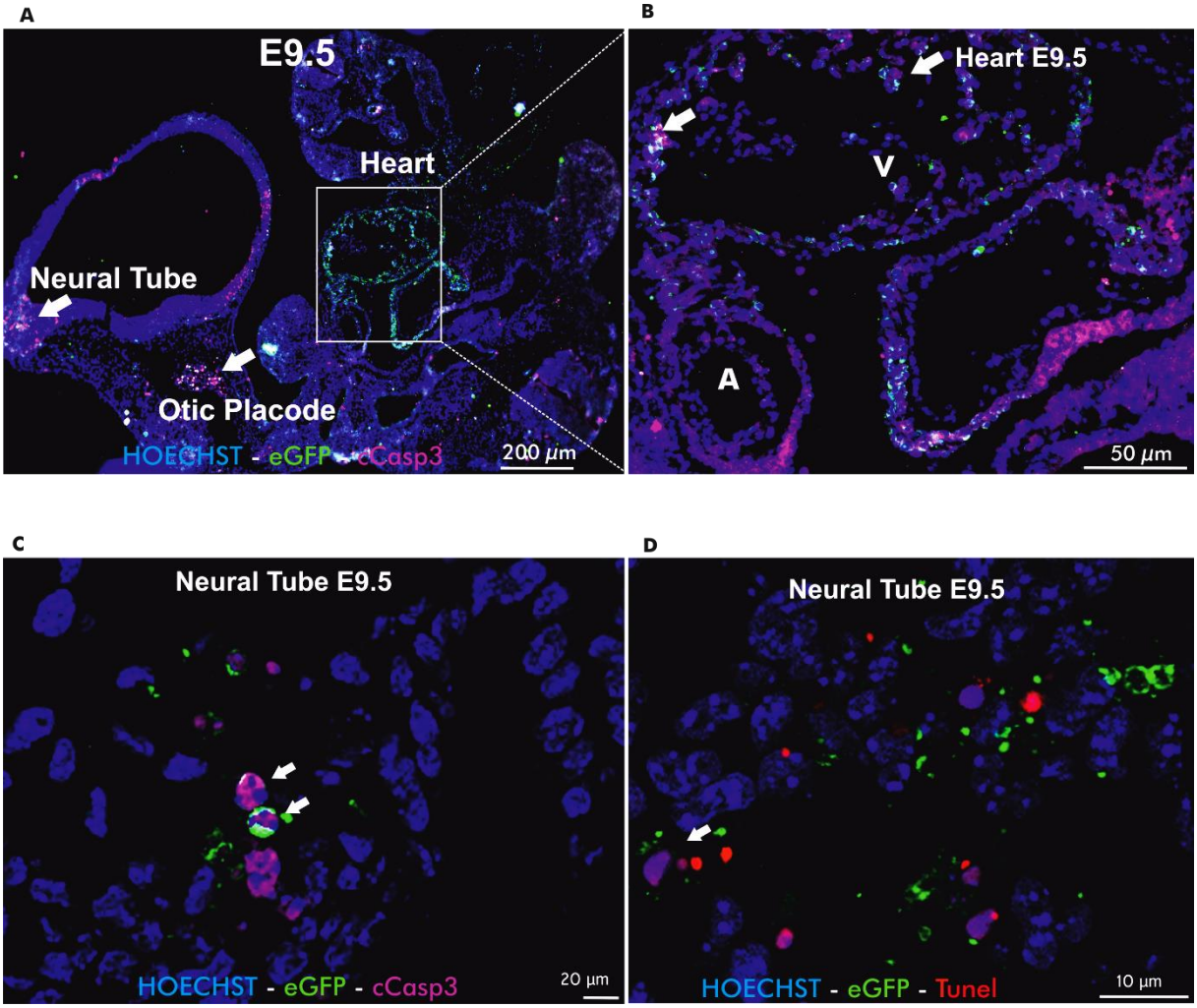

Fig. 22. sA5-YFP marks apoptotic cells during mouse development.

(A) Sagittal section of a transgenic E9.5 embryo showing co-localization of bright positive sA5-YFP^{+} signals (white arrows) with cCasp3 positive signals within the heart, the neural tube and the otic placode. **(B)** Magnification of the heart as indicated by white box in (A). **(C, D)** Frozen sections of the neural tube region of a sA5-YFP E9.5 embryo demonstrating co-localization of bright sA5-YFP^{+} signals with cCasp3 and TUNEL positive signals (white arrows), respectively. TL = transmission light, TUNEL = Terminal deoxynucleotidyl transferase dUTP nick end labeling and cCasp3 = cleaved caspase 3, V = ventricle and A = atria. *Sections were stained with eGFP antibody after Antigen Retrieval treatment to detect sA5-YFP signal. Bars are 200 µm (A), 50 µm (B), 20 µm (C) and 10 µm (D).

As mentioned in section 3.3, it was observed that not all the bright sA5-YFP^{+} particles co-localized with cCasp3 in EBs. One of the possible reasons for this is the fact that cells die at different time points and our system marks cells at different stages of the apoptosis cascade. Therefore, co-stainings for cleaved caspase 3, 8 and 7 (cCasp3, cCasp8 and cCasp7) were performed in sections of sA5-YFP embryos at E10.5 (Fig. 23). The pro-caspase 8 is the first caspase that gets activated after a death signal is sensed by death receptors (Fig. 5) and it further activates other caspases or molecules in both, the extrinsic and intrinsic apoptosis pathways. The effector casp-7 is a key protease, such as cCasp3, that further activates some

molecules in the nucleus; it is considered to be a point of no-return and the cell will definitely die. Immunostaings showed co-localization of bright sA5-YFP signals with the three markers (Fig. 23). It was noticed that the sA5-YFP particles co-localizing with cCasp8 had a clear ring-like membrane, condensed nucleus and cCasp8 was entirely distributed in the cytoplasm. These cells appeared to be whole and in a phase before blebbing started, indicating that they were at the beginning of the apoptosis cascade

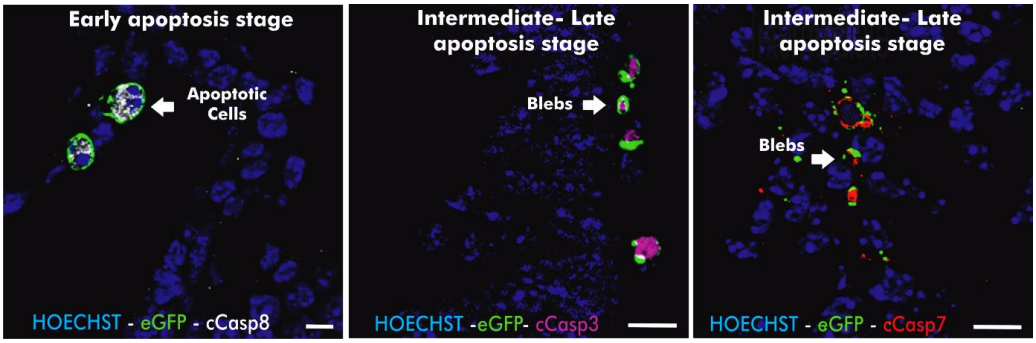

Fig. 23. sA5-YFP marks cells at different time points of apoptosis cascade during embryonic development.
Frozen sections of sA5-YFP embryos at E10.5 showing co-localization of bright sA5-YFP^{+} particles with cCasp3, 7 and 8. Notice that cells positive for cCasp8 were intact, contained condensed nuclei and presented a clear membrane YFP ring (early apoptosis). Small blebs were detected to co-localize with cCasp3 and cCasp7 (intermediate-late apoptosis). *Sections were stained with eGFP antibody after Antigen Retrieval treatment to detect sA5-YFP signal. Bars are 10 µm, 10 µm and 2 µm, respectively from left to right.

This was different for particles that were positive for cCasp3 and cCasp7, where very small blebs were also stained and had no nuclei, indicating that these cells already were in an intermediate/late stage of apoptosis. Finally, I could also show that few green particles co-localized with TUNEL staining (Fig. 22). This means that the sA5-YFP^{+} signals co-localize with markers for early and late apoptosis.

3.6. sA5-YFP marks apoptosis during mouse heart development

There is a need for studies that reveal detailed information about the contribution of apoptosis in the shaping of the developing mouse heart (24). Therefore, using the sA5-YFP mice, an analysis of rates and localization of PCD events was performed at different embryonic stages of murine hearts (E9.5 – E18.5) and postnatal day 2 (P2) hearts. Bright sA5-YFP particles were found in histological sections from all heart stages examined (Fig. 24, Fig. 25, Fig. 26). This detection system was sensitive enough for the identification of apoptotic cells at very early stages (e.j. E9.5,Fig. 24) of mouse heart development. It could also be observed that the presence of the bright green particles (white arrows) decreased as the embryonic heart got older.

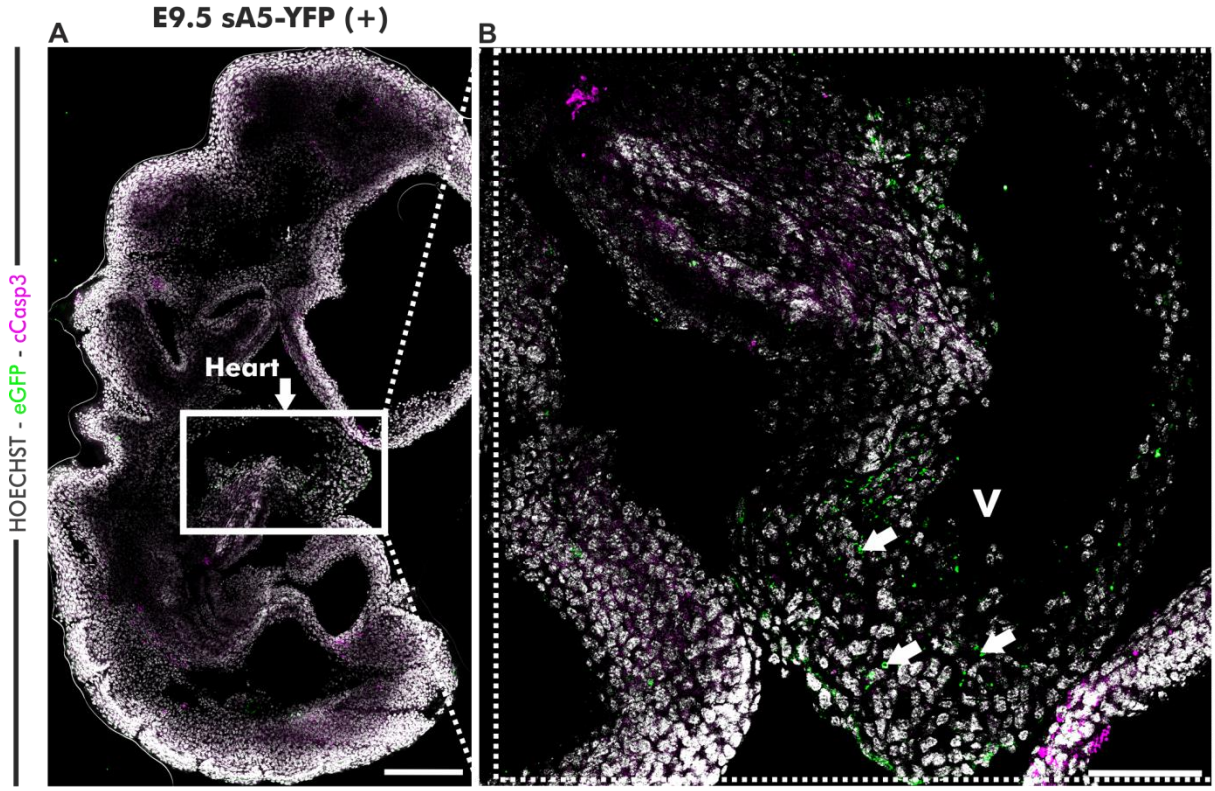

Fig. 24. Apoptosis patterns during mouse heart development at E9.5.

(A) Sagittal section of a transgenic embryo at E9.5. **(B)** Magnification of the heart from (A) where very bright YFP^{+} signals (white arrows) mark the apoptotic cells or blebs. These were mainly found in the ventricular myocardium. cCasp3 = cleaved caspase 3 and V = ventricle. *Sections were stained with eGFP antibody after Antigen Retrieval treatment to detect sA5-YFP signals. Bars are 200 µm (A) and 100 µm (B).

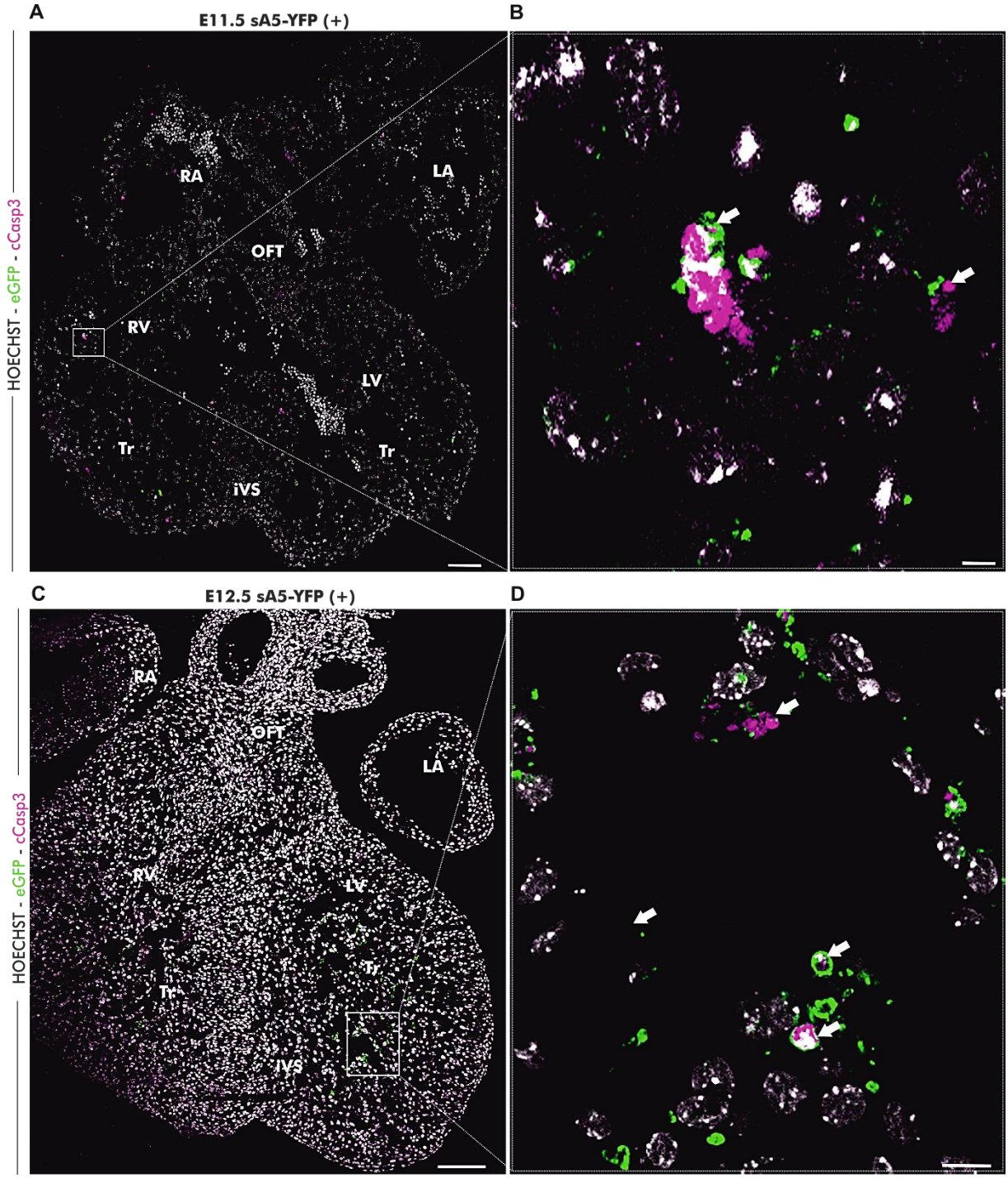

Fig. 25. Apoptosis patterns during mouse heart development at E11.5-E12.5.

Frontal sections of transgenic hearts at E11.5 **(A)** and E12.5 **(C). (B and D)** Magnification of areas marked in white boxes (A, D), where very bright sA5-YFP^{+} signals (white arrows) mark the apoptotic cells or blebs. These events were found predominantly at the ventricular trabeculae. cCasp3 = cleaved caspase 3, OFT = outflow tract, RA = right atrium, LA = left atrium, Tr = trabeculae, iVS = intra ventricular septum. *Sections were stained with eGFP antibody after Antigen Retrieval treatment to detect sA5-YFP signals. Bars are 100 µm (A), 20µm (B), 200 µm (C) and 10µm (D).

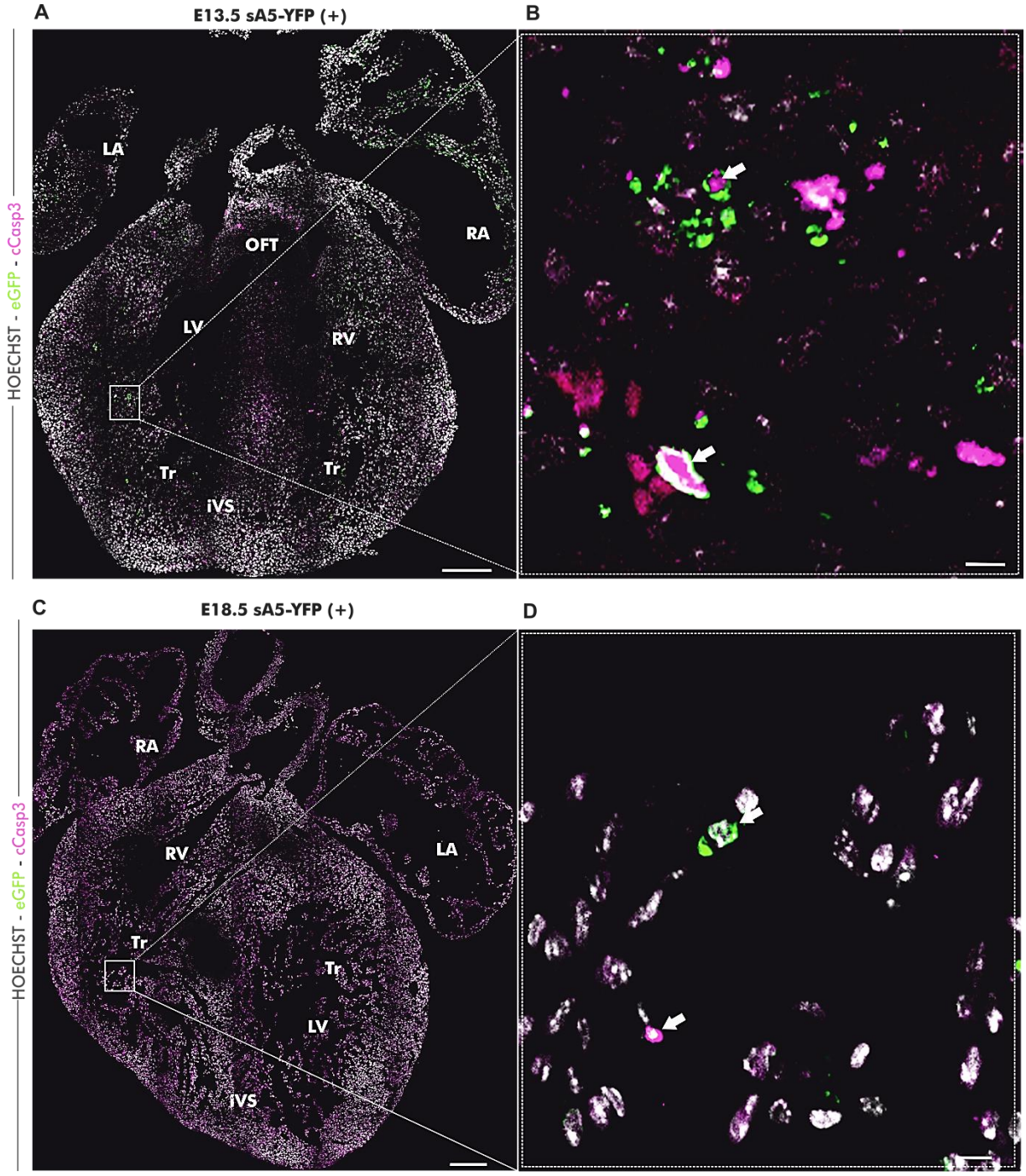

Fig. 26. Apoptosis patterns during mouse heart development at E13.5 and E18.5.

Frontal sections of transgenic hearts at E13.5 **(A)** and E18.5 **(C). (B and D)** Magnification of areas marked in white boxes (left) where very bright sA5-YFP^{+} signals (white arrows) mark the apoptotic cells or blebs. These events were found predominantly at the ventricular trabeculae. Notice that apoptotic events decreased as the heart grows older. cCasp3 = cleaved caspase 3, OFT = outflow tract, RA = right atrium, LA = left atrium, Tr = trabeculae, iVS = intra ventricular septum. *Sections were stained with eGFP antibody after Antigen Retrieval treatment to detect sA5-YFP signals. Bars are 200 µm (A, C), 20 µm (B), and 10µm (D).

As mentioned in section 3.5, I could observe that in the sA5-YFP embryonic hearts there were diverse types of labeled particles, similar to the ones present in other regions of the embryo (i.e. neural tube). There were bright sA5-YFP spots—with an approximate diameter of 5-10 µm—that showed clear ring-like membrane accumulation, often co-localized with cCasp3 positive signals in the cytoplasm and presenting a condensed nucleus. These cells were defined as "apoptotic cells" because they appeared to be intact and in a phase before membrane blebbing, indicating that they were at the beginning of the apoptosis cascade (Fig. 27A). On the other hand, small particles—ranging from a diameter of 2-4 µm —appeared to be fragments of apoptotic cells. They often did not contain nuclei and sometimes co-localized with cCasp3, indicating that these cells already were in a late stage of apoptosis. I defined these particles as "blebs" (Fig. 27B).

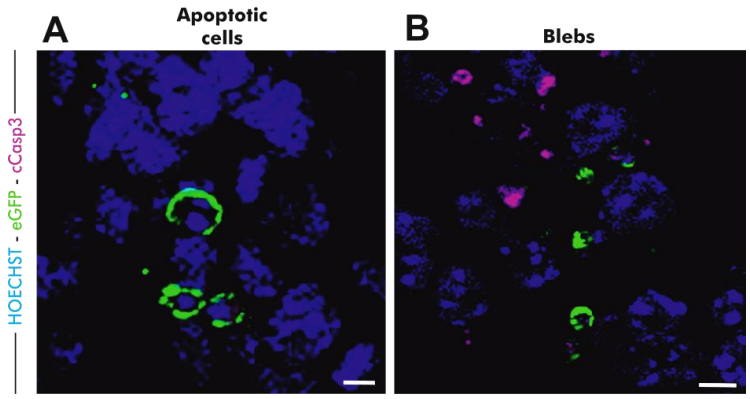

Fig. 27. Size and morphology of apoptotic cells and blebs detected by the sA5-YFP transgenic system.
(A) Apoptotic cells marked by sA5-YFP were defined as bigger particles (5-10 µM) that presented condensed nuclei and at least one of the following features: a clear ring-like membrane sA5-YFP accumulation, cCasp3 positive signal. **(B)** Blebs were defined as smaller particles (2-4 µm) without nuclear signal and positive for either YFP or cCasp3 or both. cCasp3 = cleaved caspase 3. *Sections were stained with eGFP antibody after Antigen Retrieval treatment to detect sA5-YFP signals. Bars are 5 µm (A, left) and 2 µm (A, right), 10 µm (B, left) and 5 µm (B, right).

In addition, TUNEL staining was also tested to evaluate if it also co-localizes with sA5-YFP$^+$ signals in E12.5 hearts. Few TUNEL$^+$ signals were found to co-localize with sA5-YFP$^+$ cells in the whole heart (Fig. 28). As there was a higher co-localization of sA5-YFP particles with cCasp3 positive signals and taking into account that cCasp3 is widely recognized to detect early apoptosis, it was used for the analysis and quantification of apoptotic events during mouse heart development in all further experiments.

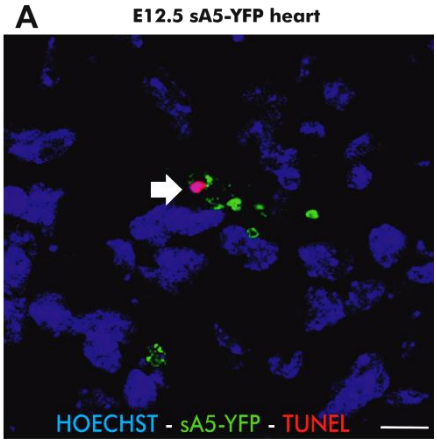

Fig. 28. TUNEL+ signals co-localize with sA5-YFP$^+$ particles in E12.5 hearts.

(A) An example of TUNEL$^+$ signal co-localizing with sA5-YFP$^+$ signal (white arrow) in frozen sections of E12.5 hearts. Very few TUNEL+ signals were found in the heart at this stage. Bar is 10 µm.

To confirm the specificity of the system, control stainings were performed in sections from E12.5 hearts. First, I check if the sA5-YFP$^+$ fluorescence signals were specific by detecting them using an anti-human Annexin V antibody. This is because the CAG-sA5-YFP plasmid contains the human sequence of Annexin V (108). I could prove that the native sA5-YFP$^+$ signals (Fig. 29A) corresponded to specific human Annexin 5 signals (white arrows in Fig. 29B). Secondly, I tested if the eGFP antibody is able to detect sA5-YFP signals after antigen retrieval. For that, E12.5 sections of sA5-YFP$^-$ (Fig. 29C) and sA5-YFP$^+$ (Fig. 29D) hearts were stained after antigen retrieval (Method 2.4.2) with anti-eGFP and anti-cCasp3. In negative hearts, no eGFP signal was detected in comparison to sA5-YFP positive signals proving the specificity of the eGFP antibody.

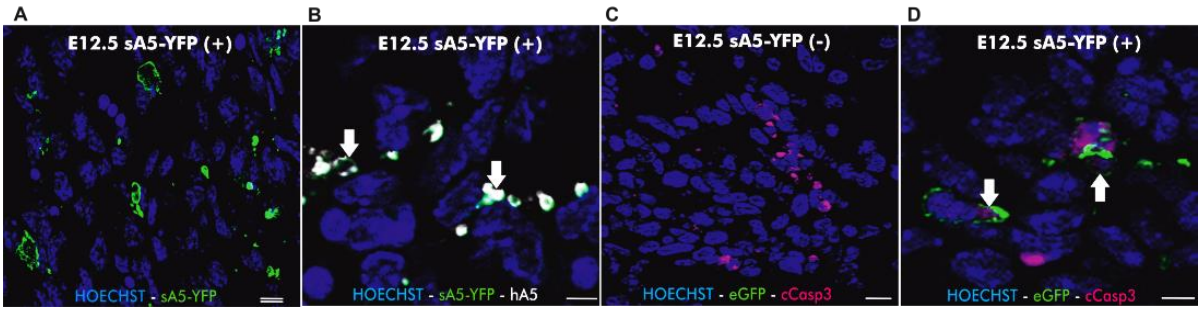

Fig. 29. Immunostainings controls in frozen sections from E12.5 hearts.

(A) Native sA5-YFP expression. **(B)** Co-localization of sA5-YFP$^+$ signals with human Annexin V antibody. **(C)** Negative E12.5 heart section co-stained against eGFP and cCasp3. No eGFP signals were detected demonstrating eGFP specificity to detect sA5-YFP signals. **(D)** eGFP antibody detects sA5-YFP$^+$ signals after Antigen Retrieval treatment in a sA5-YFP E12.5 heart stained against eGFP and cCasp3. *Sections were stained with eGFP antibody after Antigen Retrieval treatment to detect sA5-YFP signals. Bars are 10 µm (A, C) and 5 µm (B, D).

3.7. Localization and quantification of dead cells undergoing apoptosis during mouse heart development

To see if apoptosis is related to morphological changes in the heart, I assessed the specific localization of apoptotic cells and blebs during the different stages of heart development. At very early stages (E9.5-10.5) sA5-YFP+ particles were mainly localized to the ventricular myocardium (Fig. 24). Some other regions were visible at E11.5 in which very bright sA5-YFP$^+$ particles localized to both ventricles (Fig. 25), to the endocardial cushions (developing valves) and to the moderator band (connects the iVS to the anterior papillary muscle) close to the intraventricular septum (Fig. 30). At E12.5, there was a clear accumulation of apoptotic cells and blebs in the left ventricle (Fig. 25). In this region there were plenty of bright sA5-YFP$^+$ apoptotic cells—co-localizing with cCasp3—as well as sA5-YFP$^+$ blebs.

One day later, at E13.5, the majority of labeled sA5-YFP cells were still localized to the left ventricle, but to a lesser extent compared to E12.5. At this stage, it was also noticed that there were sA5-YFP$^+$ blebs in the trabecular region, in the developing mitral valve and in the right atria (Fig. 31). Another study (21) has shown that apoptosis is also present in the outflow tract at E13.5. However in this present work, I could only distinguish very dim and small sA5-YFP$^+$ signals, indicating that dying cells in this area could have already been engulfed or have been in a later stage of the apoptosis cascade (Fig. 26). At later stages of heart development, the apoptotic events were less frequent (Fig. 26). E.g. in P2 hearts, the apoptotic events were sporadically found in the ventricles and close to the mitral and tricuspid valves (Fig. 32). Finally, the incidence of apoptotic cells and blebs in adult hearts (11 months old) was scarce, indicating that the embryonic heart is primed for apoptosis, while the adult heart is not Fig. 32. This coincides with the recent findings of Sarosiek and colleagues, who showed that the expression of apoptosis genes decreased in the adult heart (63). However a deeper characterization of sA5-YFP$^+$ cells in the adult heart should be performed.

As one of my aims was to provide a complete map of the apoptosis rates, I quantified all types of labeled sA5-YFP particles throughout heart development from E9.5 to P2 in at least 3 hearts per developmental stage (Fig. 33). In order to summarize this information, I classified these particles into “apoptotic cells” and “blebs” as mentioned in section 3.6 (Fig. 23). For quantification, an “apoptotic cell” was defined as the one containing nucleus and being positive for cCasp3, sA5-YFP or both. Similarly, a “bleb” was defined as an entity not containing nucleus and being positive for either cCasp3 or YFP or both. The quantitation data

indicated that apoptosis peaks at early stages of heart organogenesis (E9.5 – E11.5), slightly decreased from E12.5 to E14.5, and started to further decrease at E15.5 confirming that apoptosis is highly active at the beginning of heart formation (Fig. 34).

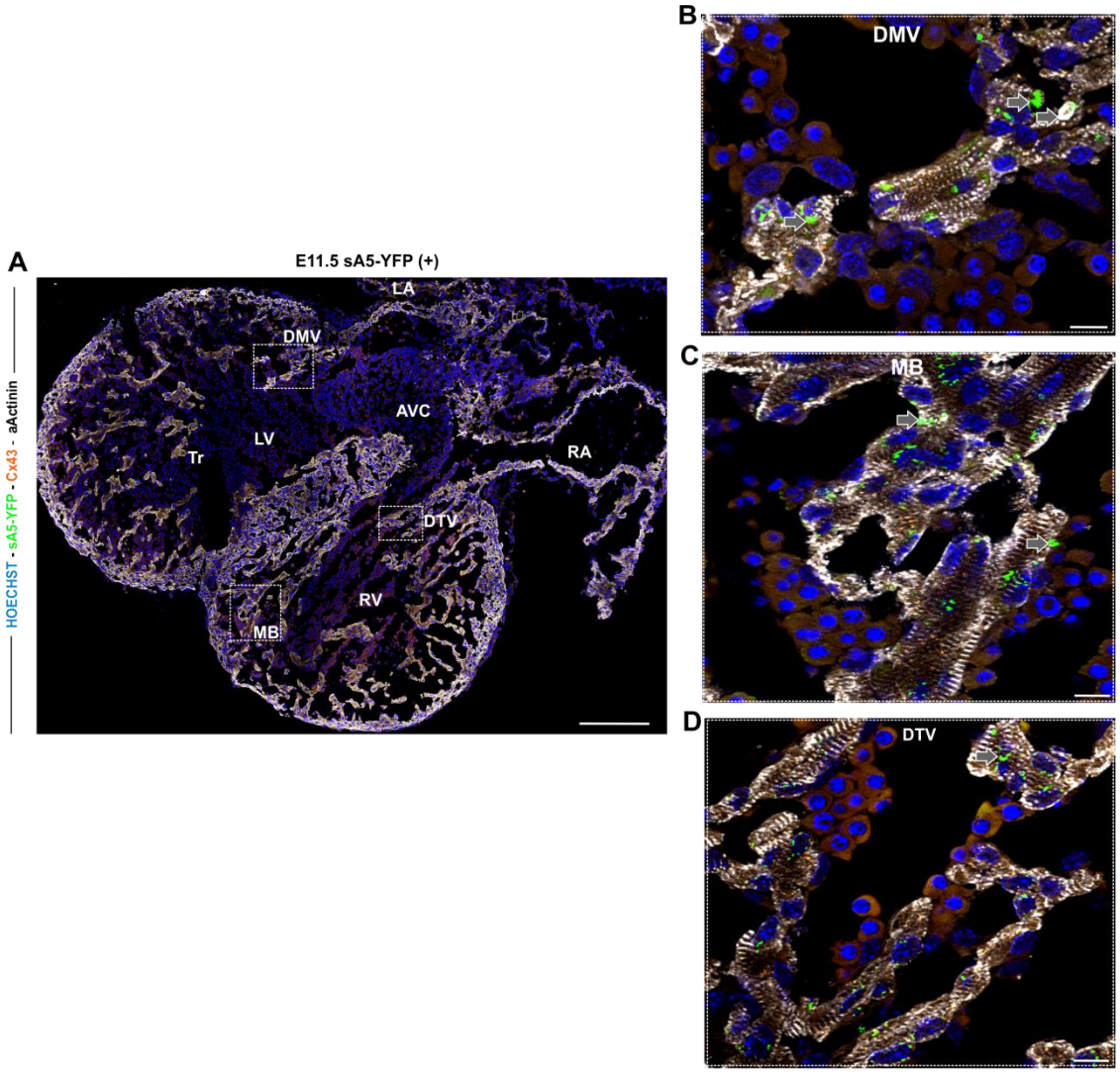

Fig. 30. Distribution pattern of apoptosis in the mouse heart at E11.5.

(A) Frontal section of a transgenic heart at E11.5. Labeled sA5-YFP apoptotic cells and blebs (white arrows) were found at the trabeculae of both ventricles, in the regions of the developing mitral and tricuspid valves, in the intraventricular septum and in the moderator band. **(B-D)** Magnifications of the heart regions marked by white boxes in (A) depicting the presence of apoptosis. V = ventricle, AVC = atrioventricular cushion, RA = right atrium, LA = left atrium, Tr = trabeculae, MB = moderator band (connects the iVS to the anterior papillary muscle), DTV = developing tricuspid valve and DMV = developing mitral valve. Bars are 200 µm (A), and 10 µm (B, C, D).

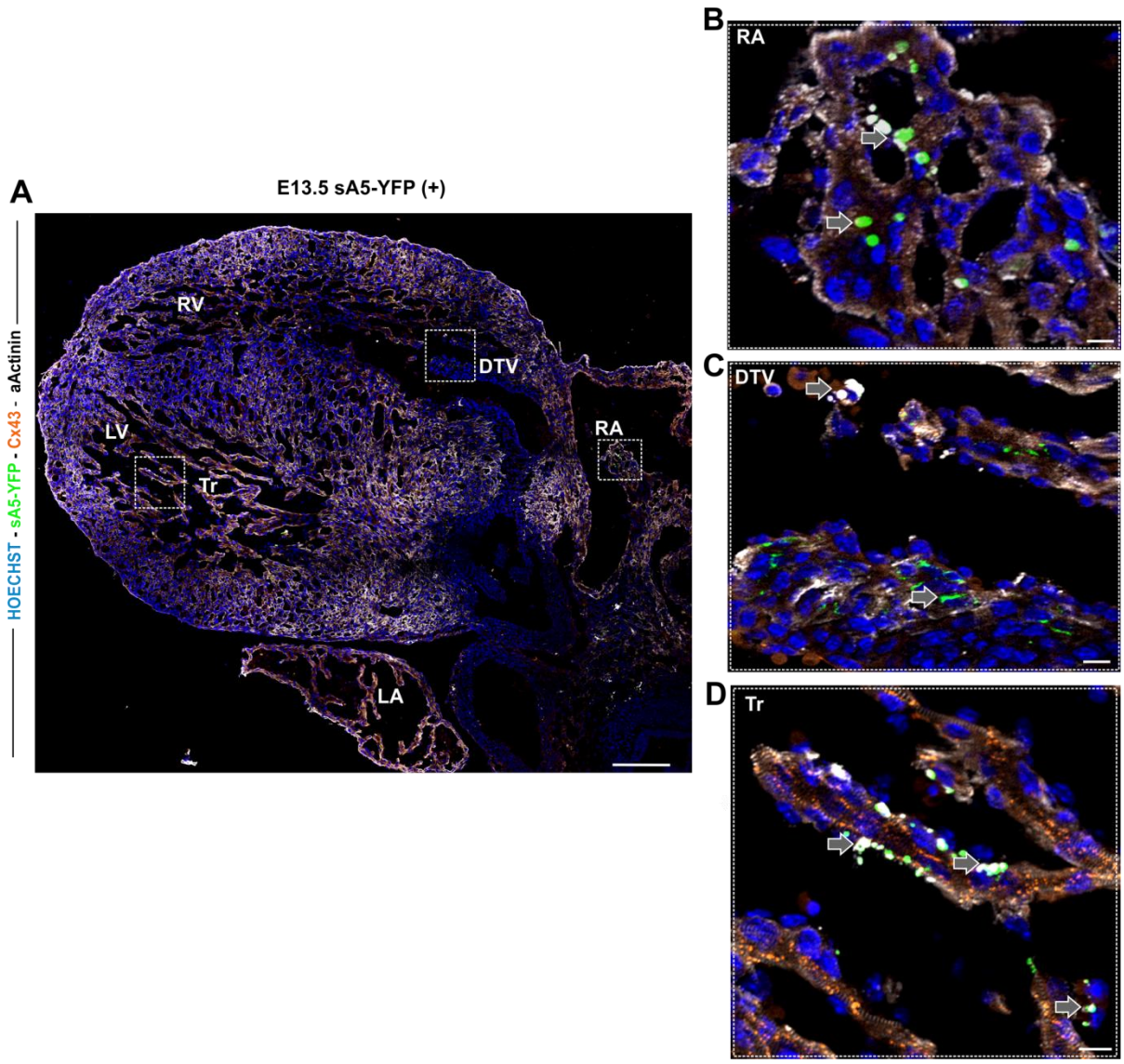

Fig. 31. Distribution pattern of apoptotic cells in the mouse heart at E13.5.

(A) Frontal sections of a transgenic heart at E13.5. Labeled sA5-YFP apoptotic cells and blebs (white arrows) were found at the trabeculae of both ventricles, in the developing mitral valve and in the right atria. **(B-D)** Magnifications of the heart regions marked by white boxes in (A) depicting the presence of apoptosis. V = ventricle, RA = right atrium, LA = left atrium, Tr = trabeculae, and DTV = developing tricuspid valve. Bars are 200 µm (A) and 10 µm (B-D).

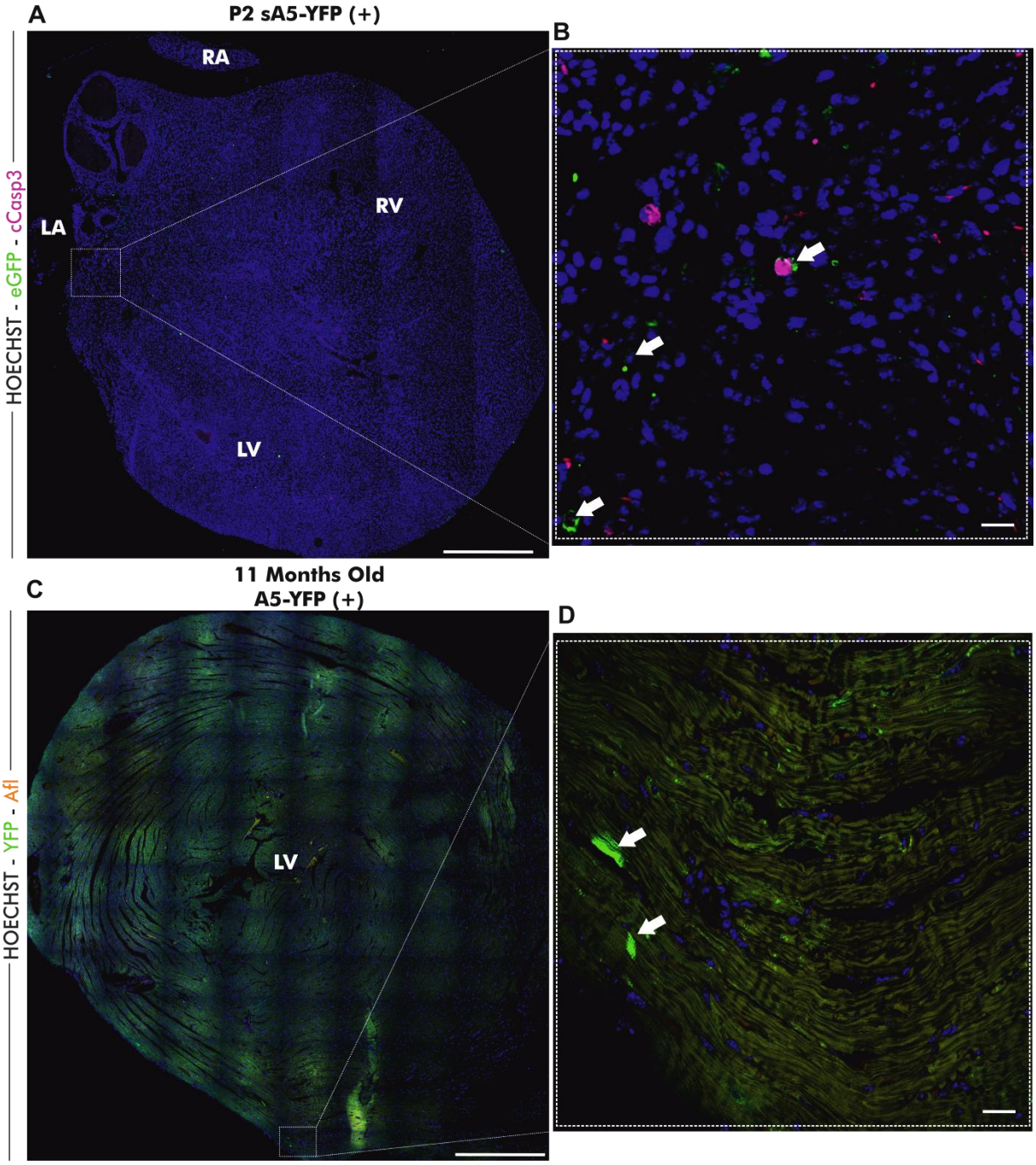

Fig. 32. Distribution pattern of apoptotic cells in P2 and adult mouse hearts.

(A) Frontal section of a transgenic heart at P2. Labeled sA5-YFP apoptotic cells and blebs (white arrows) were scarcely found in the epicardium. **(B)** Magnification of the heart region marked by white boxe in (A) depicting the presence of apoptosis. **(C)** Transversal section of a transgenic heart at 11 months old. Labeled sA5-YFP apoptotic cells and blebs (white arrows) were scarcely found in the compact zone of the left ventricle. **(D)** Magnification of the heart region marked by white boxe in (C) depicting the presence of apoptosis. RA = right atrium, LA = left atrium, LV = left ventricle, RV = right ventricle, YFP = yellow fluorescence protein, Afl = autofluorescence channel. Bars are 500 µm (A, C) and 20 µm (B,D).

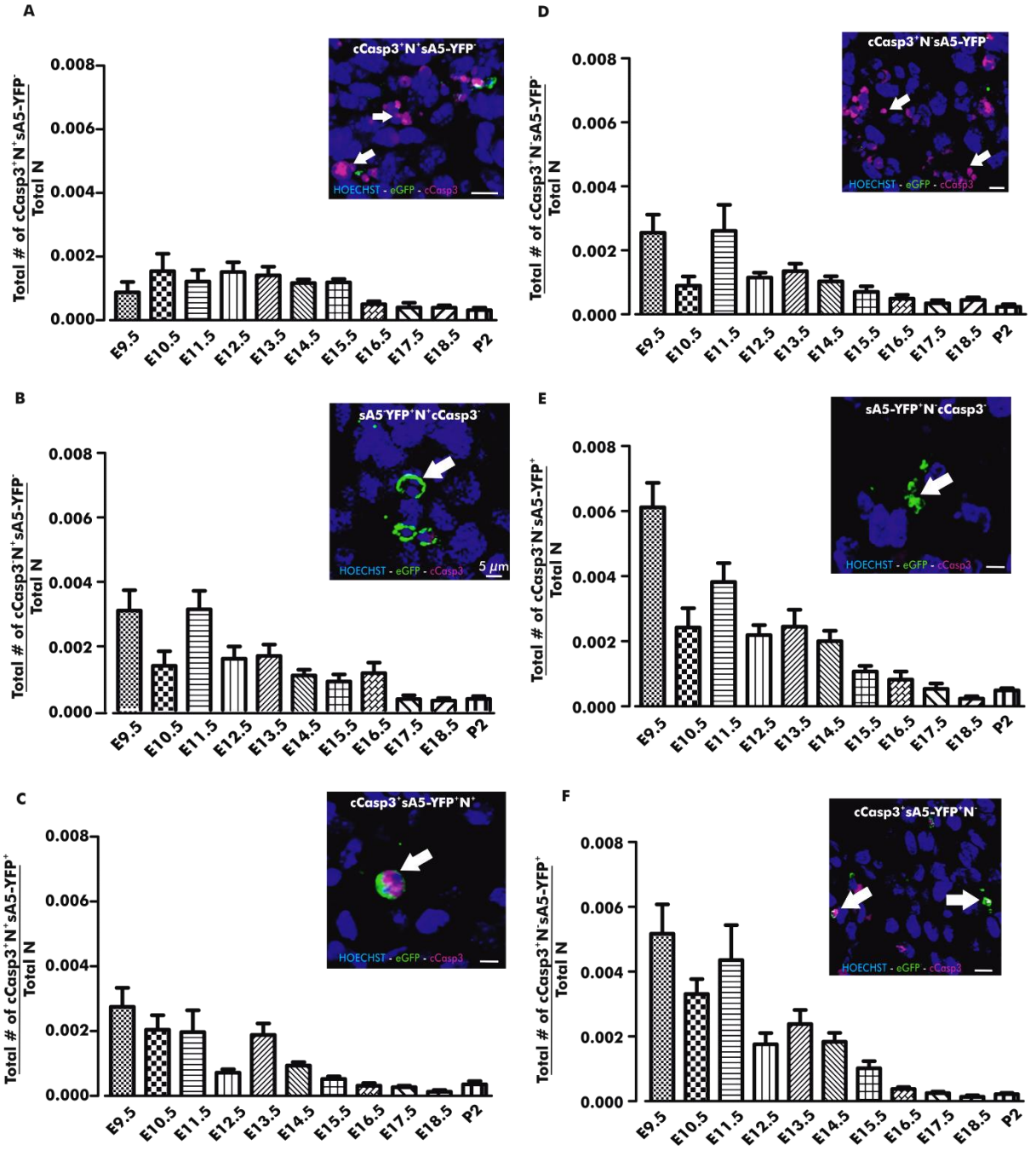

Fig. 33. Quantification of all different types of particles marked with sA5-YFP and cCasp3 during embryonic heart development.

(A, B, C) The graphs at the left show normalized rates of cells marked by sA5-YFP, cCasp3 or both, containing condensed nuclei to all nuclei. **(D, E, F)** Graphs at the right revealed the normalized rates to all nuclei of cells marked by sA5-YFP, cCasp3 or both, but without nuclei. Pictures in each graph are example of each type of quantified particle. eGFP = enhanced green fluorescent protein* and cCasp3 = cleaved caspase 3. *Sections were stained with eGFP antibody after Antigen Retrieval treatment to detect YFP signals. Bars are 10 µm in (A and D) and 5 µm in (B, C, D, E).

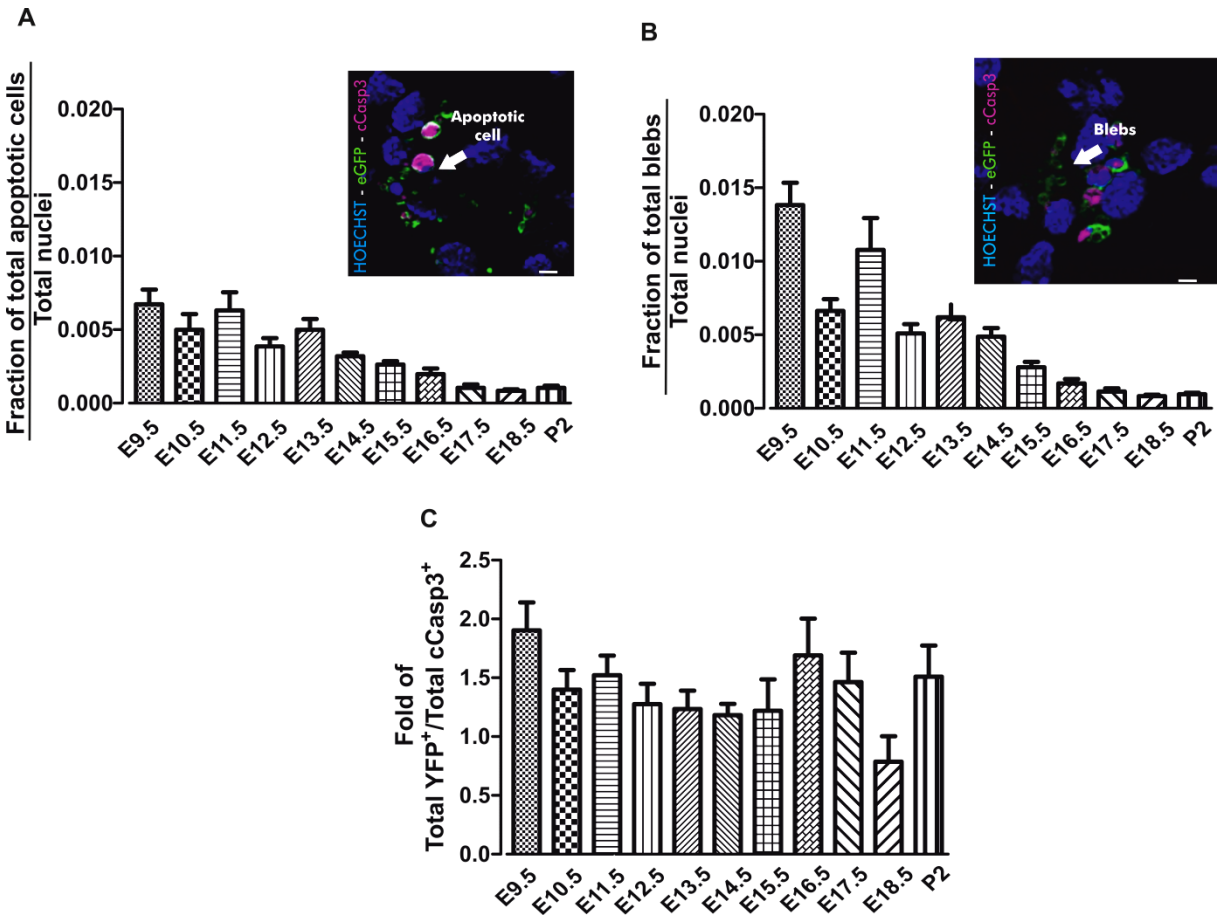

Fig. 34. Apoptotic cells and blebs rates during heart development.

(A) Quantitation of total apoptotic cells. Apoptosis peaks at early stages of heart development (E9.5 - E11.5) and it decreases significantly after E15.5 (T-test between E9.5 vs E15.5, p-value = 0.011). **(B)** Quantitation of total blebs. Apoptosis peaks at early stages of heart development (E9.5 - E11.5) and it decreases significantly after E15.5 (T-test between E9.5 vs E15.5, p-value = 0.011). **(C) F**old of YFP^+ per $cCasp3^+$ signals at different stages of mouse heart organogenesis. YFP^+ signals were approximately twice the $cCasp3^+$ signals mainly found at the trabeculae while $cCasp3^+$ signals were mostly found at the outflow tract. Data are shown as mean ± s.e.m., n=3. *Sections were stained with eGFP antibody after Antigen Retrieval treatment to detect YFP signals. Bars are 5 µm.

An advantage of the sA5-YFP detection system is that it allows detecting blebs of dying cells enabling the identification of cells in later stages of the apoptosis cascade, which is not possible with antibodies specific to either earlier or later stages at which most of the cells have been engulfed already. There were approximately two fold more sA5-YFP signals than cCasp3 signals (Fig. 34C) indicating that this system allows the detection of a broader spectrum of apoptotic stages and it can probably also detect other types of programmed cell death.

3.8. Cardiomyocytes predominantly undergo apoptosis during mouse heart development

An advantage of the sA5-YFP system is that it allows for the detection of apoptosis at early stages prior to the disruption of the cell membrane. To identify the cell types undergoing apoptosis in the embryonic heart, co-stainings in sections of transgenic E13.5 embryonic hearts with typical markers for cardiomyocytes (α-actinin and MF20), endothelial cells (PECAM), leukocytes (CD45) and smooth muscle cells (α-smooth muscle actin, ASMAC) were performed. Immunostainings revealed a strong co-localization between cardiomyocytes and sA5-YFP positive signals (Fig. 35A, B). Quantification indicated that approximately 66% of the sA5-YFP^{+} cells were cardiomyocytes, 12% smooth muscle cells, 7% leukocytes, 8% endothelial cells and 7% mesenchymal cells. This data clearly show that cardiomyocytes are the most abundant apoptotic cell type during heart development (Fig. 35G).

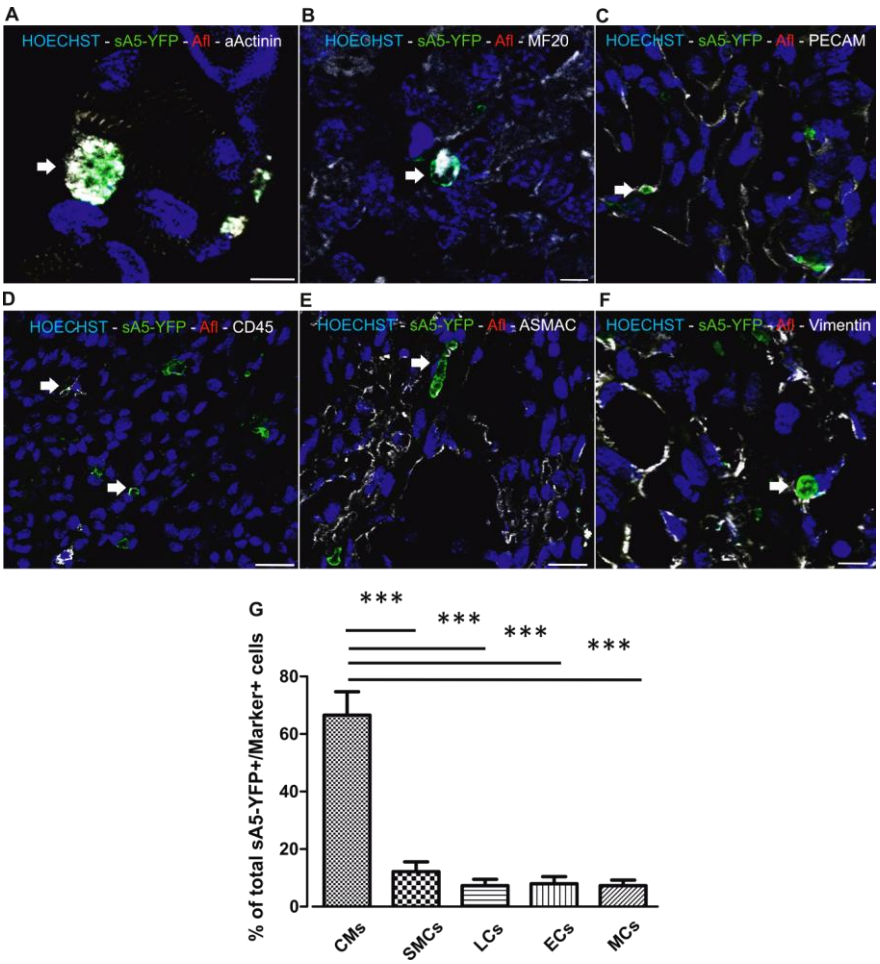

Fig. 35. Identification of cell types undergoing apoptosis during heart development.

(A, F) Co-stainings in Sections of transgenic embryonic hearts (E13.5) stained for markers of cardiomyocytes (CMs, α-actinin and MF20), endothelial cells (ECs, PECAM), leukocytes (LCs, CD45), smooth muscle cells (SMCs, ASMAC) and mesenchymal cells (MCs, vimentin). **(G)** Quantitation of the different cell types that undergo apoptosis during heart development. Data are shown as mean ± s.e.m.,*P < 0.05 (Student's t-test), n=3. Bars are 5 µm (A, B), 10 µm (C, F) and 20 µm (D, E).

3.9. Real-time detection of massive apoptosis by sA5-YFP during mouse development

To prove that the sA5-YFP transgenic mouse line is a powerful tool to visualize apoptotic cells in living embryos, I monitored the accumulation of sA5-YFP at the membrane of dying cells in transgenic embryos at E8.75 over time. After dissecting the sA5-YFP embryos from the uterus and yolk sac, I placed them in an imaging chamber filled with IMDM-imaging medium. Then, I induced massive cell death by medium starvation and analyzed the onset of apoptotic cells under an inverted confocal microscope at 37°C and 5% CO2 for 15 - 20 h taking z-stack pictures every 6 - 10 min (Fig. 14).

As shown in Fig. 36-B, I observed a clear increase in accumulation and fluorescence intensity of sA5-YFP in the membrane of dying cells throughout the whole embryo. Very bright sA5-YFP signals, with a ring-like morphology, were visible around the heart area after 2 h of induction (white arrows). After 6 - 10 h more cells rounded up and detached from the tissue in the regions close to the otic ring and neural tube. Approximately after 11 h, some of the bright sA5-YFP+ signals seem to disappear, indicating that they could have been phagocytosed by surrounding cells or macrophages. It is important to mention that the embryo shrinks and dies after 8 h of imaging.

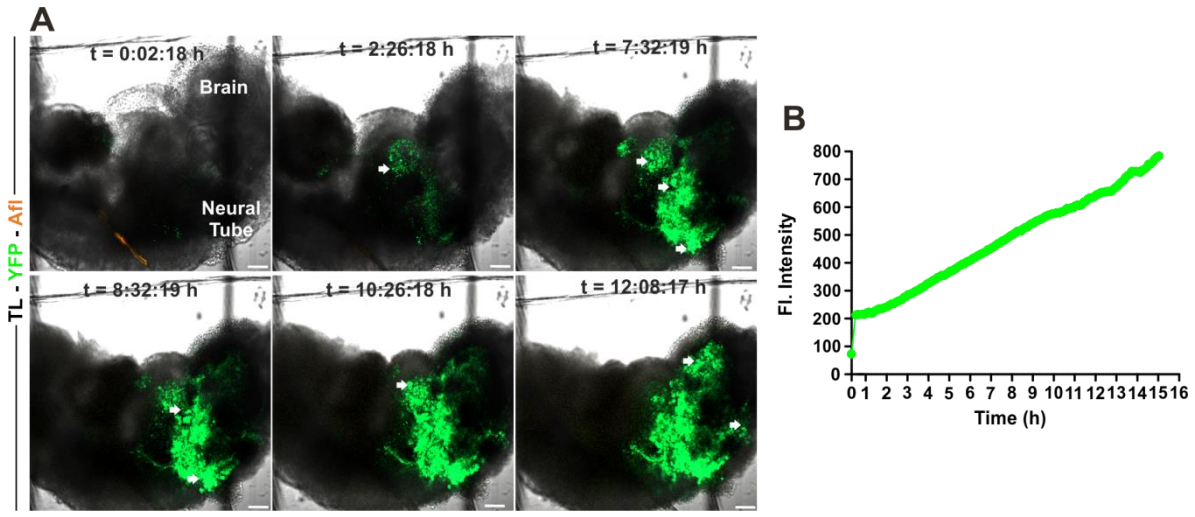

Fig. 36. Long term observation of cell death in a E8.75 sA5-YFP embryo.

(A) A transgenic sA5-YFP embryo was observed under an inverted confocal microscope. Massive cell death was induced by medium starvation. After 2 h, the first rounded cells (white arrows) appeared. Time-lapse images were recorded every 5 min for 15 h. 33 z-stack slices of 4 µm were taken. Images in this figure are from the z-stack #17. **(B)** Quantitation of sA5-YFP fluorescence signals from (A) over time. Bars are 100 µm.

3.10. Real-time detection of apoptosis by sA5-YFP during cranial neural tube closure and heart development

After proving that sA5-YFP detects dying cells *in vivo* after induction of apoptosis, it was of interest to evaluate physiological cell death during embryonic development *in vivo*. Yamaguchi and colleagues (107) demonstrated that apoptosis occurs during neural tube closure (NTC) by using their specific transgenic mouse (SCAT). This system enables the monitoring of caspase-3 activity based on fluorescence energy transfer (FRET) between two fluorescent proteins (ECFP and Venus), which are linked by the cleavage sequence of caspase 3 (DEVD).

In analogy, the sA5-YFP system should also detect apoptotic cells at the neural ridges and midline of the neural tube during fusion.

In a collaboration, Prof. Masayuki Miura and Dr. Yoshifumi Yamaguchi from the University of Tokyo, Japan kindly imaged the neural tube closure in sA5-YFP embryos. Transgenic E8 sA5-YFP embryos were dissected from the uterus and their yolk sacs. Embryos expressing sA5-YFP were placed into a 35mm glass-bottom dish filled with culture medium and imaged under an inverted confocal microscope at 37°C and 5% CO_2 for 10 h. After 18 min, the first rounded cells labeled by sA5-YFP appeared (Fig. 37A-B). In a similar way as with the SCAT system, “dancing apoptotic cells” were detected, which kept their round shape and moved to the dorsal ridges of the neural plate—without being engulfed—for about 6h. With these experiments, I could conclude that sA5-YFP is able to detect apoptotic cells *in-vivo* in specific tissues during mouse development.

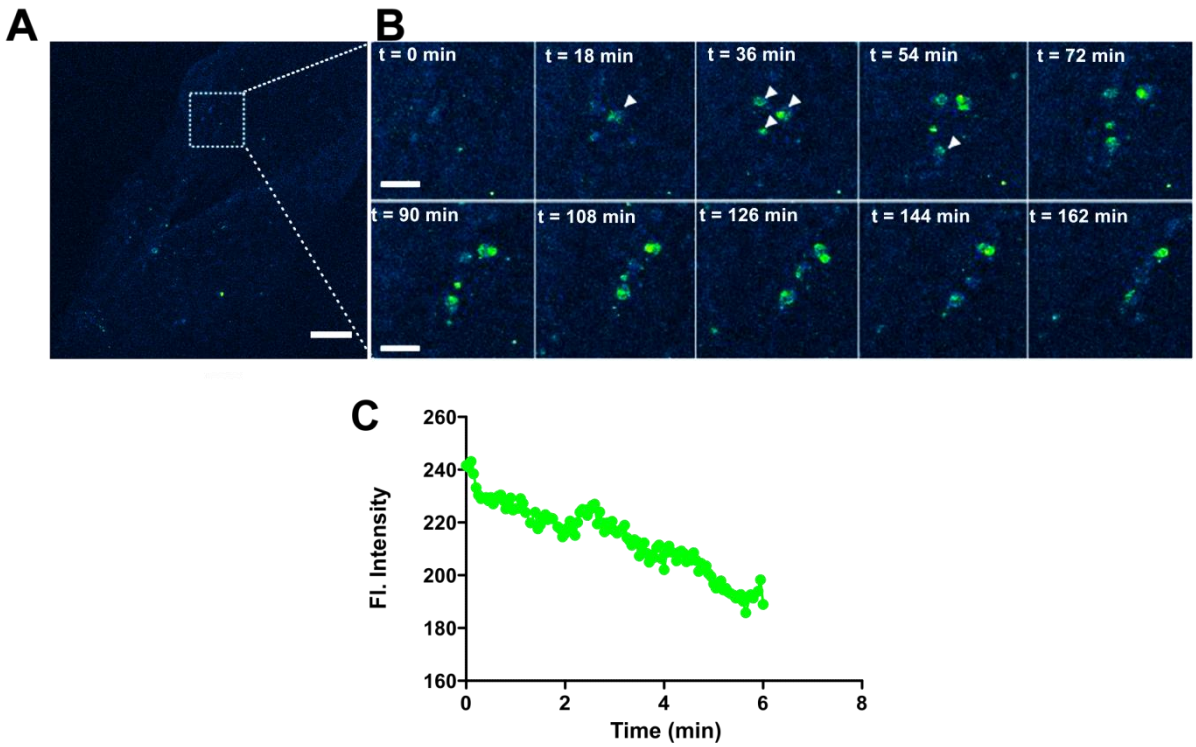

Fig. 37. Real-time detection of apoptosis by sA5-YFP during cranial neural tube closure.

(A) A transgenic E8 sA5-YFP embryo was dissected from the uterus and its yolk sac. It was transferred to a 35mm glass-bottom dish filled with culture medium and positioned under an inverted confocal microscope. The embryo was imaged at 37°C and 5% CO_2. **(B)** Time lapse of the area marked by a white box in A. After 18 min, the first rounded cells labeled by sA5-YFP (white arrows) appeared. Notice that these cells stayed (dancing like) in this area without being engulfed for about 6h. **(C)** Quantitation of sA5-YFP fluorescence signals from (B) over time. Bars are 100 (A), 40 μm (B, C). (Images and graph were kindly provided by Dr. Yoshifuma Yamaguchi and Prof. Masayuki Miura from the University of Tokyo, Japan)

A similar experimental protocol was performed to observe apoptosis during heart development. Transgenic embryos were isolated at E9 and immersed into 2% low-melting agarose in a glass imaging chamber filled with culture medium. The same culture conditions, as in section 3.9, were used (Method 2.6). The imaging was performed by using confocal microscopy for 20 h. A clear increase in accumulation of sA5-YFP in the membrane of dead cells in the ventricle, the epicardium and the outflow tract was observed. After 6 h, the first rounded cells and blebs (indicated by a white plus sign in Fig. 38A) appeared in the right ventricle, the left epicardium, and the outflow tract. Furthermore, it was noticed that some dying cells appeared and disappeared over time (yellow box in Fig. 38A) indicating that they could have been phagocytized by macrophages or by other engulfing cells. Some of the sA5-YFP^+ cells preserved their roundish morphology for the whole time imaging of (arrows in the ventricle). This can be also observed by the increase in fluorescence when the dying cells appeared, the drop in intensity when they disappeared and finally another increase when new dying cells appeared (Fig. 38B).

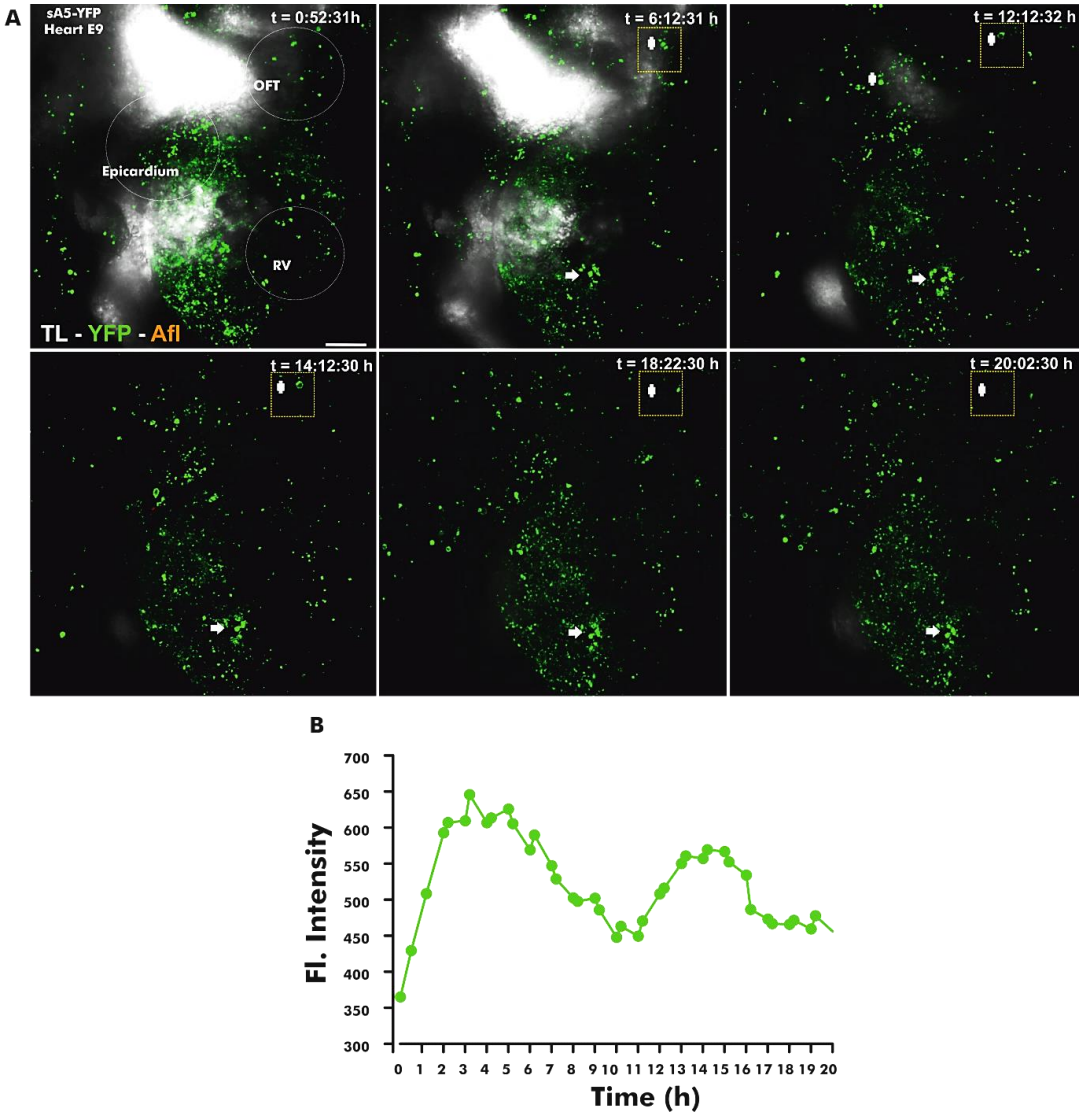

Fig. 38. Long term observation of physiological cell death in a sA5-YFP embryonic heart at E9.

A transgenic sA5-YFP embryo was dissected from the uterus and yolk sac at E9. It was placed sagittal into 2% low temperature-melting agarose contained in a special chamber filled with culture medium. The embryonic heart was observed under an inverted confocal microscope under 37°C and 5% CO_2 conditions for 20 h. **(A)** A clear increase in accumulation of sA5-YFP in the membrane of dead cells was observed in the ventricle, epicardium and outflow tract. Bar is 100 µm. After 1 hour, the first rounded cells and blebs (white plus signal in yellow square) appeared in the outflow track. Notice that cells marked with a white arrow stayed there during the whole time of imaging. **(B)** Fluorescence intensity of the region marked in yellow box in (A). Time-lapse images were recorded every 10 min, Z-stack slices were taken and the images in this figure are maximum projections.

4. DISCUSSION

The motivation of this work was to expand the current knowledge of the role of apoptosis in the developing mouse heart. This might serve as the basis for developing new therapies to treat cardiovascular diseases. For that, I established the CAG-sA5-YFP genetic system to visualize and analyze the rates, localization and identity of apoptotic cells in the embryonic mouse heart *in vivo*.

The functionality and specificity of the CAG-sA5-YFP reporter was first evaluated *in vitro*, in undifferentiated and differentiated mESCs, as well as *in vivo* in a transgenic mouse model generated from the sA5-YFP mESCs. *In vitro,* I showed that the sA5-YFP mESCs ubiquitously expressed sA5-YFP and that ectopically induction of apoptosis by 4-OHT, led to accumulation of the protein in the membrane of apoptotic cells, resulting in an increased intensity of yellow fluorescence. In addition, it was also proven that the sA5-YFP system can detect physiological apoptosis in differentiated mESCs (EBs). I observed several sA5-YFP labeled apoptotic cells in the middle and peripheral regions of the EBs. In addition, I noticed that these cells were mostly in early stages of the apoptosis cascade as marked by the early apoptosis marker, cCaps3, and that very few cells co-localized with the late marker of apoptosis, TUNEL.

The *in vivo* validation consisted of generating a sA5-YFP transgenic mouse line and demonstrating that sA5-YFP^{+} cells were localized in embryonic regions where apoptosis occurs (i.e. brain, yolk sac and otic ring). In addition, these sA5-YFP labeled cells were classified as “apoptotic cells” and “blebs” and were confirmed to be apoptotic cells by co-immunostainings for cCasp3. Moreover, this system proved to be reliable to visualize apoptotic cells in living-embryos. As positive controls, massive cell death was induced in living E8.75 sA5-YFP embryos and sA5-YFP^{+} cells appeared, detached from the tissues and presented typical apoptosis features. Additionally and very importantly, the sA5-YFP system enabled the detection of apoptotic cells during neural tube formation as has already been shown by Yamaguchi and colleagues (107).

After all these validation steps, I evaluated if apoptosis occurs during mouse embryonic development and provided a complete map of the distribution and frequencies of apoptotic cells and blebs during the complete heart embryogenesis (E9.5 to P2). Apoptosis peaked at early stages of development and decreased as the heart grew older. Apoptotic events were

observed in the ventricular trabeculae, indicating that apoptosis might be critical for trabecular formation. In addition, I confirmed that mainly cardiomyocytes undergo apoptosis in the embryonic heart.

In the following sections, I will discuss the advantages and limitations of the sA5-YFP system, the possible role of apoptosis in the developing heart, as well as the probable applications of this live-imaging tool.

4.1. The sA5-YFP system: a straight forward genetic reporter to visualize apoptosis during mouse development *in vivo*

The sA5-YFP mouse line, established in this work, is one of the few genetically encoded reporter tools available, which can reveal spatiotemporal changes and dynamics of apoptotic cells during mouse development *in vivo*. Labeled sA5-YFP cells show typical morphological and biochemical features of apoptotic cells. They round up, detach from tissue boundaries and their chromatin condenses. The sA5-YFP protein binds to PS residues exposed in the outer layer of the apoptotic membrane and it co-localizes with active forms of pro-caspases (caspase 8), effector caspases (active caspase 3 and 7) and with TUNEL staining. Furthermore, blebs of sA5-YFP labeled cells can be detected before they are engulfed, proving that the sA5-YFP reporter allows the visualization of cells in different stages (early-intermediate-late) of apoptosis. Moreover, the sA5-YFP system allows isolation of these blebs also called membrane-bound extracellular vesicles, by fluorescence-activated cell sorting (FACS) or centrifugation, for further analysis.

According to the Nomenclature Committee on Cell Death (NCCD) "*in vivo* studies constitute the ultimate tool to recognize the true importance of cell death signaling pathways and to understand their regulation" (8). However, there are still very few live-imaging tools to visualize different types of programmed cell death in mammals (21, 24, 95, 107, 149-152). Of those, the transgenic mouse line (SCAT3) developed by the group of Professor Masayuki Miura stands out. It enables the monitoring of casp-3 activity based on fluorescence energy transfer (FRET) between two fluorescent proteins (ECFP and Venus), which are linked by the cleavage sequence of caspase 3 (DEVD). Yamaguchi and colleagues used this mouse to describe the role of apoptosis during neural tube closure (107).

The SCAT3 system provides reliable detection of apoptosis. However, the quantification of caspase activation depends on a complex post-imaging processing. To track apoptotic cells, Yamaguchi and colleagues calculated the Venus/ECFP (V/C) ratio. These measurements require a considerable amount of time to make a precise analysis and involve different criteria to discard the noise (±10%) of the V/C. In contrast, the sA5-YFP model allows direct visualization and quantification of apoptotic cells and blebs during long-term observation. The sA5-YFP intensity can be automatically calculated directly after the time-lapse experiment. In addition, the appearance, trajectory and disappearance of apoptotic cells and blebs can be distinguished without the need of further measurements. This is not possible to track with probes or antibodies which are specific to only one time point of the apoptotic cascade (early or late), when the caspase signal disappear or when most of the apoptotic blebs have been engulfed already.

The SCAT3 and the sA5-YFP are powerful live-imaging systems. Both can track physiological and non-physiological apoptosis in living mouse embryos at earlier stages (E8-9.5) for about 8 hours, continuously (107). Using these reporter lines, distribution and morphological changes of apoptotic cells within specific tissues can be described over time. For example, with the SCAT3 transgenic mouse line, it was possible to identify two different types of dying cells during neural tube closure. The "dancing" ones (D-type) that were localized at the edge of the neural ridge. These cells present non-typical apoptosis characteristics, they seem to detach from the rest of the tissue and stay there without undergoing fragmentation (bleb formation) for more than 3 hours of imaging time. They are round in shape and with a diameter size of around 10 µm. The second type (C-type), were cells with typical apoptotic features. They appeared within the tissue, they have smaller diameter size (3 -7 µm), they form blebs after casp-3 activation and finally, they disappear from the tissue. Similarly, sA5-YFP^{+} apoptotic cells and blebs were observed during the neural tube closure using the sA5-YFP.

These apoptotic features and cell patterns were found in E8.75 sA5-YFP embryos after exposition to massive cell death. Different bright sA5-YFP^{+} cells detaching from the neural tube, the heart, and the otic ring were detected. It is known that environmental stress caused by medium depletion induces different types of programmed cell death such as apoptosis, necroptosis and autophagy (97, 153, 154) due to the lack of nutrients, changes in pH and oxygen availability. However, it was clearly demonstrated in tissue sections of E9.5 – 10.5

sA5-YFP embryos that the bright sA5-YFP$^+$ particles co-localized with cleaved caspase 8, 3 and 7, meaning that they were mainly apoptotic cells. These cells presented the typical series of morphological and biochemical features of apoptotic cells, including plasma membrane blebbing, rounding up and shrinkage of the cell and nuclear condensation-fragmentation (155).

One big advantage of sA5-YFP over the SCAT3 system is the stability of sA5-YFP after tissue fixation. Embryos at different developmental stages can be fixed and co-stained with other apoptosis and cell type markers. While embryos in the SCAT3 system have to be stained for casp-3 or 7 and it is not possible to observe co-localization of SCAT3 expression with these markers. In this way, the sA5-YFP is an all-inclusive tool specific for apoptosis, provides more information about cell types undergoing cell death and apoptosis rates in fixed tissue, *ex-vivo,* and *in-vivo*.

4.2. Apoptosis is present in the embryonic mouse heart during all stages of development

Tracking dying cells is very challenging due to the fast speed and asynchrony of the apoptosis cascade. Different cells within tissues are engulfed, shed or dispersed within minutes (72). It is known that each cell has different dying progression kinetics (71, 98). Therefore, techniques based on end time point detection (e.g. TUNEL assay or caspases activation) can lead to misinterpretations or false-positive quantitative results. This is one of the reasons for the many uncertainties and discrepancies in the estimation of apoptosis rates in the myocardium (20). Despite the effort of several research groups in investigating the role of apoptosis in the developing heart (21, 40, 44, 156-159) and in the diseased heart (47, 57, 92, 101, 102, 160, 161), still many questions remain unsolved such as: the time course and duration of the apoptosis cascade (morphological and morphological changes of apoptotic cells), the mechanism of removal of dead corpses, the cell types undergoing apoptosis and an accurate quantification throughout the stages of heart organogenesis.

Using the CAG-sA5-YFP mice, it was possible for the first time to give a complete map of the distribution and incidence of apoptotic cells and blebs in the embryonic mouse heart from E9.5 to P2. The quantitation data indicated that apoptosis peaks at early stages of heart organogenesis (E9.5 – E13.5) and decreases from E15.5 onwards. With both quantified parameters, marked sA5-YFP$^+$ apoptotic cells with condensed nuclei and sA5-YFP$^+$ blebs without nuclei, the percentage of apoptosis was less than 1.5 % between E9.5-E11.5, less than

0.5% from E12.5 – E14.5 and less than 0.25% from E15.5 to P2. This correlates with the results presented by Sharma and colleagues (43). They quantified the number of high-intense and low-intense TUNEL$^+$ signals divided by the total number of cells per template (apoptosis index) in mouse hearts from E10.5-E11.5. Similarly to the sA5-YFP quantification, they claimed that less than 1% of the apoptotic cells with low-intense signals were found throughout the analyzed embryonic mouse hearts.

On the other side, Sharma et al., also observed that high levels of apoptosis (more than 4%) as measured by TUNEL$^+$ nuclei, occur at E12.5-E13.5 at the endocardial cushions in the OFT. Likewise, Abdelwahid and coworkers (44) reported that between 2 - 4 % of apoptotic cells (TUNEL$^+$ signals) are present in the ventricular wall of hearts among E11.5 – E14.5 decreasing to less than 0.5 % after E16.5. This was not observed in E12.5 sA5-YFP hearts in which TUNEL$^+$ signals were rarely found per section and from these very few co-localized with apoptotic cells marked by sA5-YFP. This observation matches the remarks made by Van Ham and colleagues (108) in the secA5-YFP zebrafish system. They noticed that the brightest TUNEL$^+$ signals were not positive for YFP and showed no nuclear staining. They concluded that these cells were in the final stage of apoptosis where DNA fragmentation is massive and apoptotic cells do not have a defined cell membrane and nucleus.

From these data, I observed that the percentage of apoptosis present in the embryonic heart is high, compared to the reported basal levels in the adult heart (≤1.5% vs. 0.001%, respectively) (162, 163). A precise estimation of apoptosis rates is critical to know, as slight variations in the apoptotic cell number could lead to heart failure. For example, Kitsis and colleagues showed that that apoptotic rates of less than 0.023% are sufficient to induce a lethal, dilated cardiomyopathy in adult mouse hearts using an elegant inducible transgenic system for caspase 8 activation (163). These levels of apoptosis are four-to tenfold lower than the one reported in other studies (101, 102). To know, if apoptosis inhibition might constitute the basis to develop new therapies, it is critical to make a precise calculation of the apoptosis rates during heart development and in the adult heart. Kitsis and coworkers proved that the specific inhibition of caspase activation by the polycaspase inhibitor IDN 1965 prevented the development of cardiomyopathy. Another study from Sarosiek and colleagues (63) confirmed that the embryonic and postnatal heart is primed for apoptosis. When young hearts are exposed to death signals such as irradiation or chemotherapy agents used in young cancer patients, these patients developed cardiotoxicity. They proved that suppression of genes from

the intrinsic apoptosis pathway (e.i. Bax and Bak) reversed the effects caused by the death ligands. In this project, I corroborated that apoptosis is high at early stages of heart development and decreases in later stages coinciding with the reports of Kitsis and Sarosiek discussed in this paragraph.

4.3. The sA5-YFP system overcomes limitations of single apoptosis endpoint measurements

One of the most used assays for detecting apoptosis in heart tissue is TUNEL. However, it has been observed that the numbers of cells undergoing apoptosis in the heart could be overestimated when techniques based on DNA end-labeling are used. For example, several groups have reported high rates (5 to 35%) (20, 101) or lower rates (0.023 to 2.5 %) (102, 163, 164) of apoptosis in hearts of patients with late-stages of dilated cardiomyopathy. This indicates that even if TUNEL assay has been widely accepted as apoptosis marker, it can lead to false-positive results (19, 100). As it is a DNA fragmentation-based method it is not known how much DNA has to be fragmented until the TUNEL method gives a positive signal (20). In addition, it has been shown that TUNEL labels not only apoptotic but also oncotic nuclei (165), as well as nuclei undergoing DNA repair (166) and duplication (100). Therefore, critical caution has to be taken whenever DNA-fragmentation-based analysis is performed.

In addition, as the NCCD recommends, it is necessary to use at least two biochemical methods besides morphological characteristics to define the type of programmed cell death (103). Therefore, the previous studies discussed in this section, have to be complemented and confirmed by other analysis using different detection techniques that cover the whole range of the apoptosis cascade. It is important to highlight that the sA5-YFP detection method meets these criteria. It combines the detection of morphological changes and the biochemical changes of PS translocation to the outer membrane of apoptotic cells and it can be combined with immunostainings to detect chromatin condensation and caspases activation.

4.4. Apoptosis may play a role in the remodeling of the ventricular chamber during heart development

It has been previously reported that apoptotic cells are present in specific areas within the developing avian and mammalian heart at specific time points. The main locations of apoptosis in chicken, mouse, rat, and human, that have been reported so far, are the outflow tract cushions, the atrioventricular cushions, walls of the aorta and pulmonary trunk and the interventricular septum (167). These areas suffer striking morphological changes, remodeling,

and septation. For example, it has been demonstrated that apoptosis in the outflow tract is needed for its correct shortening and its separation into the aorta and pulmonary trunk (21, 40, 42, 158). Likewise, the incidence of apoptosis in the atrioventricular cushions correlates with their reshaping to form the atrioventricular valvar leaflets at E13.5 in the mouse heart (43). Using the sA5-YFP mice, it was possible to identify apoptotic cells and blebs in the ventricles, in the endocardial cushions at E11.5 - E12.5, in the atrium and in the apex of the interventricular septum from E11.5 – E13.5 (Fig. 25, Fig. 31), confirming previous research.

In despite of the efforts of several groups, the role of apoptosis in the developing of the heart chambers and trabeculae is still not clear, especially in a complex model such as the mouse heart, due to the lack of accurate detection techniques. Until to date, different studies have shown that the most prominent area of apoptosis in the ventricles is the interventricular septum and compact myocardium in the early embryonic mouse heart. Abdelwahid and colleagues (44) found that the peak of $TUNEL^{+}$ foci at E13.5 was in the apex of the interventricular septum, in the compact myocardium and to a lesser extent in the trabeculae of the murine heart. In contrast, one year later another study showed that the number of apoptotic cells marked by TUNEL staining in the trabeculae increased progressively from E13.5 to P2 (168). However, Sharma and colleagues (43) as well as Barbosky and colleagues (21) have shown that apoptosis in the trabeculae occurs only at very low level than in other regions (21, 43). Due to the low detected apoptosis incidence in this region, cell death in the trabeculae can be easily missed.

In contrast to earlier studies, apoptotic events in sA5-YFP hearts were observed for the first time in the primitive ventricle at E9.5 and in the trabeculae of both ventricles from E10.5 - E14.5. The early detection of apoptotic cells by sA5-YFP, before they are engulfed, is the difference of these clear findings in comparison with the techniques (TUNEL, Lysotracker Red) used in previous studies. The sA5-YFP apoptotic bodies were localized at the lining of the ventricular trabeculae (Fig. 30, Fig. 31) coinciding with episodes of trabeculae formation, differentiation, remodeling, and compaction. As reviewed in section 1.2.1 remodeling of trabeculation of both, ventricles and atria, is a critical process for chamber maturation and formation of papillary muscles and pectinate muscles, respectively.

According to the review articles of Sedmera and colleagues (28) and Samsa and colleagues (25), trabeculations are first evident after cardiac looping around E9.5 - E10.5 in the mouse

heart. They are formed due to the self-contraction and differentiation of the myocardial cells adjacent to the luminal side of the primitive ventricle (Fig. 3A-B). Here, the trabecular ridges are spaced at regular intervals along the ventricle. These first signs of trabeculae formation were observed in sA5-YFP embryos at E9.5 and coincided with the presence of bright sA5-YFP^{+} particles throughout the ventricle (Fig. 24). In further developmental stages, between E11.5 - E13.5, the trabeculae are extensive, they grow centripetally towards the lumen and have a similar pattern in both ventricles. Cardiomyocytes in the trabecular luminal side are more differentiated than those in the compact myocardium (Fig. 3). Surprisingly, numerous labeled sA5-YFP apoptotic bodies were mainly found in the ventricular trabeculae close to the developing valves and in the non-compact zone, where the cardiomyocytes are more differentiated, at E12.5 and E13.5. This occurs just before the trabeculae fuse to form the papillary muscles and re-orientate towards the outer myocardium at E14.5 to start compaction. From E14.5 onwards, cardiac septation ends and the trabeculae start thickening due to compaction. It is here where the myocardial mass increases, the proliferation rates in the compact layer and coronary vessels rise and capillaries invade the chambers (Fig. 3D). Apoptotic bodies marked by sA5-YFP were scarcely found in the compact myocardium from E15.5 onwards suggesting that apoptosis is switched off as the heart grows older in agreement with other studies (63, 159, 169).

Trabeculae are needed to provide sufficient pumping function during growth, to separate blood currents in the pre-septation heart and to facilitate oxygen and nutrient exchange in the embryonic myocardium before coronary vascularization (33). Changes in shape and proportions of compact and trabecular myocardium have been observed in congenital morphological and functional abnormalities. Human hearts with different cardiomyopathies have shown left ventricular non-compaction, hypertrabeculation (abnormal numbers and thickness of trabeculae) and right ventricular disorders (170).

Genes such as NRG1 (Neuregulin-1), ERBB2 (Receptor tyrosine-protein kinase), FKBP12 (Peptidyl-prolyl cis-trans isomerase), Bmp10 (Bone morphogenetic protein), Nkx2.5 (Homeobox 5-containing transcription factor), among others, are involved in trabecular formation and remodeling (25, 28, 171). For example, it has been demonstrated that transgenic over-expression of Bmp10 in developing heart leads to excessive trabeculation and severe heart failure (171). FKBP12-deficient mice die around E14.5 due to severe cardiac defects. These embryonic hearts present increased number and thickness of ventricular

trabeculae, deep inter-trabecular spaces, thin compact area and prominent ventricular septal defect. These features are similar to those of patients with left ventricular non-compaction (172). In addition, NRG1, ERBB2, and ERBB4 deficiency results in embryonic lethality due to the absence of trabeculation (25).

The exact role of apoptosis in congenital heart diseases, such as non-compaction defects, is still not completely determined. However, there is some evidence that apoptosis dysfunction is associated with heart anomalies. Left ventricular non-compaction is related with mutations in the mitochondrial genome that leads to downregulation of apoptosis (53). This coincides with studies showing that apoptosis in the ventricular wall during development is mediated by proteins of the mitochondrial pathway (44, 63, 169). In addition, hearts of knockout mice of apoptosis genes such as casp-3, 7, 8, FADD and c-FLIP developed noncompact myoarchitecture (53, 61). Taking all together, the sA5-YFP mouse model can help to further investigate the role of apoptosis in normal and abnormal trabeculae formation. Co-stainings for genes such as Nrg1, ErbB2, ErbB4 and Bmp10 can be performed in sA5-YFP heart sections to evaluate if apoptosis is related to trabeculae formation and remodeling. In addition, the sA5-YFP mouse can be crossed to knockout models such as the FKBP12-deficient mice mentioned above to further investigate in detail the role of apoptosis in non-compaction defects.

4.5. Cardiomyocyte apoptosis in the embryonic mouse heart correlates with changes in remodeling and differentiation

For several years, it was not completely clear which cells will undergo apoptosis to achieve a proper heart formation. In the 60's, degenerating cardiac muscle cells in the developing ventricular muscle were observed in the developing chick ventricle using electron microscopy. These cells were mainly found in large intercellular spaces or engulfed by phagocytes (39). Other studies in the 90's, claimed that apoptotic cells in the endocardial cushions were mainly from non-myocardial origin (i.e. neural crest-derived) (46, 157, 167, 173). In the 2000s, some works in chick (42, 158) and mouse (21, 43, 44) (174) suggested that cardiomyocytes undergo apoptosis in the outflow tract, endocardial cushions, and ventricular chamber. Consistently, in this work it was clearly demonstrated that the labeled sA5-YFP apoptotic cells, found in the trabeculae, co-localize mainly with cardiomyocytes around days E13.5 – E14.5 of mouse heart development.

These results are consistent with previous research in which it was observed that cleaved caspase 3 staining co-localized with cardiomyocyte markers (α-Actinin and MF20) in the developing mouse heart (21). These apoptotic cardiomyocytes were localized in the OFT and the lining of trabeculae in E13.5 – E14.5 heart sections. This study provided good evidence that many dying cells at these sites were apoptotic cardiomyocytes. However, it was limited by not showing co-localization of cardiomyocytes markers with the apoptotic cells labeled by LTR or TUNEL. The authors, themselves, mentioned that these techniques are not the most adequate to determine the cell type undergoing apoptosis because they label lots of apoptotic debris which lack membrane epitopes or apoptotic particles that have been already phagocytized by neighboring cells.

In contrast, by using the sA5-YFP system it was possible to identify and for the first time quantify the correlation of apoptotic cells and blebs with their specific cell type before cell membrane disruption. It is known that around E13.5 - E14.5 the mouse heart consists of 4 cell layers (Fig. 3). Through co-stainings for different cell types in sA5-YFP heart sections, it was found that more than 66% of the labeled sA5-YFP cells were cardiomyocytes at E13.5. The rest were smooth muscle cells, leukocytes, endothelial cells and mesenchymal cells (Fig. 35). This is consistent with other studies that have qualitatively identified by using electron microscopy and histological analysis that endocardial, mesenchymal, and mainly myocardial cells undergo apoptosis in the embryonic mouse heart (21, 44, 174).

Cardiomyocyte apoptosis in the developing heart has been related to areas of remodeling and differentiation. Apoptotic cells have been found to be distributed mainly in the differentiated parts of the mesenchyme of the endocardial cushion around E11 – E14 of mouse heart development. Differentiation of endocardial cushions into valvuseptal tissue correlates with expression of the bone morphogenic proteins Bmp-2, Bmp-4 and the homeobox gene Msx-2 (158, 174). These proteins are generally involved in morphogenesis, cell differentiation and induction of apoptosis (174, 175). In addition, work performed in embryonic chick heart suggest that apoptosis is related to differentiation of the cardiac conduction system as apoptotic cells were found in the trabeculae (158). Furthermore, apoptosis might be related to perinatal maturation of cardiac muscle fibers in the ventricular chamber (49). Similarly, in the sA5-YFP hearts at E11.5 – E14.5 apoptosis was mainly found in the ventricular trabeculae where cardiomyocytes are more differentiated than in the compact zone (28, 176). These findings imply a role of cardiomyocyte apoptosis in ventricular differentiation. However, gene

expression patterns for genes involved in trabeculae formation, as suggested in section 4.4, should be performed to clearly correlate apoptosis with areas of differentiation.

4.6. Relevance of the sA5-YFP system as in vivo marker of cardiovascular diseases

As already mentioned, inhibition of apoptosis might be used as a treatment for heart diseases. For example, Sarosiek and colleagues (63) have recently shown that young patients treated with radiation or genotoxic chemotherapies develop cardiotoxicity. Hearts of these children were characterized by reduced ejection fraction, thin ventricular walls, and altered myocyte architecture. This side effect was not present in adult patients. The cause was linked to a high activity of the intrinsic apoptosis pathway at early stages of life. Mitochondrial pro-apoptosis factors such as BAK and BAX, are highly expressed in young hearts, but they are nearly absent in adulthood. Thus, young hearts are prone to apoptosis in response to genotoxic damage. Inhibition of both of these proteins in mice mitigates the cardiotoxicity effects. Similarly, stimulation of the expression of anti-apoptotic proteins in the mitochondria, such as Bcl-xL protein, may reduce myocyte cell loss caused by high apoptosis rates found in hearts of E17.5 and P1 mice lacking cardiac muscle α-actin (49). These results are consistent with the findings presented in this work. Using the sA5-YFP mouse it was shown that apoptosis strongly decreases from E15.5 onwards. Thus, confirming that apoptosis is switched off in later adult stages and it may be switched on again (44, 159) after a strong cellular stress caused by, for example, myocardial infarction or ischemia reperfusion (177).

It is noteworthy to again mention that the accurate detection of apoptosis in healthy or diseased hearts is critical to understand to which extent apoptosis leads to heart disease. For example, it is known that hearts of normal rodents and humans present a baseline frequency of apoptosis of 1 - 10 apoptotic cells/10^5 nuclei (162), while only 23 apoptotic cells/10^5 nuclei are able to induce a lethal, dilated cardiomyopathy in mice (163). Kitsis and Mann (177) claim that there are still critical gaps in knowledge concerning the true rates of cardiac myocyte apoptosis in heart failure as well as the mechanisms controlling it. As apoptosis is an asynchronous process, single apoptosis endpoint measurements do not provide enough information about dynamics and extent of apoptosis. The only way to detect these small changes in apoptosis rates, which can lead to heart diseases, is by *in vivo*-imaging of the heart using probes that can identify cells in different stages of the apoptosis cascade.

As it was validated in this work, the sA5-YFP system allows the quantitative, *in vivo* imaging of apoptotic cells during development (Figs. 33-35). Therefore, it can be used to monitor natural occurring and ectopic levels of apoptosis over time. Fluorescence labeled Annexin V has been proven to be a suitable imaging marker of cardiovascular risk and apoptosis (151). Dumont and colleagues (149) could visualize membrane changes of single cardiomyocytes undergoing apoptosis in adult mouse hearts with an ischemia-reperfusion injury in real-time by Annexin-V-Oregon Green (Anx-V-OG). Similarly, high uptake of radiolabeled Annexin V has been found in rabbit, swine and human hearts with atherosclerosis, left ventricular dysfunction and ischemia reperfusion (151, 178-181). The greatest disadvantages of the systemic injection of Annexin V into adult animals are its elevated cost derived from high concentrations needed to penetrate the tissues and the variation in signal intensity depending on the efficacy of the injection protocol (99). In contrast, the genetically encoded aA5-YFP system expresses continuously the protein, thereby avoiding these problems. It detects clearly apoptotic signals *in vivo*, *ex vivo* and in fixed tissue sections. In addition, it can be crossed with mouse models of cell death and heart disorders to get further insights into the mechanisms of apoptosis.

4.7. Limitations of the sA5-YFP system as apoptosis marker during mouse development

There are some limitations concerning the detection of apoptosis by the sA5-YFP reporter system. First, the sA5-YFP detection specificity is determined by the time kinetics of phosphatidylserine (PS) externalization on the surface of the apoptotic cell membrane. Taking into account that PS distribution varies in each cell type, that the mechanisms of externalization are not completely understood (182) and that in this model A5-YFP is secreted to the extracellular space, it cannot be assured that sA5-YFP will not bind to intracellular PS. It has been shown that intracellular PS is mainly distributed in the inner plasma membrane, nuclear membrane, endoplasmic reticulum and secretory vesicles (182, 183). For instance, I identified two types of sA5-YFP$^+$ signals in sA5-YFP heart sections at E10.5 – E11.5: bright punctate sA5-YFP$^+$ cytoplasmic signals and the typical sA5-YFP membrane ring-like signal. This can be explained by recent evidence showing that extensive plasma membrane-derived cytoplasmic vesicles are formed during apoptosis (182). However, as it was not verified that these cytoplasmic signals were apoptotic cells, I defined only clear and bright sA5-YFP$^+$ signals surrounding the cell membrane as apoptotic cells or blebs for quantification.

Another issue related to the dynamics of PS externalization is the difficulty in defining the exact time in which sA5-YFP will bind to PS in different apoptotic tissues. In sA5-YFP embryoid bodies and transgenic mouse hearts, the co-localization of sA5-YFP with cCasp3 was not 100%. This may be due to different possible reasons. First, the exposure of PS to the outer membrane of apoptotic cells occurs before or later than caspase-3 activation (69, 184, 185). Second, sA5-YFP detects apoptotic blebs where cleaved caspase-3 is not present due to its different distribution in the numerous membrane blebs formed after fragmentation. Third, YFP^+ signals may co-localize with other executing caspases such as cleaved caspase 7 or 6. And finally, the sA5-YFP detection is caspase independent indicating that Annexin V detects other types of cell death such as necrosis or necroptosis (186, 187).

The potential binding of Annexin V to necrotic, oncotic cells (65, 142, 181) or to cells undergoing other programmed cell death types such as necroptosis (188), pharanathos or netosis (8) can be seen as a drawback in its specificity. It is known that apoptosis and necroptosis may occur in the same organ (79). In this work, it was proven in transgenic ESCs that the sA5-YFP system detects caspase independent cell death after inhibition of caspases (Fig. 17). However, it was not possible to detect necroptosis by the pan-caspases inhibitor zVAD-fmk in sA5-YFP embryos during neural tube closure (these experiments were performed by Prof. Miura and Dr. Yoshifumi; data not shown). This result could be due to low tissue penetration of the drug. Therefore, further experiments in the future are needed to confirm *in vivo,* the results observed in the sA5-YFP mESCs. One way to confirm that caspase independent cell death occurs in the embryonic heart, the sA5-YFP mouse model should be crossed with knockout models of necroptosis (e.g. RIPK3 or MLKL deficient mice) (89). If in these mice the amount of sA5-YFP^+ particles is less than in transgenic sA5-YFP embryonic hearts, then necroptosis should be present together with apoptosis during mouse heart development. On the contrary, if the number of sA5-YFP^+ particles is approximately the same than in sA5-YFP hearts, then it means that only apoptosis takes place.

Despite these restrictions, the sA5-YFP system used with time lapse imaging is more advantageous in comparison to one time-point apoptosis detection methods. Approximately two fold more sA5-YFP signals than cCasp3 signals could be detected (Fig. 31), indicating that this system allows the detection of a broader spectrum of apoptosis stages. In addition, the sA5-YFP transgenic mouse allows the *in-vivo* monitoring of apoptotic cells and blebs in early to late apoptotic stage during mouse embryonic development. Moreover, its potential to

detect caspase independent cell death can help to elucidate different programmed cell death mechanisms occurring under physiological and non-physiological conditions in the embryonic mouse heart.

The feasibility of the sA5-YFP reporter to study apoptosis in healthy postnatal and adult mouse hearts and after acute myocardial infarction remains to be validated. Based on preliminary analysis, I could observe that apoptosis rates significantly decreased in P2 hearts and that it was scarcely present in the adult heart (Fig. 32). However, as the focus of this study was the embryonic heart, a deeper characterization of the sA5-YFP signals in the adult heart has to be performed. First, it needs to be assessed carefully, whether the strong sA5-YFP expression in muscle cells driven by the chicken β-actin promoter with CMV enhancer element (CAG) (189) allows to distinguish bright sA5-YFP$^+$ signals from "background" expression. I found in these preliminary experiments the background fluorescence to be quite high probably because of the prominent release of the transgene product into the extracellular space. In addition, also co-localization of these signals with cCasp3 should be performed. Afterwards, in case that the signal to noise ratios is sufficient to detect proper apoptotic signals, it would be very interesting to evaluate if apoptosis is induced after ischemia-reperfusion as it has been reported before (149). As discussed in section 4.2 there is a huge discrepancy in the reported numbers of apoptotic cells present in the diseased heart and it is still unclear whether apoptosis is the main cell death mechanism after infarction (20).

4.8. Outlook

This work has confirmed and extended the current literature about apoptosis rates and localization of apoptotic cells during mouse heart development. Using the sA5-YFP reporter system, it was possible to report that less than 1.5% of the cells in the embryonic heart undergo physiological apoptosis. For the first time, it was shown that apoptosis is common at early stages of heart development starting from E9.5. It was confirmed that apoptosis rates decrease as the heart ages. Furthermore, it was clearly observed that apoptosis is highly present in the ventricular trabeculae and in other regions such as the outflow tract, interventricular septum, and atria. However, there are still some questions to be addressed to understand the role of apoptosis during mouse heart development. For example, it would be insightful to know which apoptosis pathway, intrinsic or extrinsic, correlates with the sA5-YFP^+ apoptotic cells and blebs. This would help to better design treatments based on apoptosis regulation for cardiovascular diseases.

Previous research suggests that both mechanisms control apoptosis in different areas of the heart during embryogenesis (190, 191). For example, expression of Fas and FasL, both members of the death receptor family that activate the extrinsic apoptosis pathway, was found in atria and ventricles, but not in the outflow tract septum or endocardial cushions (43). Other studies have shown that pro-apoptotic members of the Bcl-2 family (e.g. Bax and Bik), which regulate the mitochondrial or intrinsic apoptosis pathway, are also expressed in the embryonic heart (44, 63, 159) in patterns similar to apoptotic cells labeled with TUNEL. To confirm these results, it is not only necessary to show a correlation of these proteins in the apoptotic regions, but a clear co-localization with apoptotic cells. The sA5-YFP system is suitable to assess this issue. In fact, in this work, I showed that labeled sA5-YFP apoptotic cells co-localized with cleaved caspase 8, a member of the extrinsic apoptotic pathway, in E10.5 embryos. In a similar way, expression of Bax or Bik and cleaved caspase 9 can be correlated to sA5-YFP positive to show that the intrinsic pathway is involved.

Another question to be answered is if the sA5-YFP system detects caspase independent cell death in tissues. This can be monitored by *in-vivo* confocal imaging of sA5-YFP embryos at E8.5 – E9.5 after inhibition of caspases using the z-VAD-fmk inhibitor. This pan-caspase inhibitor has been widely used to detect caspase independent cell death and necroptosis (86, 188, 192). If bright sA5-YFP^+ signals are still detected after caspase inhibition then the system can detect other programmed cell death types. As it has been recently identified that

autophagic cell death occurs during heart organogenesis (95), it will not be surprising to find an interplay between apoptosis, necroptosis and autophagic cell death regulating cardiac morphogenesis.

These caspase inhibition experiments can also be performed to investigate if downregulation of apoptosis in the embryonic heart leads to hypertrabeculation or ventricular chamber malformation. Watanabe and colleagues have shown that inhibition of apoptosis in the chick embryonic heart leads to abnormal outflow tract shortening and ventriculo-arterial connections, associated with congenital conal heart defects (54). This together with the assessment of gene expression patterns for genes involved in trabeculae formation can help to elucidate the role of apoptosis during heart development.

In conclusion, the CAG-sA5-YFP system has the potential to mark apoptotic cells in different tissues and cell types. This makes it feasible to explore not only the role of apoptosis in mouse heart development but also in a variety of diseases. In addition, it can be crossed with different knockout models of apoptosis genes to reveal mechanistic insights and new modulators of the apoptosis cascade that may be used as therapeutic targets.

5. CREDITS

I would like to give credit to the colleagues mentioned below for their contribution to this work:

Name	Experiment
Dr. Michael Hesse and Patricia Freitag from the Institute of Physiology I, University of Bonn, Germany.	Diploid aggregation to generate the CAG-sA5-YFP mouse line.
Prof. Masayuki Miura and Dr. Yoshifumi Yamaguchi from the University of Tokyo, Japan.	Live-imaging of apoptotic cells during neural tube closure in sA5-YFP mice.
Dr. Alexandra Raulf and Katia Herz from the Institute of Physiology I, University of Bonn, Germany.	Guidance and support to optimize the live-imaging experiments.
Dr. Carolina Geisen from the Institute of Physiology I, University of Bonn, Germany.	Guidance and support to optimize the cloning strategy to generate the CAG-sA5-YFP plasmid.

6. SUMMARY

All living organisms face death since the beginning of their lives. Cells commit suicide to sculpt correctly all organs during animal development. Currently, there exist at least 13 cell death modalities through which a cell is programmed to die. From these, the most studied is apoptosis. Despite the huge progress made in the field of apoptosis, little is known about its role in mouse heart development and it is still not clear if its upregulation or downregulation can lead to heart disease. One of the main reasons for this uncertainty is the lack of techniques that mark apoptotic cells at different time points *in vivo* and in fixed tissue. With a specific and broad detection method that overcomes the asynchrony and rapidity in which apoptotic cells die and disappear from tissues, it should be possible to confirm if apoptosis takes place during mouse heart development, in which areas and at which specific rates occurs during different embryonic stages and which are the cells that undergo apoptosis during heart morphogenesis.

In this work, I addressed these issues by establishing a genetically encoded reporter tool used to visualize and quantify apoptosis during mouse heart development *in vivo*. This system is based on the detection of phosphatidylserine (PS) residues—exposed in the outer membrane of apoptotic cells—by Annexin V (A5). Commercial probes of A5 linked to fluorescent probes have been developed. These probes provide excellent results in cells, but have some limitations such as high cost and not-specific for fixed tissue, when used in fixed tissue or in living organisms by systemic injection. Therefore, this system was aimed to overcome these drawbacks by ubiquitously expressing a secreted human Annexin V (sA5) fused to the yellow fluorescent protein (YFP). The ubiquitous expression was ensured by the chicken β-actin promoter with CMV enhancer element (CAG). As cells undergo apoptosis, sA5-YFP binds with high affinity to its PS residues resulting in bright fluorescent signals. In this way, it was possible to better characterize, quantify and monitor apoptotic signals in the developing mouse heart over time.

In summary, this study consisted of two major goals. The first one was to validate the sA5-YFP system, *in vitro* and *in vivo*, to specifically label apoptotic cells. The second goal was to use this system to describe the apoptotic patterns and rates during all stages of embryonic heart development in more detail. For the first part, I could show that the labeled sA5-YFP signals in transgenic mESCs, in EBs, and in sA5-YFP mice were apoptotic cells after inducing apoptosis ectopically or in entities (EBs and embryonic tissue such as neural tube,

otic placode and yolk sac) in which apoptosis is a physiological process. These cells presented the typical morphological and biochemical changes of apoptotic cells. They rounded up, detached from the culture plate or tissue compound, formed membrane blebs or fragmented, and displayed condensed chromatin. Moreover, the sA5-YFP protein co-localized with active forms of pro-caspases (casp-8), effector caspases (active casp-3 and 7) and with TUNEL staining. Thus, I proved that the sA5-YFP system allows the visualization of cells and blebs (fragments of apoptotic cells) in different stages (early-intermediate-late) of apoptosis.

For the second goal, I used the transgenic CAG-sA5-YFP mouse line to provide detailed information about apoptosis rates, distribution of apoptotic events and cells undergoing apoptosis during mouse heart development. I could show that apoptosis takes place at all stages of the mouse heart development starting from E9.5. I observed than less than 1.5% of the cells in the embryonic heart undergo physiological apoptosis and the apoptosis rates decrease as the heart ages. In contrast to earlier studies, apoptotic cells were observed very clearly in the primitive ventricle at E9.5 and in the lining of the trabeculae of both ventricles from E10.5 - E14.5 in sA5-YFP hearts. These events coincide with episodes of trabeculae formation, differentiation, remodeling, and compaction, suggesting that apoptosis might be necessary for chamber maturation. In addition, I noticed apoptotic events in the outflow tract, the interventricular septum, and atria, coinciding with previous reports. Lastly, I demonstrated that the labeled sA5-YFP apoptotic cells, found in the trabeculae, co-localize mainly with cardiomyocytes around days E13.5 - E14.5 of mouse heart development. These findings imply a role of cardiomyocyte apoptosis in ventricular differentiation. However, more experiments are needed to undercover the biological role of apoptosis in trabeculae formation.

Last but not least, I provided evidence that the CAG-sA5-YFP mouse model enables the real-time imaging of induced apoptosis and physiological occurring apoptosis in the developing mouse embryo at E8.75 and in the embryonic mouse heart at E9. Apoptotic signals can be identified by their roundish morphology and bright sA5-YFP^{+} signals. Fluorescence intensity of sA5-YFP can be used as quantitative parameter to evaluate changes in apoptosis *in vivo*. This means that this reporter line can be used to monitor the distribution and morphological changes of apoptotic cells within specific tissues over time in living organisms. In conclusion, the sA5-YFP mouse has the potential to unravel the physiological role of apoptosis in the

developing heart, its role in the formation of other mammalian organs, and in diseases displaying aberrant patterns of apoptosis.

7. REFERENCES

1. TheFamousPeople. 8 Famous Quotes By Arthur Schopenhauer [cited 2017]. Available from: http://quotes.thefamouspeople.com/arthur-schopenhauer-237.php.
2. Clarke PG, Clarke S. Nineteenth century research on naturally occurring cell death and related phenomena. Anat Embryol (Berl). 1996;193(2):81-99.
3. Jacobson MD, Weil M, Raff MC. Programmed cell death in animal development. Cell. 1997;88(3):347-54.
4. Reynaud K, Driancourt MA. Oocyte attrition. Mol Cell Endocrinol. 2000;163(1-2):101-8.
5. Fuchs Y, Steller H. Programmed cell death in animal development and disease. Cell. 2011;147(4):742-58.
6. Elmore S. Apoptosis: a review of programmed cell death. Toxicol Pathol. 2007;35(4):495-516.
7. Thompson CB. Apoptosis in the pathogenesis and treatment of disease. Science. 1995;267(5203):1456-62.
8. Galluzzi L, Vitale I, Abrams JM, Alnemri ES, Baehrecke EH, Blagosklonny MV, et al. Molecular definitions of cell death subroutines: recommendations of the Nomenclature Committee on Cell Death 2012. Cell death and differentiation. 2012;19(1):107-20.
9. Hockenbery DM, Oltvai ZN, Yin XM, Milliman CL, Korsmeyer SJ. Bcl-2 functions in an antioxidant pathway to prevent apoptosis. Cell. 1993;75(2):241-51.
10. Sarosiek KA, Letai A. Directly targeting the mitochondrial pathway of apoptosis for cancer therapy using BH3 mimetics - recent successes, current challenges and future promise. FEBS J. 2016;283(19):3523-33.
11. Li NL, Nie H, Yu QW, Zhang JY, Ma AL, Shen BH, et al. Role of soluble Fas ligand in autoimmune diseases. World J Gastroenterol. 2004;10(21):3151-6.
12. Liu Y, Shoji-Kawata S, Sumpter RM, Jr., Wei Y, Ginet V, Zhang L, et al. Autosis is a Na+,K+-ATPase-regulated form of cell death triggered by autophagy-inducing peptides, starvation, and hypoxia-ischemia. Proc Natl Acad Sci U S A. 2013;110(51):20364-71.
13. Alberts B, Johnson, A., Lewis, J., et al. Molecular Biology of the Cell. 4th edition. . New York: Garland Science; 2002. Available from: http://www.ncbi.nlm.nih.gov/books/NBK26837/.
14. Baehrecke EH. How death shapes life during development. Nat Rev Mol Cell Biol. 2002;3(10):779-87.
15. Manesso E, Toffolo GM, Saisho Y, Butler AE, Matveyenko AV, Cobelli C, et al. Dynamics of beta-cell turnover: evidence for beta-cell turnover and regeneration from sources of beta-cells other than beta-cell replication in the HIP rat. Am J Physiol Endocrinol Metab. 2009;297(2):E323-30.
16. Fuchs Y, Steller H. Live to die another way: modes of programmed cell death and the signals emanating from dying cells. Nat Rev Mol Cell Biol. 2015;16(6):329-44.
17. WHO. The top 10 causes of death 2017 [cited 2017]. Available from: http://www.who.int/mediacentre/factsheets/fs310/en/.
18. WHO. Cardiovascular diseases (CVDs) 2017 [cited 2017]. Available from: http://www.who.int/mediacentre/factsheets/fs317/en/.
19. Takemura G, Kanoh M, Minatoguchi S, Fujiwara H. Cardiomyocyte apoptosis in the failing heart--a critical review from definition and classification of cell death. Int J Cardiol. 2013;167(6):2373-86.
20. Rodriguez M, Schaper J. Apoptosis: measurement and technical issues. J Mol Cell Cardiol. 2005;38(1):15-20.
21. Barbosky L, Lawrence DK, Karunamuni G, Wikenheiser JC, Doughman YQ, Visconti RP, et al. Apoptosis in the developing mouse heart. Dev Dyn. 2006;235(9):2592-602.
22. Inc. M-W. Heart 2017 [cited 2017]. Available from: https://www.merriam-webster.com/dictionary/heart?src=search-dict-hed.
23. Vincent SD, Buckingham ME. How to make a heart: the origin and regulation of cardiac progenitor cells. Curr Top Dev Biol. 2010;90:1-41.
24. Schaefer K, Watanabe M. Visualizing cell death in the developing heart. Anat Rec B New Anat. 2004;279(1):2-3.

25. Samsa LA, Yang B, Liu J. Embryonic cardiac chamber maturation: Trabeculation, conduction, and cardiomyocyte proliferation. Am J Med Genet C Semin Med Genet. 2013;163C(3):157-68.
26. Olson EN. Gene regulatory networks in the evolution and development of the heart. Science. 2006;313(5795):1922-7.
27. Bruneau BG. The developmental genetics of congenital heart disease. Nature. 2008;451(7181):943-8.
28. Sedmera D, Pexieder T, Vuillemin M, Thompson RP, Anderson RH. Developmental patterning of the myocardium. Anat Rec. 2000;258(4):319-37.
29. de Boer BA, van den Berg G, de Boer PA, Moorman AF, Ruijter JM. Growth of the developing mouse heart: an interactive qualitative and quantitative 3D atlas. Dev Biol. 2012;368(2):203-13.
30. Christoffels VM, Habets PE, Franco D, Campione M, de Jong F, Lamers WH, et al. Chamber formation and morphogenesis in the developing mammalian heart. Dev Biol. 2000;223(2):266-78.
31. Lin CJ, Lin CY, Chen CH, Zhou B, Chang CP. Partitioning the heart: mechanisms of cardiac septation and valve development. Development. 2012;139(18):3277-99.
32. Armstrong EJ, Bischoff J. Heart valve development: endothelial cell signaling and differentiation. Circ Res. 2004;95(5):459-70.
33. Sedmera D, Thomas PS. Trabeculation in the embryonic heart. Bioessays. 1996;18(7):607.
34. Staudt DW, Liu J, Thorn KS, Stuurman N, Liebling M, Stainier DY. High-resolution imaging of cardiomyocyte behavior reveals two distinct steps in ventricular trabeculation. Development. 2014;141(3):585-93.
35. Arbustini E, Weidemann F, Hall JL. Left ventricular noncompaction: a distinct cardiomyopathy or a trait shared by different cardiac diseases? J Am Coll Cardiol. 2014;64(17):1840-50.
36. Sedmera D, Thompson RP. Myocyte proliferation in the developing heart. Dev Dyn. 2011;240(6):1322-34.
37. Gitler AD, Lu MM, Jiang YQ, Epstein JA, Gruber PJ. Molecular markers of cardiac endocardial cushion development. Dev Dyn. 2003;228(4):643-50.
38. Sakamaki K, Inoue T, Asano M, Sudo K, Kazama H, Sakagami J, et al. Ex vivo whole-embryo culture of caspase-8-deficient embryos normalize their aberrant phenotypes in the developing neural tube and heart. Cell death and differentiation. 2002;9(11):1196-206.
39. Manasek FJ. Myocardial cell death in the embryonic chick ventricle. J Embryol Exp Morphol. 1969;21(2):271-84.
40. Pexieder T. The tissue dynamics of heart morphogenesis. I. The phenomena of cell death. A. Identification and morphology. Z Anat Entwicklungsgesch. 1972;137(3):270-84.
41. Schaefer KS, Doughman YQ, Fisher SA, Watanabe M. Dynamic patterns of apoptosis in the developing chicken heart. Dev Dyn. 2004;229(3):489-99.
42. Watanabe M, Choudhry A, Berlan M, Singal A, Siwik E, Mohr S, et al. Developmental remodeling and shortening of the cardiac outflow tract involves myocyte programmed cell death. Development. 1998;125(19):3809-20.
43. Sharma PR, Anderson RH, Copp AJ, Henderson DJ. Spatiotemporal analysis of programmed cell death during mouse cardiac septation. Anat Rec A Discov Mol Cell Evol Biol. 2004;277(2):355-69.
44. Abdelwahid E, Pelliniemi LJ, Niinikoski H, Simell O, Tuominen J, Rahkonen O, et al. Apoptosis in the pattern formation of the ventricular wall during mouse heart organogenesis. Anat Rec. 1999;256(2):208-17.
45. Haunstetter A, Izumo S. Apoptosis: basic mechanisms and implications for cardiovascular disease. Circ Res. 1998;82(11):1111-29.
46. Pexieder T. Cell death in the morphogenesis and teratogenesis of the heart. Adv Anat Embryol Cell Biol. 1975;51(3):3-99.
47. Bromme HJ, Holtz J. Apoptosis in the heart: when and why? Mol Cell Biochem. 1996;163-164:261-75.
48. James TN. Apoptosis in congenital heart disease. Coron Artery Dis. 1997;8(10):599-616.

49. Abdelwahid E, Pelliniemi LJ, Szucsik JC, Lessard JL, Jokinen E. Cellular disorganization and extensive apoptosis in the developing heart of mice that lack cardiac muscle alpha-actin: apparent cause of perinatal death. Pediatr Res. 2004;55(2):197-204.
50. NIH. What are congenital heart defects? 2011 [15/10/2016]. Available from: https://www.nhlbi.nih.gov/health/health-topics/topics/chd.
51. Huang JB, Liu YL, Sun PW, Lv XD, Du M, Fan XM. Molecular mechanisms of congenital heart disease. Cardiovasc Pathol. 2010;19(5):e183-93.
52. Zhu C, Liu YQ, Chen FK, Hu DL, Yu ZB, Qian LM. LYRM1, a gene that promotes proliferation and inhibits apoptosis during heart development. Molecules. 2010;15(10):6974-82.
53. Tang S, Batra A, Zhang Y, Ebenroth ES, Huang T. Left ventricular noncompaction is associated with mutations in the mitochondrial genome. Mitochondrion. 2010;10(4):350-7.
54. Watanabe M, Jafri A, Fisher SA. Apoptosis is required for the proper formation of the ventriculo-arterial connections. Dev Biol. 2001;240(1):274-88.
55. Kloesel B, DiNardo JA, Body SC. Cardiac Embryology and Molecular Mechanisms of Congenital Heart Disease: A Primer for Anesthesiologists. Anesth Analg. 2016;123(3):551-69.
56. Fisher SA, Langille BL, Srivastava D. Apoptosis during cardiovascular development. Circ Res. 2000;87(10):856-64.
57. James TN, St Martin E, Willis PW, 3rd, Lohr TO. Apoptosis as a possible cause of gradual development of complete heart block and fatal arrhythmias associated with absence of the AV node, sinus node, and internodal pathways. Circulation. 1996;93(7):1424-38.
58. James TN. Normal and abnormal consequences of apoptosis in the human heart. From postnatal morphogenesis to paroxysmal arrhythmias. Circulation. 1994;90(1):556-73.
59. James TN, Nichols MM, Sapire DW, DiPatre PL, Lopez SM. Complete heart block and fatal right ventricular failure in an infant. Circulation. 1996;93(8):1588-600.
60. Mallat Z, Tedgui A, Fontaliran F, Frank R, Durigon M, Fontaine G. Evidence of apoptosis in arrhythmogenic right ventricular dysplasia. N Engl J Med. 1996;335(16):1190-6.
61. Lakhani SA, Masud A, Kuida K, Porter GA, Jr., Booth CJ, Mehal WZ, et al. Caspases 3 and 7: key mediators of mitochondrial events of apoptosis. Science. 2006;311(5762):847-51.
62. Ranger AM, Malynn BA, Korsmeyer SJ. Mouse models of cell death. Nat Genet. 2001;28(2):113-8.
63. Sarosiek KA, Fraser C, Muthalagu N, Bhola PD, Chang W, McBrayer SK, et al. Developmental Regulation of Mitochondrial Apoptosis by c-Myc Governs Age- and Tissue-Specific Sensitivity to Cancer Therapeutics. Cancer Cell. 2017;31(1):142-56.
64. Kerr J. WA, and Currie A. Apoptosis: a basic biological phenomenon with wide-ranging implications in tissue kinetics. Br J Cancer. 1972;26:239.
65. Balvan J, Krizova A, Gumulec J, Raudenska M, Sladek Z, Sedlackova M, et al. Multimodal holographic microscopy: distinction between apoptosis and oncosis. PLoS One. 2015;10(3):e0121674.
66. Vandenabeele P, Galluzzi L, Vanden Berghe T, Kroemer G. Molecular mechanisms of necroptosis: an ordered cellular explosion. Nat Rev Mol Cell Biol. 2010;11(10):700-14.
67. Silva MT. Secondary necrosis: the natural outcome of the complete apoptotic program. FEBS Lett. 2010;584(22):4491-9.
68. Ashkenazi A, Salvesen G. Regulated cell death: signaling and mechanisms. Annu Rev Cell Dev Biol. 2014;30:337-56.
69. Suzuki K, Kostin, S., Person, V., Elsässer, A., and Schaper, J. Time Course of the Apoptotic Cascade and Effects of Caspase Inhibitors in Adult Rat Ventricular Cardiomyocytes. J Mol Cell Cardiol. 2001;33:983–94.
70. Green DR. Apoptotic pathways: ten minutes to dead. Cell. 2005;121(5):671-4.
71. Takemoto K, Nagai T, Miyawaki A, Miura M. Spatio-temporal activation of caspase revealed by indicator that is insensitive to environmental effects. J Cell Biol. 2003;160(2):235-43.
72. Miura M. Active participation of cell death in development and organismal homeostasis. Dev Growth Differ. 2011;53(2):125-36.

73. Ellis HM, Horvitz HR. Genetic control of programmed cell death in the nematode C. elegans. Cell. 1986;44(6):817-29.
74. Hengartner MO, Horvitz HR. Programmed cell death in Caenorhabditis elegans. Current opinion in genetics & development. 1994;4(4):581-6.
75. Hengartner MO. Programmed cell death. A rich harvest. Curr Biol. 1994;4(10):950-2.
76. Hengartner MO. The biochemistry of apoptosis. Nature. 2000;407(6805):770-6.
77. Thornberry NA, Rano TA, Peterson EP, Rasper DM, Timkey T, Garcia-Calvo M, et al. A combinatorial approach defines specificities of members of the caspase family and granzyme B. Functional relationships established for key mediators of apoptosis. J Biol Chem. 1997;272(29):17907-11.
78. de Almagro MC, Vucic D. Necroptosis: Pathway diversity and characteristics. Seminars in cell & developmental biology. 2015;39:56-62.
79. Linkermann A, Green DR. Necroptosis. N Engl J Med. 2014;370(5):455-65.
80. Su Z, Yang Z, Xie L, DeWitt JP, Chen Y. Cancer therapy in the necroptosis era. Cell Death Differ. 2016;23(5):748-56.
81. Cai Z, Jitkaew S, Zhao J, Chiang HC, Choksi S, Liu J, et al. Plasma membrane translocation of trimerized MLKL protein is required for TNF-induced necroptosis. Nat Cell Biol. 2014;16(1):55-65.
82. Moriwaki K, Bertin J, Gough PJ, Orlowski GM, Chan FK. Differential roles of RIPK1 and RIPK3 in TNF-induced necroptosis and chemotherapeutic agent-induced cell death. Cell Death Dis. 2015;6:e1636.
83. Luedde M, Lutz M, Carter N, Sosna J, Jacoby C, Vucur M, et al. RIP3, a kinase promoting necroptotic cell death, mediates adverse remodelling after myocardial infarction. Cardiovascular research. 2014;103(2):206-16.
84. Hitomi J, Christofferson DE, Ng A, Yao J, Degterev A, Xavier RJ, et al. Identification of a molecular signaling network that regulates a cellular necrotic cell death pathway. Cell. 2008;135(7):1311-23.
85. Chan FK, Shisler J, Bixby JG, Felices M, Zheng L, Appel M, et al. A role for tumor necrosis factor receptor-2 and receptor-interacting protein in programmed necrosis and antiviral responses. J Biol Chem. 2003;278(51):51613-21.
86. Degterev A, Huang Z, Boyce M, Li Y, Jagtap P, Mizushima N, et al. Chemical inhibitor of nonapoptotic cell death with therapeutic potential for ischemic brain injury. Nat Chem Biol. 2005;1(2):112-9.
87. Declercq W, Vanden Berghe T, Vandenabeele P. RIP kinases at the crossroads of cell death and survival. Cell. 2009;138(2):229-32.
88. Wilson NS, Dixit V, Ashkenazi A. Death receptor signal transducers: nodes of coordination in immune signaling networks. Nature immunology. 2009;10(4):348-55.
89. Vanden Berghe T, Linkermann A, Jouan-Lanhouet S, Walczak H, Vandenabeele P. Regulated necrosis: the expanding network of non-apoptotic cell death pathways. Nat Rev Mol Cell Biol. 2014;15(2):135-47.
90. AB NM. The 2016 Nobel Prize in Physiology or Medicine - Press Release: Nobelprize.org.; 2016 [cited 2017 Nov 8]. Available from: https://www.nobelprize.org/nobel_prizes/medicine/laureates/2016/press.html.
91. Larsson NGaM, M.G. Scientific Background. Discoveries of Mechanisms for Autophagy: Nobelprize.org; 2016 [cited 2017 Nov 8]. Available from: https://www.nobelprize.org/nobel_prizes/medicine/laureates/2016/advanced-medicineprize2016.pdf.
92. Whelan RS, Kaplinskiy V, Kitsis RN. Cell death in the pathogenesis of heart disease: mechanisms and significance. Annu Rev Physiol. 2010;72:19-44.
93. Schneider JL, Cuervo AM. Autophagy and human disease: emerging themes. Curr Opin Genet Dev. 2014;26:16-23.
94. Denton D, Shravage B, Simin R, Mills K, Berry DL, Baehrecke EH, et al. Autophagy, not apoptosis, is essential for midgut cell death in Drosophila. Current biology : CB. 2009;19(20):1741-6.

95. Lee E, Koo Y, Ng A, Wei Y, Luby-Phelps K, Juraszek A, et al. Autophagy is essential for cardiac morphogenesis during vertebrate development. Autophagy. 2014;10(4):572-87.
96. Shimizu S, Kanaseki T, Mizushima N, Mizuta T, Arakawa-Kobayashi S, Thompson CB, et al. Role of Bcl-2 family proteins in a non-apoptotic programmed cell death dependent on autophagy genes. Nature cell biology. 2004;6(12):1221-8.
97. Tsujimoto Y, Shimizu S. Another way to die: autophagic programmed cell death. Cell death and differentiation. 2005;12 Suppl 2:1528-34.
98. PROMEGA. Timing your apoptosis assays. Cell Notes. 2006(16).
99. Watanabe M, Hitomi M, van der Wee K, Rothenberg F, Fisher SA, Zucker R, et al. The pros and cons of apoptosis assays for use in the study of cells, tissues, and organs. Microsc Microanal. 2002;8(5):375-91.
100. Roche. In Situ Cell Death Detection Kit, Fluorescein. In: Science RA, editor. 2012.
101. Narula J, Haider N, Virmani R, DiSalvo TG, Kolodgie FD, Hajjar RJ, et al. Apoptosis in myocytes in end-stage heart failure. N Engl J Med. 1996;335(16):1182-9.
102. Olivetti G, Abbi R, Quaini F, Kajstura J, Cheng W, Nitahara JA, et al. Apoptosis in the failing human heart. N Engl J Med. 1997;336(16):1131-41.
103. Galluzzi L, Aaronson SA, Abrams J, Alnemri ES, Andrews DW, Baehrecke EH, et al. Guidelines for the use and interpretation of assays for monitoring cell death in higher eukaryotes. Cell death and differentiation. 2009;16(8):1093-107.
104. Shalini S, Dorstyn L, Dawar S, Kumar S. Old, new and emerging functions of caspases. Cell death and differentiation. 2015;22(4):526-39.
105. Kroemer G, Galluzzi L, Brenner C. Mitochondrial membrane permeabilization in cell death. Physiol Rev. 2007;87(1):99-163.
106. Bardet PL, Kolahgar G, Mynett A, Miguel-Aliaga I, Briscoe J, Meier P, et al. A fluorescent reporter of caspase activity for live imaging. Proceedings of the National Academy of Sciences of the United States of America. 2008;105(37):13901-5.
107. Yamaguchi Y, Shinotsuka, N., Nonomura, K., Takemoto, K., Kuida, K., Yosida, H., and Miura, M. . Live imaging of apoptosis in a novel transgenic mouse highlights its role in neural tube closure. J Cell Biol 2011;195:1047–60
108. van Ham TJ, Mapes J, Kokel D, Peterson RT. Live imaging of apoptotic cells in zebrafish. FASEB J. 2010;24(11):4336-42.
109. Solnica-Krezel L, Stemple DL, Driever W. Transparent things: cell fates and cell movements during early embryogenesis of zebrafish. BioEssays : news and reviews in molecular, cellular and developmental biology. 1995;17(11):931-9.
110. George SH, Gertsenstein M, Vintersten K, Korets-Smith E, Murphy J, Stevens ME, et al. Developmental and adult phenotyping directly from mutant embryonic stem cells. Proceedings of the National Academy of Sciences of the United States of America. 2007;104(11):4455-60.
111. EMBL. Cloning. Cloning Methods Cloning using restriction enzymes 2016 [cited 2016 18.03]. Available from: https://www.embl.de/pepcore/pepcore_services/cloning/cloning_methods/restriction_enzymes/.
112. QIAGEN®. QIAquick® Spin Handbook 2006 [cited 2016 18.03]. Available from: http://mvz.berkeley.edu/egl/inserts/QIAquick_Spin_Handbook.pdf.
113. Rossi RM, A; Ciarrocchi, G; Biamonti, G. Functional characterization of the T4 DNA ligase: a new insight into the mechanism of action. Nucleic Acids Res. 1997;25(11):2106-13.
114. QIAGEN®. QIAprep® Miniprep Handbook 2015. Available from: https://www.qiagen.com/.
115. Morrison DaR, J. Endotoxins and Disease Mechanisms. Ann Rev Med. 1987;38:417-32.
116. QIAGEN®. EndoFree® Plasmid Purification Handbook. 2005.
117. Potter H, and Heller, R. Transfection by Electroporation. Curr Protoc Mol Biol. 2003:CHAPTER: Unit–9.3.
118. Life-Technologies. Real-time PCR handbook. 2012.
119. Stotz M. Green Fluorescent Protein (GFP) and it's relatives. Biomolecular Structure. 2005.

120. Livak K, and Schmittgen, T. Analysis of Relative Gene Expression Data Using Real-Time Quantitative PCR and the 22DDCT Method. Methods 2001;25:402-8.
121. Mullis K, Faloona, F., Scharf, S., Saiki, R., Horn, G., and Erlich, H. Specific Enzymatic Amplification of DNA In Vitro: The Polymerase Chain Reaction. Cold Spring Harbor Symposia on Quantitative Biology. 1986;LI.
122. QIAGEN®. Gentra® Puregene® Handbook. 2011.
123. Mandlekar S, and Kong, A. Mechanisms of tamoxifen-induced apoptosis. Apoptosis. 2001;6:469-77.
124. Malet C, Compel, A., Spritzer, P., Bricout, N., Yaneva, M., Mowszowicz, I., et al. Tamoxifen and Hydroxytamoxifen Isomers versus Estradici Effects on Normal Human Breast Cells in Culture. Cancer Research. 1988;48:7196-9.
125. Riss T, and Moravec, R. Use of Multiple Assay Endpoints to Investigate the Effects of Incubation Time, Dose of Toxin, and Plating Density in Cell-Based Cytotoxicity Assays. ASSAY and Drug Development Technologies. 2004;2(1).
126. Galvao J, Davis B, Tilley M, Normando E, Duchen MR, Cordeiro MF. Unexpected low-dose toxicity of the universal solvent DMSO. FASEB J. 2014;28(3):1317-30.
127. Doetschman TC, Eistetter H, Katz M, Schmidt W, Kemler R. The in vitro development of blastocyst-derived embryonic stem cell lines: formation of visceral yolk sac, blood islands and myocardium. J Embryol Exp Morphol. 1985;87:27-45.
128. Kurosawa H. Methods for Inducing Embryoid Body Formation: In Vitro Differentiation System of Embryonic Stem Cells. JOURNAL OF BIOSCIENCE AND BIOENGINEERING. 2007;103(5):389-98.
129. Fuegemann CJ, Samraj AK, Walsh S, Fleischmann BK, Jovinge S, Breitbach M. Differentiation of mouse embryonic stem cells into cardiomyocytes via the hanging-drop and mass culture methods. Curr Protoc Stem Cell Biol. 2010;Chapter 1:Unit 1F 11.
130. SERVIER LL. Medical Art: LES LABORATOIRES SERVIER; 2017 [cited 2017]. Available from: http://www.servier.de/medical-art.
131. Shi S, and Taylor, C. Antigen Retrieval. Protocol. Dako.
132. Tanaka M, Hadjantonakis, A.K., Vintersten, K., and Nagy, A. Aggregation Chimeras: Combining ES Cells, Diploid, and Tetraploid Embryos. Methods Mol Biol. 2009;530:287-309.
133. Takahashi M, Osumi N. The method of rodent whole embryo culture using the rotator-type bottle culture system. J Vis Exp. 2010(42).
134. Barak H, Boyle SC. Organ culture and immunostaining of mouse embryonic kidneys. Cold Spring Harb Protoc. 2011;2011(1):pdb prot5558.
135. Clipart.printcolorcraft. microscope clipart 13 id-46406 2017 [cited 2017 Nov. 13]. Available from: http://clipart.printcolorcraft.com/2015/11/microscope-clipart-13/.
136. GmbH i. Open slides 2017 [cited 2017 Nov. 13]. Available from: https://ibidi.com/open-slides/35--slide-2-well.html.
137. Miyazaki J, Takaki S, Araki K, Tashiro F, Tominaga A, Takatsu K, et al. Expression vector system based on the chicken beta-actin promoter directs efficient production of interleukin-5. Gene. 1989;79(2):269-77.
138. Okabe M, Ikawa M, Kominami K, Nakanishi T, Nishimune Y. 'Green mice' as a source of ubiquitous green cells. FEBS Lett. 1997;407(3):313-9.
139. Xu ZL, Mizuguchi H, Ishii-Watabe A, Uchida E, Mayumi T, Hayakawa T. Optimization of transcriptional regulatory elements for constructing plasmid vectors. Gene. 2001;272(1-2):149-56.
140. Hesse M, Raulf A, Pilz GA, Haberlandt C, Klein AM, Jabs R, et al. Direct visualization of cell division using high-resolution imaging of M-phase of the cell cycle. Nat Commun. 2012;3:1076.
141. Bruegmann T, Malan, D., Hesse, M., Beiert, T., Fuegemann, C., Fleischmann, B., and Sasse, P. Optogenetic control of heart muscle in vitro and in vivo. Nature Methods. 2010;7(11).
142. Huerta S, Goulet, E., Huerta-Yepz, S., and Livingston, E. Screening and Detection of Apoptosis. Journal of Surgical Research. 2007;139:143–56.
143. Koike M, Sakaki, S., Amano Y., and Kurosawa, H. Characterization of Embryoid Bodies of Mouse Embryonic Stem Cells Formed under Various Culture Conditions and Estimation of

Differentiation Status of Such Bodies. JOURNAL OF BIOSCIENCE AND BIOENGINEERING. 2007;104(4):294–9.
144. Penaloza C, Lin, L., Lockshin, R., and Zakeri, Z. . Cell death in development: shaping the embryo. Histochem Cell Biol. 2006;126:149–58.
145. Boyd S, Hooper, M., and Wyllie, A. . The mode of cell death associated with cavitation in teratocarcinoma-derived embryoid bodies. J Embryol exp Morph. 1984;80:63-74.
146. Kaczmarek A, Vandenabeele P, Krysko DV. Necroptosis: the release of damage-associated molecular patterns and its physiological relevance. Immunity. 2013;38(2):209-23.
147. Slee EA, Zhu H, Chow SC, MacFarlane M, Nicholson DW, Cohen GM. Benzyloxycarbonyl-Val-Ala-Asp (OMe) fluoromethylketone (Z-VAD.FMK) inhibits apoptosis by blocking the processing of CPP32. Biochem J. 1996;315 (Pt 1):21-4.
148. Vandenabeele P, Vanden Berghe T, Festjens N. Caspase inhibitors promote alternative cell death pathways. Sci STKE. 2006;2006(358):pe44.
149. Dumont EA, Reutelingsperger CP, Smits JF, Daemen MJ, Doevendans PA, Wellens HJ, et al. Real-time imaging of apoptotic cell-membrane changes at the single-cell level in the beating murine heart. Nat Med. 2001;7(12):1352-5.
150. Blankenberg FG. In vivo detection of apoptosis. J Nucl Med. 2008;49 Suppl 2:81S-95S.
151. Laufer EM, Reutelingsperger CP, Narula J, Hofstra L. Annexin A5: an imaging biomarker of cardiovascular risk. Basic Res Cardiol. 2008;103(2):95-104.
152. Yivgi-Ohana N, Eifer M, Addadi Y, Neeman M, Gross A. Utilizing mitochondrial events as biomarkers for imaging apoptosis. Cell Death Dis. 2011;2:e166.
153. Hauser H, Wagner R. Mammalian Cell Biotechnology in Protein Production. Berlin, Germany: Walter de Gruyter; 1997. Available from: https://books.google.de/books?id=_-OQM5eQa5YC&pg=PA27&lpg=PA27&dq=medium+depletion+and+programmed+cell+death&source=bl&ots=kA79qMCq6v&sig=xxbLkzmd1GqVijmo8le4ZcT54cA&hl=de&sa=X&ved=0ahUKEwiDvvG-o6POAhVJJpoKHc8eDEgQ6AEIZTAJ#v=onepage&q=medium%20depletion%20and%20programmed%20cell%20death&f=false.
154. Franek F. Starvation-induced programmed death of hybridoma cells: Prevention by amino acid mixtures. Biotechnol Bioeng. 1995;45(1):86-90.
155. Fadeel B, Orrenius S. Apoptosis: a basic biological phenomenon with wide-ranging implications in human disease. J Intern Med. 2005;258(6):479-517.
156. Jerse M, Zidar N. Apoptosis in the developing human heart resembles apoptosis in epithelial tissues. Cell Tissue Res. 2011;343(3):537-43.
157. Poelmann RE, Gittenberger-de Groot AC. Apoptosis as an instrument in cardiovascular development. Birth Defects Res C Embryo Today. 2005;75(4):305-13.
158. Cheng G, Wessels A, Gourdie RG, Thompson RP. Spatiotemporal and tissue specific distribution of apoptosis in the developing chick heart. Dev Dyn. 2002;223(1):119-33.
159. Fernandez E, Siddiquee Z, Shohet RV. Apoptosis and proliferation in the neonatal murine heart. Dev Dyn. 2001;221(3):302-10.
160. Schaper J, Elsasser A, Kostin S. The role of cell death in heart failure. Circ Res. 1999;85(9):867-9.
161. Lesauskaite V, Epistolato MC, Ivanoviene L, Tanganelli P. Apoptosis of cardiomyocytes in explanted and transplanted hearts. Comparison of results from in situ TUNEL, ISEL, and ISOL reactions. Am J Clin Pathol. 2004;121(1):108-16.
162. Mani K, Kitsis RN. Myocyte apoptosis: programming ventricular remodeling. J Am Coll Cardiol. 2003;41(5):761-4.
163. Wencker D, Chandra M, Nguyen K, Miao W, Garantziotis S, Factor SM, et al. A mechanistic role for cardiac myocyte apoptosis in heart failure. J Clin Invest. 2003;111(10):1497-504.
164. Kostin S, Pool L, Elsasser A, Hein S, Drexler HC, Arnon E, et al. Myocytes die by multiple mechanisms in failing human hearts. Circ Res. 2003;92(7):715-24.
165. Ohno M, Takemura G, Ohno A, Misao J, Hayakawa Y, Minatoguchi S, et al. "Apoptotic" myocytes in infarct area in rabbit hearts may be oncotic myocytes with DNA fragmentation: analysis

by immunogold electron microscopy combined with In situ nick end-labeling. Circulation. 1998;98(14):1422-30.
166. Kanoh M, Takemura G, Misao J, Hayakawa Y, Aoyama T, Nishigaki K, et al. Significance of myocytes with positive DNA in situ nick end-labeling (TUNEL) in hearts with dilated cardiomyopathy: not apoptosis but DNA repair. Circulation. 1999;99(21):2757-64.
167. Poelmann RE, Molin D, Wisse LJ, Gittenberger-de Groot AC. Apoptosis in cardiac development. Cell Tissue Res. 2000;301(1):43-52.
168. Zhao Z, Rivkees SA. Programmed cell death in the developing heart: regulation by BMP4 and FGF2. Dev Dyn. 2000;217(4):388-400.
169. Kajstura J, Mansukhani M, Cheng W, Reiss K, Krajewski S, Reed JC, et al. Programmed cell death and expression of the protooncogene bcl-2 in myocytes during postnatal maturation of the heart. Exp Cell Res. 1995;219(1):110-21.
170. Shieh JT, Jefferies JL, Chin AJ. Disorders of left ventricular trabeculation/compaction or right ventricular wall formation. Am J Med Genet C Semin Med Genet. 2013;163C(3):141-3.
171. Chen H, Zhang W, Li D, Cordes TM, Mark Payne R, Shou W. Analysis of ventricular hypertrabeculation and noncompaction using genetically engineered mouse models. Pediatr Cardiol. 2009;30(5):626-34.
172. Shou W, Aghdasi B, Armstrong DL, Guo Q, Bao S, Charng MJ, et al. Cardiac defects and altered ryanodine receptor function in mice lacking FKBP12. Nature. 1998;391(6666):489-92.
173. Takeda K, Yu ZX, Nishikawa T, Tanaka M, Hosoda S, Ferrans VJ, et al. Apoptosis and DNA fragmentation in the bulbus cordis of the developing rat heart. J Mol Cell Cardiol. 1996;28(1):209-15.
174. Abdelwahid E, Pelliniemi LJ, Jokinen E. Cell death and differentiation in the development of the endocardial cushion of the embryonic heart. Microsc Res Tech. 2002;58(5):395-403.
175. Abdelwahid E, Rice D, Pelliniemi LJ, Jokinen E. Overlapping and differential localization of Bmp-2, Bmp-4, Msx-2 and apoptosis in the endocardial cushion and adjacent tissues of the developing mouse heart. Cell Tissue Res. 2001;305(1):67-78.
176. Sedmera D. Form follows function: developmental and physiological view on ventricular myocardial architecture. Eur J Cardiothorac Surg. 2005;28(4):526-8.
177. Kitsis RN, Mann DL. Apoptosis and the heart: a decade of progress. J Mol Cell Cardiol. 2005;38(1):1-2.
178. Kietselaer BL, Reutelingsperger CP, Boersma HH, Heidendal GA, Liem IH, Crijns HJ, et al. Noninvasive detection of programmed cell loss with 99mTc-labeled annexin A5 in heart failure. J Nucl Med. 2007;48(4):562-7.
179. Johnson LL, Schofield L, Donahay T, Narula N, Narula J. 99mTc-annexin V imaging for in vivo detection of atherosclerotic lesions in porcine coronary arteries. J Nucl Med. 2005;46(7):1186-93.
180. Kolodgie FD, Petrov A, Virmani R, Narula N, Verjans JW, Weber DK, et al. Targeting of apoptotic macrophages and experimental atheroma with radiolabeled annexin V: a technique with potential for noninvasive imaging of vulnerable plaque. Circulation. 2003;108(25):3134-9.
181. van Heerde WL, Robert-Offerman S, Dumont E, Hofstra L, Doevendans PA, Smits JF, et al. Markers of apoptosis in cardiovascular tissues: focus on Annexin V. Cardiovasc Res. 2000;45(3):549-59.
182. Lee SH, Meng XW, Flatten KS, Loegering DA, Kaufmann SH. Phosphatidylserine exposure during apoptosis reflects bidirectional trafficking between plasma membrane and cytoplasm. Cell death and differentiation. 2013;20(1):64-76.
183. Leventis PA, Grinstein S. The distribution and function of phosphatidylserine in cellular membranes. Annu Rev Biophys. 2010;39:407-27.
184. Denecker G, Dooms, H., Van Loo, G., Vercammen, D., Grooten, J., , Fiers W, Declercq, W., and Vandenabeele, P. . Phosphatidyl serine exposure during apoptosis precedes release of cytochrome c and decrease in mitochondrial transmembrane potential. FEBS Letters. 2000;465:47-52.
185. Goldstein JC, Waterhouse NJ, Juin P, Evan GI, Green DR. The coordinate release of cytochrome c during apoptosis is rapid, complete and kinetically invariant. Nat Cell Biol. 2000;2(3):156-62.

186. Wu T, Tan, H., Huang, Q., Sun, X., Zhu, X., Shen, H. zVAD-induced necroptosis in L929 cells depends on autocrine production of TNFa mediated by the PKC–MAPKs–AP-1 pathway. Cell death and differentiation. 2011;18:26-37.
187. Kroemer G, and Martin, S. Caspase-independent cell death. Nature Medicine. 2005;11(7).
188. Gong YN, Guy C, Olauson H, Becker JU, Yang M, Fitzgerald P, et al. ESCRT-III Acts Downstream of MLKL to Regulate Necroptotic Cell Death and Its Consequences. Cell. 2017;169(2):286-300 e16.
189. Fleischmann M, Bloch W, Kolossov E, Andressen C, Muller M, Brem G, et al. Cardiac specific expression of the green fluorescent protein during early murine embryonic development. FEBS Lett. 1998;440(3):370-6.
190. van den Hoff MJ, van den Eijnde SM, Viragh S, Moorman AF. Programmed cell death in the developing heart. Cardiovasc Res. 2000;45(3):603-20.
191. Keyes WM, Sanders EJ. Regulation of apoptosis in the endocardial cushions of the developing chick heart. Am J Physiol Cell Physiol. 2002;282(6):C1348-60.
192. Koshinuma S, Miyamae M, Kaneda K, Kotani J, Figueredo VM. Combination of necroptosis and apoptosis inhibition enhances cardioprotection against myocardial ischemia-reperfusion injury. J Anesth. 2014;28(2):235-41.

8. ABBREVIATIONS

A	atria
Afl	autofluorescence
AIF	apoptosis-inducing factor
ALS	Amyotrophic Lateral Sclerosis
AO	acridine orange
Apaf1	apoptotic protease-activating factor 1
AR	antigen retrieval
α-SMCs	alpha smooth muscle cells
ASMAC	alpha smooth muscle actin
Atgs	autophagy related genes
AVC	atrioventricular canal
A5	annexin A5
Bak	Bcl-2 antagonist/killer 1
Bax	Bcl-2-associated X protein, apoptosis regulator
Bcl-2	B-cell lymphoma 2, apoptosis regulator
Bcl-X_L	B-cell lymphoma X long, apoptosis regulator
BF	bright field
Bid	BH3-interacting domain death agonist
Bmp10	bone morphogenetic protein 10
CAG	chicken β-actin promoter with CMV enhancer element
Casp	caspase
cCasp	cleaved caspase
CD	cluster of differentiation
CD1-Tg	CD1 mice-transgenic
CDH	congenital heart diseases
CED	identified cell-death gene
CIAP	calf Intestine alkaline phosphatase
cIAPS	cellular inhibitors of apoptosis
c-FLIP	cellular FLICE-like inhibitory protein
CMs	cardiomyocytes
CO_2	carbon dioxide
Ct	threshold cycle

cytC	cytochrome c
DAI	DNA-dependent activator of interferon regulatory factor
DEVD	caspase 3-cleavage site: Asp-Glu-Val-Asp
DIABLO	direct IAP-binding protein with low pI
DISC	death-inducing signaling complex
DMSO	dimethyl sulfoxide
DNA	Deoxyribonucleic acid
dNTP	Deoxyribonucleotide triphosphate
DPBS	Dulbecco's Phosphate-Buffered Saline
DR	death receptor
DS	donkey serum
E	embryonic day
EBs	Embryiod bodies
ECFP	enhanced cyan fluorescent protein
EDTA	Ethylenediaminetetraacetic acid
eGFP	enhanced green fluorescent protein
ERBB2	Receptor tyrosine-protein kinase 2
EtBr	ethidium bromide
FADD	Fas-associated death domain protein
FAM	Carboxyfluorescein
FasL	Fas Ligand
FCS	fetal calf serum
FHF	first heart field
FKBP12	Peptidyl-prolyl cis-trans isomerase
FMK	Fluoromethyl ketone
FRET	Fluorescence resonance energy transfer
Fw	forward primer
GFP	green fluorescent protein
hA5	human annexin A5
HIV	human immunodeficiency virus
HS4	Chromatin insulator: chicken β-globin locus control region hypersensitive site 4
IAP	inhibitors of apoptosis
IMDM	Iscove's Modified Dulbecco's Medium

iVS	intraventricular septum
KO-DMEM	Knockout Dulbecco’s Modified Eagle Medium
LA	left atrium
LED	light-emitting diode
LIF	Leukemia inhibiting factor
LTR	LysoTracker Red
LV	left ventricle
LVNC	left ventricular non-compaction
MEM	Non-Essential Aminoacids
mESCs	Mouse embryonic stem cells
MF20	anti-myosin heavy chain monoclonal Clone MF20
MGB	minor groove binder probes
MLS	Mitochondrial Leader Sequence
MLKL	Pseudokinase mixed lineage kinase domain-like
MOMP	Mitochondrial outer membrane permeabilization
MOPS	3-Morpholinopropanesulfonic Acid
N	Nuclei
NBS	Nile blue sulfate
NCCD	Nomenclature Committee on Cell Death
Nec-1	Necrostatin 1
Neo3	Neomycin resistant cassette
NF-kβ	Nuclear factor kappa-light-chain-enhancer of activated B cells
NIH	National Institute of Health
Nkx2.5	Homeobox 5-containing transcription factor
NR	Neutral red
NRG1	Neuregulin-1
OFT	Outflow Tract
4-OHT	4-hydroxytamoxifen
P	postnatal day
pBH	Bleeding heart vector
PBS	Phosphate-Buffered Saline
PCD	Programmed Cell Death
PCR	Polymerase chain reaction
PECAM	Platelet endothelial cell adhesion molecule

PFA	Paraformaldehyde
PMEF-NL	Embryonic Fibroblast
PS	Phosphatidylserine
RA	right atrium
Rev	reverse primer
RIPK1/3	Receptor-interacting protein kinase-1/3
RNA	Ribonucleic acid
RT	Room temperature
RT-qPCR	real-time quantitative PCR
RV	right ventricle
sA5	secreted Annexin A5
SHF	secondary heart field
Smac	second mitochondria derived activator of caspases
SV	sinus venosus
SV129;BL/6	substrain 129;black six mice
TAE	Tris-Acetate-EDTA
TdT	Terminal deoxynucleotidyl transferase
TEM	Transmission electron microscopy
TFRC	Transferrin receptor gene
TMRM	Tetramethylrhodamine methylester
TNF	Tumor Necrosis Factor
TNFα	Tumor necrosis factor alpha
TNFR1	Tumor necrosis factor receptor 1
Tr	Trabeculae
TRADD	Tumor necrosis factor receptor type 1-associated death domain protein
TRIF	Toll/IL-1 receptor domain-containing adaptor inducing IFN-β
Tris-HCl	Tris-(Hydroxymethyl)-Aminomethan-Hydrochlorid
TUNEL	Terminal deoxynucleotidyl transferase dUTP nick end labeling
UAS	Upstream Activating Sequences, DNA-binding motif of GAL4
V	ventricle
Vps34	Phosphoinositide 3-kinase (PI3K) class III isoform
YFP	yellow fluorescent protein
zVAD-fmk	N-benzyloxycarbonyl-Val-Ala-Asp- fluoromethyl ketone

LIST OF PUBLICATIONS

Publications

Kristel Martínez-Lagunas, Michael Hesse, Yoshifumi Yamaguchi, Masayuki Miura and Bernd K. Fleischmann. *A straight forward genetic reporter to visualize apoptosis during mouse heart development in vivo.*

*On preparation. To be submitted to Nature Communications.

Oral Talks

Martínez-Lagunas K, Fleischmann BK and Hesse M. *In vivo detection of programmed cell death during mouse heart development.* 96th Annual Meeting of the Deutsche Physiologische Gesellschaft, Greifswald, Germany, March 2017.

Martínez-Lagunas K, Fleischmann BK and Hesse M. *In vivo detection of programmed cell death during mouse heart development.* 24th Conference of the European Cell Death Organization, "Cell Death in Health and Disease", Barcelona, Spain, September 2016.

Poster Presentations

Martínez-Lagunas K, Fleischmann BK and Hesse M. *Establishment of a novel system for in vivo detection of cardiomyocyte apoptosis*. 23rd Conference of the European Cell Death Organization, "Death pathways and beyond' Geneva, Switzerland, October 2015.

Martínez-Lagunas K, Fleischmann BK and Hesse M. *Establishment of a novel system for in vivo detection of cardiomyocyte apoptosis*.94th Annual Meeting of the German Physiological Society, Magdeburg Germany, March 2015.

Martínez-Lagunas K, Fleischmann BK and Hesse M. *Establishment of a novel system for in vivo detection of cardiomyocyte apoptosis*. Mechanisms of cardiovascular diseases and the road to therapy. Hannover, Germany, September 2014.

Martínez-Lagunas K, Fleischmann BK and Hesse M. *Establishment of a novel system for in vivo detection of cardiomyocyte apoptosis*. 93rd Annual Meeting of the German Physiological Society, Mainz Germany, April 2014**.**

ACKNOWLEDGEMENTS

"Making a decision was only the beginning of things. When someone makes a decision, he is really diving into a strong current that will carry him to places he had never dreamed of when he first made the decision." (Paulo Coelho, The Alchemist)

This thesis is more than the results of my research. It is a fulfilled dream. It is a pile of conquered challenges. It is the answer to frustration and loneliness. It is a self-discovery. It is the result of endurance and of the stand ups after several falls. It is beautiful moments shared with indescribable people. It is laughter and tears. It is all what the universe conspired for me to arrive here. It is the potter who has shaped my personal and professional life. It is a team work. It is the reflection of all the persons and institutions who held me out a hand.

In the following lines, I would like to mention and give thanks to all who made possible my PhD. Trip and to all who shared it with me making it special and happy.

In first place, I would like to thank my advisor Prof. Dr. Bernd Fleischmann for opening me the doors of his laboratory and for providing me all the necessary resources to finish this project. Thank you for your mentoring, questioning and feedback, which led me to give more than 100 percent in each experiment. In second place, I give my special gratitude to my direct supervisor, Dr. Michael Hesse. Thank you so much Michael for believing in me, for leaving on my hands your project's idea, for being my guide in theory and practice, for having always the doors open to discuss our ideas, for your constructive commentaries, for your kindness, and nice sense of humor, for all those curious stories, and for teaching me to be more pragmatic.

My arrival to the University of Bonn was possible thanks to the Ph.D. program from the *NRW International Graduate School Biotech-Pharma,* who offered me a three-year scholarship to be part of their academic program. Thank you so much to Prof. Dr. Alexander Pfeifer and Dr. Elisabeth Mies-Klomfass for all their economic, administrative and academic support. In addition, I would like to extend my gratitude to the *International Graduate School BIGS-DrugS* from the University of Bonn, the DFG research group FOR1352, and the one of the Mexican National Board of Science of Technology (CONACYT) for offering me financial help to finish my research study.

I want also to thank to Prof. Dr. Christa Müller from the Institute of Pharmacology, to Prof. Dr. Evi Kostenis from the Institute of Pharmaceutical Biology, and Prof. Dr. Jörg Höhfeld from the Institute Cell Biology from the University of Bonn, for their kind willingness to be part of my thesis committee and for evaluating this investigation.

Moreover, I am deeply grateful with Prof. Masayuki Miura and Dr. Yoshifumi Yamaguchi from the University of Japan, for showing their genuine interest on my project, for the kind and useful academic counseling, for the insightful feedback and for performing the real-time experiments to validate my reporter system.

I want to give my sincere acknowledgment to all members of the Institute of Physiology I for their comradeship and for creating a nice working atmosphere. Here, I would like to mention several people who led me a hand in several aspects. Thanks a lot Birgit for your valuable help with all administrative issues during all my stay in this institute. Patricia, Sabine and Carolina one thousand thanks for teaching me cloning and cell culture techniques, but mostly *Vielen Lieben Dank* for opening me the doors of your heart and for integrate me inside and outside the lab. I will always be grateful towards you for sharing the nice walking tours, grills, coffees, for pushing me to speak in German and having me patience to improve it. I also give thanks to Alex Raulf for introducing me to the experimental world in this lab, for guiding me and being my master of microscopy. Finally, many thanks to my dear colleagues Daniel, Katia and Ken for your moral support, for all those shared moments, for your cheering words and for your help in optimizing some of my experiments.

My biggest appreciation and recognition is for my parents Toñita and Miguel and for my siblings Vane, Migue y Chino. My lovely *papis* the word "thanks" is not enough to express how much I value your unconditional LOVE. Infinitely thank you for all your sacrifices for helping me to reach my dreams, for being my example of life, for teaching me to fight as a warrior, for teaching me to be brave, for your wise advice, for letting me fly high despite the pain of the distance, for being always present, for sharing my achievements and failures. This trip wouldn't have been possible without the foundation you have left in my life. *Hermanitos,* I deeply thank you for your affection, for helping me in all that is on your hands and for all the beautiful moments we have shared. *Hermanita,* thanks thanks for being my biggest example, for showing me the way of fighting for our dreams, and for introducing me to the German culture.

Finally, I am eternally thankful with the Universe for putting on my way to my great family in Germany, my friends, my siblings to whom I will mention in order of appearance. My dear musketeers Marisa and David thank from the bottom of my heart for all these years of adventures, for sharing our dreams, laughter and happiness, for each hug and cheerful word that you give me, and most of all for teaching me the true value of friendship. Next, thanks to the beautiful empathy and kindness of Omneya I was able to meet the rest of the family. Omneya thank you so much for approaching me that day in the kitchen of the lab, for opening

me the door of your friendship and for introducing me to Eli. My sweet angel you have been the sun of my trip. Many many thanks from the bottom of my soul for showing me the GOODNESS in person, for every angel action that you have done for me, for taking out the best of me, for your genuine interest for all what happens in my life, for your awesome sense of humor and happiness that shine my life up, for bear my “gracias”, but most of all for being my Spanish sister and trip comrade. My days in the lab were more fun and special thanks to my dear Viki. Vik, one million thanks from the bottom of my heart for your warm hugs in those difficult moments, for your cuteness and support, for laughing and crying with me, for all the lunch moments, and for each shared instant inside and outside the lab. And lastly, thank you so much to all my friends, who arrived in the middle or at the end of my Ph.D. trip, for all your help and for making this experience more memorable and happy.

AGRADECIMIENTOS

"Las decisiones son solamente el comienzo de algo. Cuando alguien toma una decisión, se zambulle en una poderosa corriente que lleva a una persona hasta un lugar que jamás hubiera soñado en el momento de decidirse" (Paulo Coelho, El Alquimista)

Esta tesis es más que los resultados de mi investigación. Es un sueño cumplido. Es un montón de retos superados. Es la respuesta a la frustración y a la soledad. Es un descubrimiento personal. Es el resultado de la perseverancia y de levantarse después de varias caídas. Es hermosos momentos compartidos con personas indescriptibles. Es risas y lágrimas. Es todo lo que el universo conspiró para que yo llegará hasta aquí. Es el alfarero que ha moldeado mi vida personal y profesional. Es un trabajo de equipo. Es el reflejo de todas las personas e instituciones que me tendieron la mano.

En las siguientes líneas quiero mencionar y agradecer a todos los que hicieron posible mi viaje de doctorado y a los que lo compartieron conmigo haciéndolo especial y feliz.

Primeramente, le agradezco a mi asesor, el Prof. Dr. Bernd Fleischmann, por abrirme las puertas de su laboratorio y por brindarme los recursos necesarios para concluir esta investigación. Gracias por darme seguimiento y por su cuestionamiento crítico, el cual me llevó a dar más del cien por ciento en cada experimento. En segundo lugar, le doy mi especial agradecimiento a mi supervisor, el Dr. Michael Hesse. Muchísimas gracias Michael por creer en mí, por dejar en mis manos tu idea de este proyecto, por ser mi guía en teoría y práctica, por tener siempre las puertas abiertas para discutir, por tus comentarios constructivos, por tu bondad, por tu buen sentido del humor, por todas esas historias curiosas y por enseñarme a ser más pragmática.

Mi llegada a la Universidad de Bonn fue posible gracias al programa de doctorado de la Escuela Internacional de Investigación "Biotech-Pharma" de Renania del Norte, quienes me otorgaron una beca de tres para participar en su programa académico. Muchísimas gracias al Prof. Dr. Alexander Pfeifer y la Dra. Elisabeth Mies-Klomfass por todo su apoyo económico, administrativo y académico. También agradezco de antemano a la Escuela Internacional de Investigación "BIGS-DrugS" de la Universidad de Bonn, al grupo de investigación FOR1352 del Consejo Alemán de Investigación (DFG) y al Consejo Nacional de Ciencia y Tecnología (CONACYT) de mi hermoso México por darme su enorme apoyo económico para poder finalizar mi investigación.

Extiendo mi agradecimiento a la Profa. Dra. Christa Müller del Instituto de Farmacología, a la Profa. Dra. Evi Kostenis del Instituto de Biología Farmacéutica y al Prof. Dr. Jörg Höhfeld del Instituto de Biología Celular de la Universidad de Bonn, por su buena disposición para ser miembros de mi comité de tesis y por evaluar esta investigación.

Además, estoy profundamente agradecida con el Prof. Masayuki Miura y el Dr. Yoshifumi Yamaguchi de la Universidad de Tokio en Japón, por mostrar un interés genuino en mi proyecto, por su asesoría, por su retroalimentación reveladora y útil, y por realizar los experimentos de tiempo real para validar mi sistema.

Mi más sincero agradecimiento a todos los miembros del Instituto de Fisiología I por su compañerismo y por crear un ambiente agradable de trabajo. Aquí quiero mencionar varias personas que me echaron la mano en diferentes aspectos. Muchísimas gracias Birgit por tu valiosa ayuda con todos los trámites administrativos durante toda mi estancia en este instituto. Patricia, Sabine y Carolina mil gracias por enseñarme varias técnicas de clonación y cultivo celular. Pero mucho más, les agradezco profundamente por abrirme las puertas de su corazón y por integrarme dentro y fuera del laboratorio. Gracias por compartir esas bonitas caminatas, carnes asadas, cafecitos, por su paciencia al escucharme hablar alemán y por ayudarme a mejorarlo. También le doy un especial agradecimiento a Alex Raulf por introducirme al mundo experimental, por guiarme cada día en mis primeros seis meses en el laboratorio y por ser mi maestra de microscopía. Finalmente, muchas gracias a mis queridos colegas Daniel, Katia, Annika y Ken por su gran apoyo moral, por todos esos momentos compartidos fuera y dentro del laboratorio, por sus palabras de aliento y por su ayuda para optimizar algunos de mis experimentos.

Mi mayor reconocimiento es para mis papás Toñita y Miguel y para mis hermanos Vane, Migue y Chino. Papis hermosos la palabra “gracias” se queda corta para expresarles cuanto valoro el AMOR incondicional que me han dado. Infinitamente gracias por todos sus sacrificios para apoyarme a lograr mis sueños locos, por ser mi ejemplo de vida, por enseñarme a luchar como guerrera, por enseñarme a ser valiente, por sus sabios consejos, por dejarme volar a pesar del dolor que causa la distancia, por estar siempre presentes, por compartir mis alegrías y fracasos. Este viaje no hubiera sido posible sin los cimientos que han forjado en mi vida. Hermanitos les agradezco de corazón por su cariño, por sus palabras de ánimo y motivación, por estar siempre atentos de lo que pasa en mi vida, por ayudarme en todo lo que está en sus manos y por todos los bonitos momentos que hemos compartido. Hermanita mil gracias por ser mi gran ejemplo, por mostrarme como luchar por nuestros sueños y por introducirme a la cultura alemana.

Finalmente, estoy eternamente agradecida con el universo por poner en mi camino a mi gran familia en Alemania, mis amigos, mis hermanos a quienes mencionaré por orden de aparición. Mis queridos mosqueteros Marisa y David mil gracias por todos estos años de aventuras, por compartir nuestros sueños, risas y alegrías, por cada abrazo y palmadita de ánimo que me han brindado y por enseñarme el verdadero valor de la amistad. Ustedes le han dado sazón a esta aventura alemana. Por otro lado, gracias a la hermosa empatía y bondad de Omneya pude conocer al resto de mi familia de amigos. Omenya gracias por acercarte a mí ese día en la cocina del laboratorio, por abrirme la puerta de tu amistad y por presentarme a Eli. Mi angelita linda tú has sido el solecito de mi viaje. Muchísimas gracias desde el fondo de mi ser Chavi por mostrarme lo que es la BONDAD en persona, por cada acción de ángel que has hecho por mí, por siempre sacar lo mejor de mí, por tu interés genuino por lo que pasa en mi vida, por tu gran sentido del humor y alegría que iluminan mi vida, por aguantar mis "gracias", pero sobre todo por ser mi hermana española y compañera de viaje. Mis días en el laboratorio fueron más divertidos y especiales gracias a mi querida Viki. Vik, muchísimas gracias desde el fondo de mi corazón por tus abrazos en esos momentos difíciles, por tu ternura y apoyo, por reír y llorar conmigo, por todas las comidas juntas y por cada momento compartido dentro y fuera del laboratorio. Y por último, muchísimas gracias a todos mis amigos, quienes llegaron a la mitad o al final de mi viaje doctoral, por todo su apoyo y por hacer esta aventura más memorable y feliz.